March 2018

LIGHT-HARVESTING AND LIGHT-RESPONSIVE MATERIALS FOR OPTOELECTRONIC AND BIOLOGICAL APPLICATIONS

youngju bae

LIGHT-HARVESTING AND LIGHT-RESPONSIVE MATERIALS FOR OPTOELECTRONIC AND BIOLOGICAL APPLICATIONS

A Dissertation Presented

by

YOUNGJU BAE

Submitted to the Graduate School of the
University of Massachusetts Amherst in partial fulfillment
of the requirements for the degree of

DOCTOR OF PHILOSOPHY

February 2018

Department of Chemistry

LIGHT-HARVESTING AND LIGHT-RESPONSIVE MATERIALS FOR OPTOELECTRONIC AND BIOLOGICAL APPLICATIONS

A Dissertation Presented

by

YOUNGJU BAE

Approved as to style and content by:

_____
Sankaran Thayumanavan, Chair

_____
Elizabeth R. Young, Member

_____
Min Chen, Member

_____
Anthony D. Dinsmore, Member

_____
Richard W. Vachet, Department Head
Chemistry

DEDICATION

For my families, the one I was born into and the one I have made.

ACKNOWLEDGMENTS

The process for Ph.D. was not possible without lots of help and support from many people throughout the six years of my doctoral study at UMass Amherst. I would like to take this opportunity to express my sincere gratitude to those who have helped and supported me to make this dissertation possible.

I am grateful to my advisor, Professor Sankaran Thayumanavan (Thai), for his training, guidance, and support throughout my doctoral degree. I appreciate the opportunity he has given me to be a part of his research group, the encouragement to execute my ideas, and his guidance to help me to develop the ability to think scientifically. I really appreciate his full effort and patience in training me to be an independent scientist. Professor Thai's guidance and support has helped me to build my confidence and has prepared me to step into my future career.

I would also like to express my gratitude to my committee members, Professor Elizabeth Young, Professor Min Chen, Professor Anthony Dinsmore, Professor Alejandro Briseno, and Professor Paul Lathi, for their valuable suggestions and support. Their productive criticisms and advice helped me with the understanding and completion of this work.

I would like to thank my supervisor in my Master's degree, Professor In Tae Kim, for his supports and inspiration that made me continue my research in chemistry. I also would like to thank to Professor Byeonghyo Kim. His lectures in organic chemistry inspired and led me to the world of organic chemistry.

I would like to thank my class-mates: Mallory Gordon, Banyuhay P. Serrano, Oyuntuya Munkhbat, Kishore Raghupathi, Moumita Ray, Ngoc Le. We shared both fun

and frustrating times together while pursuing our Ph.D.'s. I have had an amazing time with you guys and will never forget our friendship.

I would also like to take this opportunity to thank all former and present Thayumanavan research group members: Dr. Bhooshan Popere, Dr. Jiaming Zhuang, Dr. Krishna Reddy Raghupathi, Dr. Wei Bai, Dr. Hatice Secinti, Dr. Mijanur Rahaman Molla, Dr. Subramanu Swaminathan, Celia Homyak, Poornima Rangadurai, Priyaa Prasad, Bo Zhao, Huan He, Bin Liu, Piyachai Khomein, Jingjing Gao, Francesca Anson, Kingshuk Dutta, Wardah Ejaz, Thameez Koyasseril, Vikash Kumar. I have enjoyed working and discussing both scientific and non-scientific topics with all of you.

I would like to express my special thanks to my collaborators, Dr Bhooshan Popere, Dr. Ambata Poe, Mallory Gordon, Oyuntuya, Munkhbat, Mine Canakci, Ziwen Jiang, Bo Zhao, Samuel Hendel, and Vijesh Tanna, for their valuable suggestions and discussions on my research.

I would like to thank Karen Hakala and Joe Connolly for all their support. They gave me a lot of love whenever I had a hard time. I will never forget their warm care.

I also would like to thank my friends in South Korea: your support and motivation have been great therapy for times when I almost gave up. Thank you for being my great friends for such a long time.

Finally, I could not have done this and be myself today without the support and care of my parents (Deoksoo Bae and Inok Yun) and brother (Mingyu Bae). Their unconditional love and support have kept me walking through this long journey. I hope you are proud of your daughter and sister. I would like to thank my husband, Dongsik Yang, for his support and patience. When I am frustrated, he is the one I can emotionally

rely on. I would like to send special love to my baby, Teo Yang. Although he delayed my graduation, he was the biggest motivation to continue to push forward. I share this thesis with my family.

ABSTRACT

LIGHT-HARVESTING AND LIGHT-RESPONSIVE MATERIALS FOR OPTOELECTRONIC AND BIOLOGICAL APPLICATIONS

FEBRUARY 2018

YOUNGJU BAE, B.S., KWANGWOON UNIVERSITY

M.S., KWANGWOON UNIVERSITY

Ph.D., UNIVERSITY OF MASSACHUSETTS AMHERST

Directed by: Professor Sankaran Thayumanavan

In photodynamic therapy, several critical standards are required of photosensitizers including high singlet oxygen quantum yield, biocompatibility in dark, and long term photochemical stability. In addition, current PDT systems lack active targeting strategies to tumor cells, and instead mainly rely on the natural distribution of PS in the body following injection and application of near-infrared light treatment in the tumor region. This thesis describes a series of BODIPY-based molecules that were designed, synthesized and studied as photosensitizers with high singlet oxygen generation capacity through utilizing the heavy atom effect. Additionally, aqueous solubility and active targeting capability were introduced by photosensitizer conjugation to hyaluronic acid, a biocompatible natural polymer that binds CD44+ receptors on cancer cells such as HeLa. A small degree of BODIPY substitution on the nontoxic hyaluronic acid polymer backbone allowed overall viability of the PS in dark, but controlled cytotoxicity was observed upon application of near-infrared LED light. Cytotoxicity studies also established the cell selective cytotoxicity of the hyaluronic acid-BODIPY conjugates, verifying their candidacy for photodynamic applications.

In the field of molecular amplification, self-immolative materials have been widely used for various biological applications including drug delivery, biomarker detection, imaging, and sensing. Traditionally, the chemical design of self-immolative polymer or dendrimer backbones include reporters or prodrugs in their monomeric structure. In such systems, the extend of stimuli-induced amplified signal and release of reporters or prodrugs is directly rely on the degree of polymerization or dendrimer generation. Here, we discuss the design, synthesis, and study of an oligomeric self-immolative polymeric system that produces a morphological signal output as a macroscopic response to a molecular-level stimulus through signal amplification. For this aim, we developed a gel that undergoes a gel-sol transition upon application of light to demonstrate this amplification behavior. In this system, stimuli triggers modification in chemical structure of self-immolative polymer that presence in catalytic amount in the gel, which leads to macroscopic morphological transition. Since this macroscopic morphological change driven by catalytic polymer, the extend of amplified signal in this system is not directly dependent on the degree of polymerization. Successful demonstration of such a system will help achieve rapid and reliable signal amplification.

Organic photovoltaics are an attractive alternate technology to traditional inorganic photovoltaics due to their relatively low weight and feasibility of processing into flexible large panels. Polymer-based organic photovoltaics have been investigated for their efficient charge carrier generation, owing to their low band gap through extensive conjugation. Simultaneously, small molecule based organic photovoltaics have also been developed due to their advantages over polymer-based organic photovoltaics, including facile purification with well-defined monodisperse structural properties, as well

as tunable frontier orbital energy alignment. One of the strategies to improve organic photovoltaics performance is developing active materials with a great light-harvesting property for optimal complementarity to the solar energy spectrum. BODIPY molecules are appropriate candidates due to their favorable features as a light-harvesting material, including high extinction coefficients, high photochemical stability, and a relatively easy preparation process. In addition, their frontier energy levels are finely tunable through incorporating with various core structures of different electronegativities. However, their strong absorption profile of simple BODIPY is narrow and limited to visible range (~500 nm). To expand upon the previously reported benefits of BODIPY molecules, we discuss broadening of light absorption profile towards near-infrared through *alpha*-conjugation extension of BODIPY molecules. Utilizing BODIPY that absorbs into the near-infrared region with high absorption coefficients would allow efficient absorbance of the incident light even in thin films, contributing to enhanced organic photovoltaic performances.

`

TABLE OF CONTENTS

Page

LIST OF TABLES

Table Page

LIST OF FIGURES

LIST OF SCHEMES

CHAPTER 1

INTRODUCTION

1.1. Introduction to Chapter 2: Photodynamic Therapy

1.1.1. Photodynamic Therapy

Photodynamic therapy (PDT) is a simple, clean, and non-invasive cancer treatment that utilizes photosensitization, a process by which a specific wavelength of light is absorbed preferentially by photosensitizer (PS) and it then used to affect chemical changes in another species. In PDT, the excited state PS leads to chemical modification of neighboring oxygen species that eventually causes cancer cell death. Specifically, when the PS absorbs a photon to become an excited singlet state (^{1}PS*), it can undergo inter-system crossing (ISC) to transform into an excited triplet state (^{3}PS*). Due to its relatively long lifetime, it is possible for ^{3}PS* to transfer its energy to oxygen ($^3O_2$) to generate reactive singlet oxygen species ($^1O_2$). Typically, this reactive $^1O_2$ either reacts with a substrate or thermally loses its excitation energy, whereas its phosphorescence emission is a relatively inefficient process. Thus, if the generation of $^1O_2$ happens in cells, it reacts rapidly with surrounding biomolecules and is consumed entirely rather than stabilized back to $^3O_2$ state[1,2]. This reactive $^1O_2$ acts as a major cytotoxic agent in PDT process, defined as the Type 2 mechanism. Alternatively, it is also possible for excited PS to transfer electrons or protons to nearby substrates, providing reactive superoxide species, defined as the Type 1 mechanism. As energy transfer to $^3O_2$ occurs as described above, ^{3}PS* is converted back to initial ground state (^{1}PS), which is available to absorb

another photon and regenerate $^1O_2$ cytotoxic agent. Therefore, many $^1O_2$ species (typically $10^3 \sim 10^5$ molecules)[2] can be generated by each PS molecule until it becomes bleached.

1.1.2. Mechanism of Photodynamic Therapy

The amount of $^1O_2$ generated by a PS depends on many factors including molar absorption coefficient of the PS, the efficiency of the energy transfer from $^3PS^*$ to $^3O_2$, and the possibility of ISC. Extensive efforts to improve ISC efficiency have been reported through the installation of heavy atoms within the PS molecular structure[3–6].

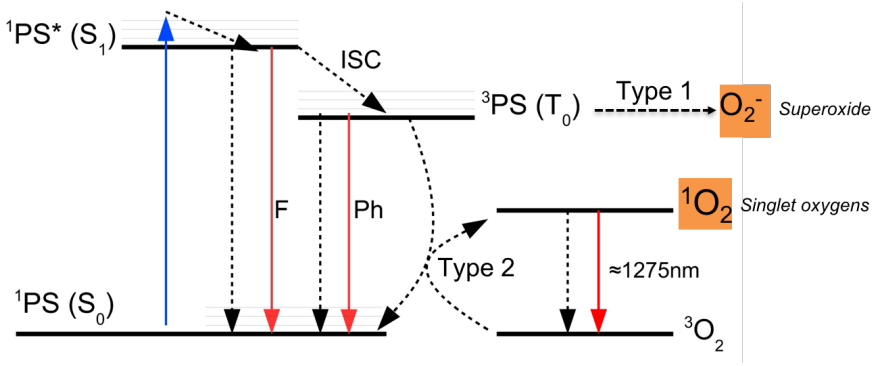

Figure 1.1 Illustration of type 1 and type 2 mechanisms of singlet oxygen generation in a Jablonski diagram.

ISC process is forbidden transition ($^1S^* \rightarrow {}^1T^*$) by the selection rule because it is a transition between pure spin states of different multiplicity. Thus, the forbidden process requires spin-orbit coupling between the singlet state and triplet state, which leads to quantum mechanical mixing between two states of different multiplicity.[7–9] Once the spins involve in an intercombinational transition, they turn to an admixture of states of another multiplicity, rather than separate pure states.[7] The spin-orbit coupling originates from the interaction of spin magnetic moment of electrons and magnetic field, which is

derived from the apparent motion of the nucleus. Since the magnetic field of the nucleus is proportional to the effective nuclear charge of the molecule, it is concluded that spin-orbit coupling increases as an atomic number of molecule increases.[8,10] This phenomenon clearly indicates that enhanced spin-orbit perturbations can be achieved by the attachment of a heavy atom directly onto the molecule of interest. The phenomenon is defined as heavy atom effect and has been widely used to enhance forbidden transition in a molecular level. In 1949, McClure[11] observed a significant decrease in the phosphorescence lifetime of aromatic compounds bearing heavy atoms. Even though he admitted that there is the quantitative limitation, he claimed a correlation between phosphorescence lifetime of the compounds with the spin-orbit coupling parameter, radial part, of the heavy atom. He claimed that the heaviest atom in the excited molecular system would be expected to have the most dominant effect on the lifetime by the assumption that heaviest atom dominates the radial part of the molecule, which consists of several different atoms. In 1959, Ermolaev and Svitashev[12] reported further experimental results on a set of naphthalene derivatives that McClure originally had reported. It was observed that an increase in the weight of the heavy atom substituent leads to (1) increase in relative phosphorescence quantum yield with respect to fluorescence quantum yield, (2) increase in ISC probability, and (3) decrease in triplet state lifetime. This result supports that installation of a heavy atom enhances not only the probability of the ISC process, but also the probability of phosphorescence. However, it is noted that their analysis based on probability could not clearly explain the decrease in triplet lifetime, because the increase in probability was found to be more profound on the phosphorescence rather than the ISC process. In 1976, Cowan[13] analyzed this data by

comparing the rate constant of each process, which successfully explains the decrease in triplet lifetime upon heavy atom attachment. It is clearly stated that the effect of a heavy atom more profound on ISC rate constant than on the rate constants of both radiative and non-radiative triplet state decay. Although the heavy atom effect on triplet lifetime is not always the same, and depends on the strength of the effect on ISC and triplet state decay, it is important to note that a heavy atom does have an influence on all forbidden intercombinational transitions with different extents.

1.1.3. Requirement of Photosensitizers

In PDT, the most beneficial feature originates from the invasive approach, such that an optimized PS is required to possess certain conditions: (1) strong absorption spectrum at the excitation wavelength of interest, (2) long enough excitation wavelength to penetrate biological tissues, (3) excitation wavelength within therapeutic window (650-900 nm) to avoid damage to biomolecules including proteins and vitamins, (4) no cytotoxicity in the dark, which impact drug dosages, and (5) high $^1O_2$ generation upon light absorption.

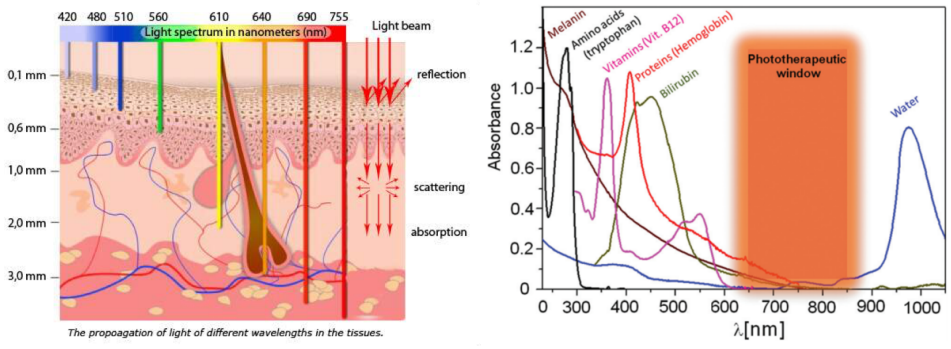

Figure 1.2 Skin penetration depth (left) and phototherapeutic window (right) of the light spectrum.

1.2. Introduction to Chapter 3: Molecular Amplification

1.2.1. Signal Amplification

Signal amplification is a crucial process in biological systems, such that minor chemical or physical changes result in a response in an efficient and rapid manner. For example, cells are exposed to enormous variety of external signals including hormones, neurotransmitters, odors, and light, and reliable rapid and complete responses to weak inputs and require signal amplification to enable normal function of cellular signaling. These naturally evolved signal amplification processes involve cascade mechanisms, which effectively preserve the form of the input signal. Specific protein cascade mechanisms exhibit well-defined signal amplification depending on their regulatory design.[14–16] The cell uses cascade pathways as complex biochemical networks for intracellular signaling.[17,18] It allows cells to integrate multiple inputs to shape a specifically defined output, regulating multiple biological functions.[19] In other words, the interaction of different pathways and the modulation of the components in the cascade enable dynamic biological outputs. These highly controlled signal amplification process and their uniquely defined outputs allow the cell to adapt and respond to a constantly changing environment.

Since at least the 1960's, biochemical cascade mechanisms have been understood as signal amplifying processes.[20] Specifically, it was reported that complex cascade reactions of enzyme and pro-enzyme are involved in physiological phenomena such as visual activation and blood clotting.[21] Successive chain reactions between the pro-enzyme and enzyme activates signal amplification of a stimulus, causing physiological responses. The kinetics of enzyme activity as an amplifier is further discussed.[20] For

linear cascades it has also been shown that its overall sensitivity is the product of the sensitivities at each level within the cascade, and understandably the system in its entirety is highly specific.[22] This explains why signal transduction pathways in cells involve a multitude of interconnecting linear and cyclic cascades acting on each other. These nature-inspired signal amplification cascades have inspired artificial amplification processes in various scientific applications including sensing, bio-imaging, and therapeutic technologies.[23–25] Furthermore, because signal amplification is a simple and efficient strategy for improving sensitivity, development of signal amplification systems has significantly improved the detection limit for medical diagnosis of various conditions and diseases. Specifically, signal amplification has enabled early detection of disease biomarkers that exist in low concentrations in the body.[23] Early-stage detection of disease provides patients with the precious chance of immediate treatment, maintenance, and even improved chances of survival.

For these reasons, fundamental development of molecular signal amplification is considered as one of the most important challenges in the fields of diagnostics, imaging, and drug delivery. A common desired feature in these application fields is the release of a imaging or therapeutic agent in response to a specific demand or stimulus.

1.2.2. Self-immolative Systems

Self-immolative systems have been widely utilized as chemical tools for molecular amplifications. Early developments of self-immolative materials were in drug delivery applications, which were achieved by degradation of dendrimers or polymers in response to a specific physiological trigger, such that break down of a molecular scaffold results in release of encapsulated drugs. It has been reported that amphiphilic self-

immolative block copolymers can self-assemble into the form of a molecular cage, encapsulating guest molecules in their interior.[26–28] The molecular vehicle is designed to release their encapsulated molecules upon triggered degradation of self-immolative polymer block, due to loss of the hydrophilic-hydrophobic balance of the assembly and resultant loss of aggregation characteristics.[28] Without the self-immolative property on their backbone, block copolymer-based polymersomes would have the severe drawback of poor permeability to small substances and membranes.[29–31] Since assembly of copolymer is formed when they are in hydrophobic-hydrophilic balance in aqueous solution, switching solubility of the vehicles is required to break the balance to release interior molecules. In this system, cooperative changes of most of the repeating units of the polymer is necessary to achieve a significant change in solubility, whereas a system with self-immolative can offer facile approach to release interior guests by complete degradation of self-immolative polymer backbone.

Another strategy of signal amplification involves the use of output-functionalities on the periphery groups of the dendrimer structure. Dendrimer-based self-immolative systems have been extensively investigated because of their well-defined molecular structure and they can possess multiple reporter units on their periphery positions for an individual dendron. The released reporter molecules upon stimuli-induced degradation of the dendrimer can function as a readout signal.[32–34] This feature has been used in various biosensor applications and the molecular design of the periphery and its responsivity has been modified depending on the desired output. For example, a prodrug installed on the dendrimer periphery can be released in the form of its active drug upon self-immolative degradation of supramolecular structure.[26,35–38] Challenges with dendrimer-based designs

include that complete degradation of the structure is crucial for efficient release of reporter molecules substituted on the periphery positions. Further, both the extent of amplified signal and number of drugs that the dendrimer can carry depend on the generation of dendrimer molecules, which could demand multi-step synthesis. Lastly, their natural steric hindrance often limits the number of functionalized periphery groups that a dendrimer can possess.

Linear polymers have also been designed with self-immolative backbones to study their signal amplification properties. Typically, reporter molecules are introduced on monomer units, so that outputs are regenerated upon degradation of the polymer backbone. Because degradation can occur all the way through the backbone and monomer branches, reporters on the end of monomers are released once degradation is complete. This system also requires complete degradation of both the polymer backbone and monomers to initiate the release of reporter molecules. In addition, similar to dendritic systems, the number of released molecules and resultant signal amplification capacity are linearly dependent on degree of polymerization at molecular scale.

1.3. Introduction to Chapter 4: Organic Photovoltaics

1.3.1. Organic Photovoltaics

The field of photovoltaic devices develops promising technologies that can generate sustainable and renewable clean energy by conversion of sunlight into electrical energy.[39] Since the birth of the first silicon-based solar cell in 1954, the silicon-based photovoltaics have been developed steadily due to their highly ordered atomic network and built-in electric field, allowing for facile charge separation and transport through

valence and conduction bands.[40] Inorganic solar cells have since reached very high efficiencies, often exceeding 40%, when their light-harvesting and power output is maximized by combining multiple inorganic layers, which are multijunction inorganic cells.[41] Although the improvement of these device efficiencies is a great achievement, their critical drawbacks is that they require inorganic materials, which generate environmentally harmful byproducts. In addition, inorganic materials are cost inefficient to process in bulk due to difficult and expensive purification.

1.3.2. Principle of BHJ Organic Photovoltaic Devices

An alternative to inorganic photovoltaics, organic photovoltaic devices use semi-conductive small molecules or polymers as an active layer in between two electrodes. The active layer is composed of two organic molecules: an electron rich p-type donor and electron deficient n-type acceptor. Organic devices undergo four processes to successfully generate electricity from sunlight. 1) Photoexcitation: once the active layer absorbs sunlight as a form of a photon, organic molecules in the active layer get excited, moving an electron from their highest occupied molecular orbital (HOMO) to their lowest unoccupied molecular orbital (LUMO) energy levels, generating an excited state. This excitation process typically occurs in the donor material preferably due to their small band gap. As a result, the donor HOMO loses an electron, leaving a hole, and the LUMO gains an electron, which is called exciton, electron-hole pair. Since solar energy has the greatest intensity in visible to NIR range (400 ~ 1,000 nm)[42], the development of low band gap organic molecules is fundamental to maximize the absorption of solar energy, which contributes to overall device efficiency. 2) Charge transfer: the electron in the LUMO of the donor will be transferred into the n-type acceptor material if an

energetically favorable condition is given, which has been defined as an energy gap between the donor and acceptor LUMO greater than 0.3 eV. If the energy gap is smaller than 0.3 eV, the charge transfer is not favorable and allows for the opposite direction of charge flow, sacrificing device efficiency. 3) Charge transport: the separated electron and hole generated by charge transfer is now transported through donor and acceptor material phases, respectively, towards their corresponding electrodes. The structure of organic materials in the active layer and the engineering of their morphology both have great influence on the efficiency of the charge transport process. Extensive investigation on the development of the bulk heterojunction (BHJ) morphology has been pursued to enhance this charge transport process, which is susceptible to various relaxation pathways that sacrifice device efficiency. The thermal deposition of mixed donor and acceptor solution to form the BHJ active layer involves the formation of randomly controlled nano-scale morphologies. It is possible to have discontinuous BHJ with the donor or acceptor phase deposition towards the respective electrodes, interfering with successful transport of the hole or electron to their electrodes. Failure to achieve well-controlled nano-scale morphology sacrifices the device efficiency. Engineering of the active layer morphology, including annealing techniques and use of solvent additives, has been widely investigated to obtain a well-organized desirable morphology with high crystallinity of each phase, enhancing charge transport efficiency. 4) Charge collection: the charges that reach their respective electrodes are collected as the electrical current, i.e. electricity. Since charge collection is influenced by the work function of the metals used as electrodes, improvement in charge collection can be achieved through adjustment of the electrode composition. Furthermore, since the efficiency of the charge collection also depends on

device architecture, a variety of device system has been explored.[43–46] The most common layout is a direct cell, which is organized with a hole transporting layer introduced between the cathode and active layer, inhibiting unwanted electrons from coming to the interface, while smoothing the collection of the hole.

1.3.3. Conjugate Polymers in Organic Photovoltaic Devices

Since the first photovoltaic effect with an organic material was reported in 1959[47], significant researches been reported with an aim of understanding the relation of device efficiency and morphology of active layer.[48] In 1994, an organic photovoltaic device was reported that composed of a blend of a conjugated polymer and electron deficient fullerene molecule as the active layer.[49] The concept of BHJ allowed for significant improvement due to their maximized contact area between n-type and p-type materials within the active layer. These findings attracted attention to the combination of conjugated polymers and fullerene as organic photovoltaics, generating extensive researches in the field.

The use of conjugated organic molecules improves light-harvesting capability due to the their delocalized π-electrons which provide a relatively low bandgap, making their absorbance fall into vis-NIR range of spectrum where most solar energy exists. One of the most commonly used molecular designs incorporated electron rich (donor) and electron deficient (acceptor) moieties alternatively through the conjugate backbone, to impart an electron push-pull and achieve a low bandgap. This system has been widely investigated as a donor material to extend orbital mixing with a variation in strength of both electron donating and electron withdrawing of the moiety. Poly(3-hexylthiophene) (P3HT) is one of the most commonly studied conjugated organic polymers in BHJ

systems, with fullerene derivative [6,6]-phenyl-C_{61}-butyric acid methyl ester (PCBM) used as an acceptor molecule.[50,51] The P3HT:PCBM blending system has been extensively studied to evaluate the impact of molecular weight, poly dispersity index, regioregularity of 3-hexylthiophene unit, choice of deposition solvent, among several other factors on the morphology and charge transfer of the active layer, and resultant device efficiency. With comprehensive understanding, the P3HT:PCBM active layer has become a standard system to which novel conjugated polymeric systems often compared.

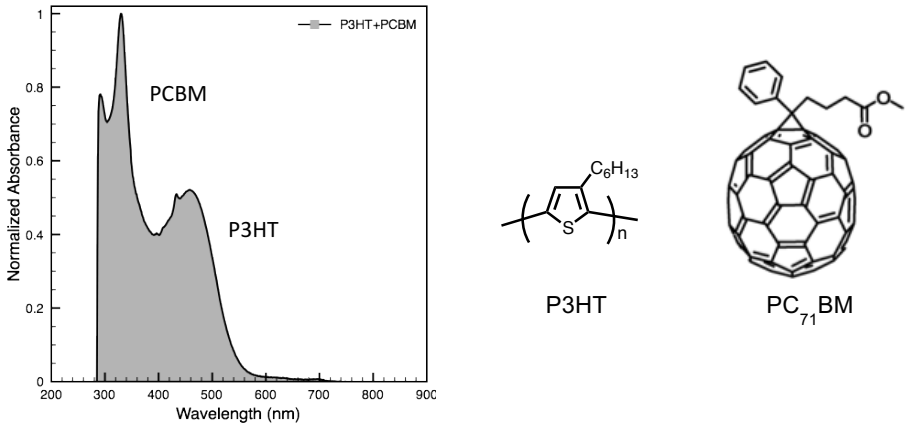

Figure 1.3 UV/vis absorption profile of P3HT:PCBM blends in chloroform (left) and their chemical structures (right).

1.3.4. Device Efficiency

Photovoltaic devices are evaluated by their efficiency under dark and illuminated conditions, providing a current density-voltage (*J-V*) curve. When a voltage is applied to the device, it shows diode-like behavior, where its current get saturated under a reverse bias and grows exponentially under a forward bias. The power conversion efficiency (*PCE*) is defined by the equation below:

$$PCE = \frac{P_{out}}{P_{in}} = \frac{J_{SC} \times V_{OC} \times FF}{P_{in}}$$

PCE is the ratio of power output over power input of irradiated light. The power output is the product of the short circuit current density (J_{SC}), open circuit voltage (V_{OC}) and fill factor (FF). J_{SC} defines the maximum current across the cell when voltage is not applied, while V_{OC} is the maximum potential across the cell when there is no current flowing. *FF*, the ratio of theoretical power output to the maximum power output (*MPP*), is defined as the equation below:

$$FF = \frac{J_{MPP} \times V_{MPP}}{J_{SC} \times V_{OC}}$$

1.4. Dissertation Outline

In this dissertation, we discuss about three different applications of light-related fields of study, including photodynamic therapy, signal amplification and organic photovoltaics. In chapter 2, a series of BODIPY-functionalized hyaluronic acid are evaluated as a photosensitizer in photodynamic therapy. Molecular structure is strategically designed with variations of conjugation extension and/or existence of heavy atom. Their capacity of reactive oxygen generation is evaluated. Furthermore, NIR absorbing photosensitizers are selected for further cytotoxicity studies as well as their selective targeting ability to CD44 receptor on HeLa tumor cells over HepG2 normal cells. In chapter 3, carbamate-based self-immolative polymer with carboxylate functionality is investigated as a platform to demonstrate signal amplification in a way of morphological change from solution to gel. Finally, in chapter 4, we discuss optoelectronic properties of alpha-extended BODIPY-based small molecules with a variation of molecular structure of cores. As an aim of improving light-harvesting

property, they are compared to their molecular analogues without alpha-extension on BODIPY units.

1.5. Reference

(1) Gorman, A.; Killoran, J.; O'Shea, C.; Kenna, T.; Gallagher, W. M.; O'Shea, D. F. In Vitro Demonstration of the Heavy-Atom Effect for Photodynamic Therapy. *J. Am. Chem. Soc.* **2004**, *126* (34), 10619–10631.

(2) Kochevar, I. E.; Redmond, R. W. Photosensitized Production of Single Oxygen. *Methods Enzymol.* **2000**, *319*, 20–28.

(3) Chen, X.; Li, Y.; Wang, A.; Zhou, L.; Lu, S.; Zhou, J.; Lin, Y.; Wei, S. Protonation Salt Derivative with Heavy-Atom Effect on Phthalocyanine for Enhanced in Vitro Photodynamic Therapy. *Dye. Pigment.* **2015**, *114* (C), 93–104.

(4) Yogo, T.; Urano, Y.; Ishitsuka, Y.; Maniwa, F.; Nagano, T. Highly Efficient and Photostable Photosensitizer Based on BODIPY Chromophore. *J. Am. Chem. Soc.* **2005**, *127* (35), 12162–12163.

(5) Rodriguez-Serrano, A.; Rai-Constapel, V.; Daza, M. C.; Doerr, M.; Marian, C. M. Internal Heavy Atom Effects in Phenothiazinium Dyes: Enhancement of Intersystem Crossing via Vibronic Spin-Orbit Coupling. *Phys. Chem. Chem. Phys.* **2015**, *17* (17), 11350–11358.

(6) Cui, G.; Fang, W. H. State-Specific Heavy-Atom Effect on Intersystem Crossing Processes in 2-Thiothymine: A Potential Photodynamic Therapy Photosensitizer. *J. Chem. Phys.* **2013**, *138* (4).

(7) Turro, N. J. The Triplet State. *J. Chem. Educ.* **1966**, *46* (1), 2–6.

(8) McClure, D. S. Spin-Orbit Interaction in Aromatic Molecules. *J. Chem. Phys.*

1952, *20* (4), 682.

(9) Lower, S.; El-Sayed, M. The Triplet State and Molecular Electronic Processes in Organic Molecules. *Chem. Rev.* **1966**, *66* (2), 199–241.

(10) Levine, I. N. Quantum Chemistry; Allyn and Bacon: Boston, 1970; pp 306–310.

(11) McClure, D. S. Triplet-Singlet Transitions in Organic Molecules. Lifetime Measurements of the Triplet State. *J. Chem. Phys.* **1949**, *17* (10), 905.

(12) Ermolaev, V. L.; Svitasbev, K. K. Quantum Yields of Phosphorescence and Fluorescence of Some 1-Derivatives of Naphthalene in Solutions at -196˚C.pdf. *Opt. Spectrosc.* **1959**, *1*, 399.

(13) Cowan, D. O. Elements of Organic Photochemistry. In *Elements of Organic Photochemistry*; Plenum Press: New York, N.Y., 1976; pp 250–262.

(14) Chock, P. B.; Stadtman, E. R. Superiority of Interconvertible Enzyme Cascades in Metabolite Regulation: Analysis of Multicyclic Systems. *Proc Natl Acad Sci U S A* **1977**, *74* (7), 2766–2770.

(15) Koshland, D. E.; Goldbeter, A.; Stock, J. B. Amplification and Adaptation in Regulatory and Sensory Systems Author (S): Daniel E . Koshland , Albert Goldbeter and Jeffry B . Stock Published by : American Association for the Advancement of Science Stable URL : http://www.jstor.org/stable/1689499 JS. **2017**, *217* (4556), 220–225.

(16) Chock, P. B.; Rhee, S. G.; Stadtman, E. R. Interconvertible Enzyme Cascades in Cellular-Regulation. *Annu. Rev. Biochem.* **1980**, *49*, 813–843.

(17) Bhalla and Ravi Iyengar, U. S. Emergent Properties of Networks of Biological Signaling Pathways. *Science (80-.).* **1999**, *283* (5400), 381–387.

(18) Weng, G. Complexity in Biological Signaling Systems. *Science (80-.).* **1999**, *284* (5411), 92–96.

(19) Jordan, J. D.; Landau, E. M.; Iyengar, R. Signaling Networks: The Origins of Cellular Multitasking. *Cell* **2000**, *103* (2), 193–200.

(20) Levine, S. N. Enzyme Amplifier Kinetics. *Science (80-.).* **1966**, *152* (3722), 651–653.

(21) Wald, G. Visual Excitation and Blood Clotting. *Science* **1965**, *150* (3699), 1028–1030.

(22) Brown, G. C.; Hoek, J. B.; Kholodenko, B. N. Why Do Protein Kinase Cascades Have More than One Level? *Trends Biochem. Sci.* **1997**, *22*, 288.

(23) Fozooni, T.; Ravan, H.; Sasan, H. Signal Amplification Technologies for the Detection of Nucleic Acids: From Cell-Free Analysis to Live-Cell Imaging. *Appl. Biochem. Biotechnol.* **2017**, 1–30.

(24) Wu, W.; Bazan, G. C.; Liu, B. Conjugated-Polymer-Amplified Sensing, Imaging, and Therapy. *Chem* **2017**, *2* (6), 760–790.

(25) Mittal, S.; Kaur, H.; Gautam, N.; Mantha, A. K. Biosensors for Breast Cancer Diagnosis: A Review of Bioreceptors, Biotransducers and Signal Amplification Strategies. *Biosens. Bioelectron.* **2017**, *88*, 217–231.

(26) Dewit, M. A.; Nazemi, A.; Karamdoust, S.; Beaton, A.; Gillies, E. R. Design, Synthesis and Assembly of Self-Immolative Linear Block Copolymers. *Non-Coventional Funct. Block Copolym.* **2011**, 9–21.

(27) Li, Y.; Liu, G.; Wang, X.; Hu, J.; Liu, S. Enzyme-Responsive Polymeric Vesicles for Bacterial-Strain-Selective Delivery of Antimicrobial Agents. *Angew. Chemie* -

Int. Ed. **2016**, *55* (5), 1760–1764.

(28) Liu, G.; Wang, X.; Hu, J.; Zhang, G.; Liu, S. Self-Immolative Polymersomes for High-Efficiency Triggered Release and Programmed Enzymatic Reactions. *J. Am. Chem. Soc.* **2014**, *136* (20), 7492–7497.

(29) Sauer, M.; Haefele, T.; Graff, a; Nardin, C.; Meier, W. Ion-Carrier Controlled Precipitation of Calcium Phosphate in Giant ABA Triblock Copolymer Vesicles. *Chem. Commun. (Camb).* **2001**, No. 23, 2452–2453.

(30) Sceince, P. Polymer Vesicles. *Science (80-.).* **2005**, *297* (17), 967–974.

(31) Wu, J.; Eisenberg, A. Proton Diffusion across Membranes of Vesicles of Poly(styrene-B-Acrylic Acid) Diblock Copolymers. *J. Am. Chem. Soc.* **2006**, *128* (9), 2880–2884.

(32) Gabrielli, L.; Mancin, F. Minimal Self-Immolative Probe for Multimodal Fluoride Detection. *J. Org. Chem.* **2016**, *81* (22), 10715–10720.

(33) Amir, R. J.; Pessah, N.; Shamis, M.; Shabat, D. Self-Immolative Dendrimers. *Angew. Chemie - Int. Ed.* **2003**, *42* (37), 4494–4499.

(34) Shamis, M.; Shabat, D. Single-Triggered AB6 Self-Immolative Dendritic Amplifiers. *Chemistry* **2007**, *13* (16), 4523–4528.

(35) Tan, X.; Li, B. B.; Lu, X.; Jia, F.; Santori, C.; Menon, P.; Li, H.; Zhang, B.; Zhao, J. J.; Zhang, K. Light-Triggered, Self-Immolative Nucleic Acid-Drug Nanostructures. *J. Am. Chem. Soc.* **2015**, *137* (19), 6112–6115.

(36) Niculescu-Duvaz, I.; Niculescu-Duvaz, D.; Friedlos, F.; Spooner, R.; Martin, J.; Marais, R.; Springer, C. J. Self-Immolative Nitrogen Mustard Prodrugs for Suicide Gene Therapy. *J. Med. Chem.* **1998**, *41* (13), 5297–5309.

(37) De Groot, F. M. H.; Albrecht, C.; Koekkoek, R.; Beusker, P. H.; Scheeren, H. W. "Cascade-Release Dendrimers" liberate All End Groups upon a Single Triggering Event in the Dendritic Core. *Angew. Chemie - Int. Ed.* **2003**, *42* (37), 4490–4494.

(38) Shamis, M.; Lode, H. N.; Shabat, D. Bioactivation of Self-Immolative Dendritic Prodrugs by Catalytic Antibody 38C2. *J. Am. Chem. Soc.* **2004**, *126* (6), 1726–1731.

(39) Dresselhaus, M.S.; Thomas, I. . Alternative Energy Technologies. *Nature* **2001**, *414* (November), 332–337.

(40) Gregg, B. A.; Hanna, M. C. Comparing Organic to Inorganic Photovoltaic Cells: Theory, Experiment, and Simulation. *J. Appl. Phys.* **2003**, *93* (6), 3605–3614.

(41) https://energy.gov/eere/solar/downloads/research-cell-efficiency-records.

(42) Potscavage, W. J.; Sharma, a; Kippelen, B. Critical Interfaces in Organic Solar Cells and Their Influence on the Open-Circuit Voltage. *Acc. Chem. Res.* **2009**, *42* (11), 1758–1767.

(43) Carsten, B.; Szarko, J. M.; Son, H. J.; Wang, W.; Lu, L.; He, F.; Rolczynski, B. S.; Lou, S. J.; Chen, L. X.; Yu, L. Examining the Effect of the Dipole Moment on Charge Separation in Donor-Acceptor Polymers for Organic Photovoltaic Applications. *J. Am. Chem. Soc.* **2011**, *133* (50), 20468–20475.

(44) Yao, K.; Intemann, J. J.; Yip, H.-L.; Liang, P.-W.; Chang, C.-Y.; Zang, Y.; Li, Z.; Chen, Y.; Jen, A. K.-Y. Efficient All Polymer Solar Cells from Layer-Evolved Processing of a Bilayer Inverted Structure. *J. Mater. Chem. C* **2014**, *2* (3), 416.

(45) Takacs, C. J.; Sun, Y.; Welch, G. C.; Perez, L. A.; Liu, X.; Wen, W.; Bazan, G. C.; Heeger, A. J. Solar Cell Efficiency, Self-Assembly, and Dipole-Dipole Interactions

of Isomorphic Narrow-Band-Gap Molecules. *J. Am. Chem. Soc.* **2012**, *134* (40), 16597–16606.

(46) Beaujuge, P. M.; Fréchet, J. M. J. Molecular Design and Ordering Effects in π-Functional Materials for Transistor and Solar Cell Applications. *J. Am. Chem. Soc.* **2011**, *133* (50), 20009–20029.

(47) Kallmann, H.; Pope, M. Photovoltaic Effect in Organic Crystals. *J. Chem. Phys.* **1959**, *30* (2), 585–586.

(48) Benanti, T. L.; Venkataraman, D. Organic Solar Cells: An Overview Focusing on Active Layer Morphology. *Photosynth. Res.* **2006**, *87* (1), 73–81.

(49) Yu, G.; Pakbaz, K.; Heeger, A. J. Semiconducting Polymer Diodes: Large Size, Low Cost Photodetectors with Excellent Visible-Ultraviolet Sensitivity. *Appl. Phys. Lett.* **1994**, *64* (25), 3422–3424.

(50) Dang, M. T.; Hirsch, L.; Wantz, G. P3HT:PCBM, Best Seller in Polymer Photovoltaic Research. *Adv. Mater.* **2011**, *23* (31), 3597–3602.

(51) Wu, P. T.; Xin, H.; Kim, F. S.; Ren, G.; Jenekhe, S. A. Regioregular poly(3-Pentylthiophene): Synthesis, Self-Assembly of Nanowires, High-Mobility Field-Effect Transistors, and Efficient Photovoltaic Cells. *Macromolecules* **2009**, *42* (22), 8817–8826.

(52) Gabe, Y.; Ueno, T.; Urano, Y.; Kojima, H.; Nagano, T. Tunable Design Strategy for Fluorescence Probes Based on 4-Substituted BODIPY Chromophore: Improvement of Highly Sensitive Fluorescence Probe for Nitric Oxide. *Anal. Bioanal. Chem.* **2006**, *386* (3), 621–626.

(53) Li, Y.; Wang, J.; Zhang, X.; Guo, W.; Li, F.; Yu, M.; Kong, X.; Wu, W.; Hong, Z.

Highly Water-Soluble and Tumor-Targeted Photosensitizers for Photodynamic Therapy. *Org. Biomol. Chem.* **2015**, *13* (28), 7681–7694.

(54) Gee, K. R.; Archer, E. A.; Kang, H. C. 4-Sulfotetrafluorophenyl (STP) Esters: New Water-Soluble Amine-Reactive Reagents for Labeling Biomolecules. *Tetrahedron Lett.* **1999**, *40* (8), 1471–1474.

(55) Hendel, S. J.; Poe, A. M.; Khomein, P.; Bae, Y.; Thayumanavan, S.; Young, E. R. Photophysical and Electrochemical Characterization of BODIPY-Containing Dyads Comparing the Influence of an A–D–A versus D–A Motif on Excited-State Photophysics. *J. Phys. Chem. A* **2016**, *120*, 8794–8803.

(56) Gollnick, K.; Griesbeck, A. Singlet Oxygen Photooxygenation of Furans. *Tetrahedron* **1985**, *41* (11), 2057–2068.

(57) Morone, M.; Beverina, L.; Abbotto, A.; Silvestri, F.; Collini, E.; Ferrante, C.; Bozio, R.; Pagani, G. A. Enhancement of Two-Photon Absorption Cross-Section and Singlet-Oxygen Generation in Porphyrins upon ??-Functionalization with Donor-Acceptor Substituents. *Org. Lett.* **2006**, *8* (13), 2719–2722.

(58) Deng, P.; Zhang, Q. Recent Developments on Isoindigo-Based Conjugated Polymers. *Polym. Chem.* **2014**, *5* (10), 3298–3305.

(59) Lin, Y.; Li, Y.; Zhan, X. Small Molecule Semiconductors for High-Efficiency Organic Photovoltaics. *Chem. Soc. Rev.* **2012**, *41* (11), 4245.

(60) Zhang, Z.; Wang, J. Structures and Properties of Conjugated Donor–Acceptor Copolymers for Solar Cell Applications. *J. Mater. Chem.* **2012**, *22* (10), 4178.

(61) Zhou, H.; Yang, L.; You, W. Rational Design of High Performance Conjugated Polymers for Organic Solar Cells. *Macromolecules* **2012**, *45* (2), 607–632.

(62) Hou, J.; Huo, L.; He, C.; Yang, C.; Li, Y. Synthesis and Absorption Spectra of poly(3-(Phenylenevinyl)thiophene)s with Conjugated Side Chains. *Macromolecules* **2006**, *39* (2), 594–603.

(63) Hou, J.; Tan, Z.; Yan, Y.; He, Y.; Yang, C.; Li, Y. Synthesis and Photovoltaic Properties of Two-Dimensional Conjugated Polythiophenes with Bi(thienylenevinylene) Side Chains. *J. Am. Chem. Soc.* **2006**, *128* (14), 4911–4916.

(64) He, G.; Li, Z.; Wan, X.; Liu, Y.; Zhou, J.; Long, G.; Zhang, M.; Chen, Y. Impact of Dye End Groups on Acceptor–donor–acceptor Type Molecules for Solution-Processed Photovoltaic Cells. *J. Mater. Chem.* **2012**, *22* (18), 9173.

(65) Liu, J.; Walker, B.; Tamayo, A.; Zhang, Y.; Nguyen, T. Q. Effects of Heteroatom Substitutions on the Crystal Structure, Film Formation, and Optoelectronic Properties of Diketopyrrolopyrrole-Based Materials. *Adv. Funct. Mater.* **2013**, *23* (1), 47–56.

(66) Yuan, J.; Huang, X.; Zhang, F.; Lu, J.; Zhai, Z.; Di, C.; Jiang, Z.; Ma, W. Design of Benzodithiophene-Diketopyrrolopyrrole Based Donor–acceptor Copolymers for Efficient Organic Field Effect Transistors and Polymer Solar Cells. *J. Mater. Chem.* **2012**, *22* (42), 22734.

(67) Sonar, P.; Ng, G.-M.; Lin, T. T.; Dodabalapur, A.; Chen, Z.-K. Solution Processable Low Bandgap Diketopyrrolopyrrole (DPP) Based Derivatives: Novel Acceptors for Organic Solar Cells. *J. Mater. Chem.* **2010**, *20* (18), 3626.

(68) Della Pelle, A. M.; Homnick, P. J.; Bae, Y.; Lahti, P. M.; Thayumanavan, S. Effect of Substituents on Optical Properties and Charge-Carrier Polarity of Squaraine

Dyes. *J. Phys. Chem. C* **2014**, *118* (4), 1793–1799.

(69) Huang, X.; Zhu, C.; Zhang, S.; Li, W.; Guo, Y.; Zhan, X.; Liu, Y.; Bo, Z. Porphyrin-Dithienothiophene π-Conjugated Copolymers: Synthesis and Their Applications in Field-Effect Transistors and Solar Cells. *Macromolecules* **2008**, *41* (19), 6895–6902.

(70) Benniston, A. C.; Copley, G. Lighting the Way Ahead with Boron Dipyrromethene (Bodipy) Dyes. *Phys. Chem. Chem. Phys.* **2009**, *11* (21), 4124.

(71) Oosterhout, S. D.; Savikhin, V.; Zhang, J.; Zhang, Y.; Burgers, M. A.; Marder, S. R.; Bazan, G. C.; Toney, M. F. Mixing Behavior in Small Molecule:Fullerene Organic Photovoltaics. *Chem. Mater.* **2017**, *29* (7), 3062–3069.

(72) Carlé, J. E. Polymers for Organic Photovoltaics Based on 1,5-bis(2-Hexyldecyloxy)-Naphthalene, Thiophene, and Benzothiadiazole. *J. Photonics Energy* **2011**, *1* (1), 11111.

(73) Guo, X.; Watson, M. D. Conjugated Polymers from Napthalene Bisimide. *Org. Lett.* **2008**, *10* (23), 5333–5336.

(74) Eggert Carlé, J.; Wenzel Andreasen, J.; Jørgensen, M.; Christian Krebs, F. Low Band Gap Polymers Based on 1,4-Dialkoxybenzene, Thiophene, Bithiophene Donors and the Benzothiadiazole Acceptor. *Sol. Energy Mater. Sol. Cells* **2010**, *94* (5), 774–780.

(75) Poe, A. M.; Della Pelle, A. M.; Subrahmanyam, A. V.; White, W.; Wantz, G.; Thayumanavan, S. Small Molecule BODIPY Dyes as Non-Fullerene Acceptors in Bulk Heterojunction Organic Photovoltaics. *Chem. Commun.* **2014**, *50* (22), 2913–2915.

(76) Matsumura, S.; Hlil, A. R.; Lepiller, C.; Gaudet, J.; Guay, D.; Shi, Z.; Holdcroft, S.; Hay, A. S. Ionomers for Proton Exchange Membrane Fuel Cells with Sulfonic Acid Groups on the End-Groups: Novel Branched Poly(ether-Ketone)s. *Am. Chem. Soc. Polym. Prepr. Div. Polym. Chem.* **2008**, *49* (1), 511–512.

(77) Wakim, S.; Beaupré, S.; Blouin, N.; Aich, B.-R.; Rodman, S.; Gaudiana, R.; Tao, Y.; Leclerc, M. Highly Efficient Organic Solar Cells Based on a poly(2,7-Carbazole) Derivative. *J. Mater. Chem.* **2009**, *19* (30), 5351.

(78) Goud, T. V.; Tutar, A.; Biellmann, J. F. Synthesis of 8-Heteroatom-Substituted 4,4-Difluoro-4-Bora-3a,4a-Diaza-S-Indacene Dyes (BODIPY). *Tetrahedron* **2006**, *62* (21), 5084–5091.

(79) Rakstys, K.; Paek, S.; Gao, P.; Gratia, P.; Marszalek, T.; Grancini, G.; Cho, K. T.; Genevicius, K.; Jankauskas, V.; Pisula, W.; et al. Molecular Engineering of Face-on Oriented Dopant-Free Hole Transporting Material for Perovskite Solar Cells with 19% PCE. *J. Mater. Chem. A* **2017**, *5* (17), 7811–7815.

CHAPTER 2

HEAVY ATOM EFFECT IN BODIPY-FUNCTIONALIZED HYALURONIC ACIDS AS BIOCOMPATIBLE PHOTOSENSITIZERS IN PHOTODYNAMIC THERAPY

2.1. Introduction

In PDT, ideal PS are required to possess great biocompatibility, photostability, high extinction molar coefficient and high $^1O_2$ quantum yield. Recently, diverse organic PS molecules, inorganic nanoparticle-based PS have been reported for PDT applications. Specifically, absorption spectrum profiles with NIR region is one of critical requirements for clinical applications. One of the way to achieve high $^1O_2$ quantum yield is introducing heavy atom onto PS. However, toxicity of halogenation could remain a major concern for the application of organic material in biological system. Other current issues in PDT mainly derive from the solubility of the PS as well as the absence of active targeting. Since neither the PS nor the $^1O_2$ has an innate selectivity towards tumor cells over normal cells, traditional PDT relies on the natural distribution of the PS over a specific and optimized time, then selective irradiation of the tumor areas in an effort to avoid damaging healthy cells. One strategy for improving selectivity is the incorporation of an active targeting moiety on the PS molecules. Further, the solubility of the PS can be one of the biggest limitations in PDT, which can adversely affect their optical properties. Various methods have been pursued to overcome PS solubility problems[52–54]. One common method involves the introduction of hydrophilic functional groups, such as carboxylic or sulfonic groups, however, this strategy can cause additional toxicity issues

in the dark. Hyaluronic acid (HA) is a biocompatible natural polymer, consisting of polysaccharide-based repetitive disaccharide. It has been a prominent interest for active targeting towards an overexpressed CD44 receptor on the surface of cancer cell membranes (Figure 2.1). CD44 receptors have been implicated in tumor progression, metastasis, drug resistance and disease prognosis and they have high binding affinity to HA through hydrogen bonding. It is theoretically reported that at least 4-6 repeat units are required to bind.

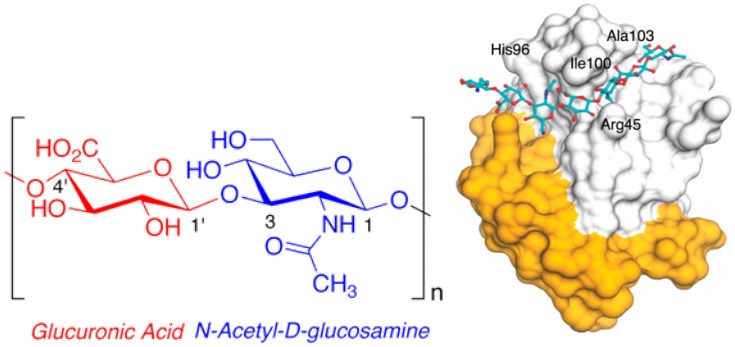

Figure 2.1 Chemical structure of hyaluronic acid (left) and illustration of binding between hyaluronic acid and amino acids of CD44 (right).

2.2. Molecular Design

We designed a series of BODIPY-based PS molecules that are incorporated onto the hydrophilic, biocompatible, and natural polymer hyaluronic acid (HA). HA is a polysaccharide-based repetitive disaccharide and has been a prominent interest for active targeting towards CD44, an overexpressed receptor on the surface of cancer cell membranes. CD44 receptors have been implicated in tumor progression, metastasis, drug resistance and disease prognosis. BODIPY molecules with variation in their structure were chosen as the core PS structure for several reasons. BODIPY derivatives have large extinction coefficients, typically $10^4 \sim 10^5$, which can help maximize the light absorbance

and the extend of excitation. They also possess relatively robust stability towards $^1O_2$. The thermodynamic and kinetic stability of BODIPY molecules would provide a decent shelf-life as a PS. Two categories of molecular variations on BODIPY were designed in an effort to understand and develop novel PS structures for PDT applications. First, the conjugation extension of the BODIPY core was lengthened to increase the onset wavelength of absorption with the aim of deeper tissue penetration. Second, substituent variants were designed to employ the heavy atom effect[3,5,6] and enhance the possibility of ISC process, which could contribute to energy transfer to $^3O_2$, leading to improved $^1O_2$ generation.

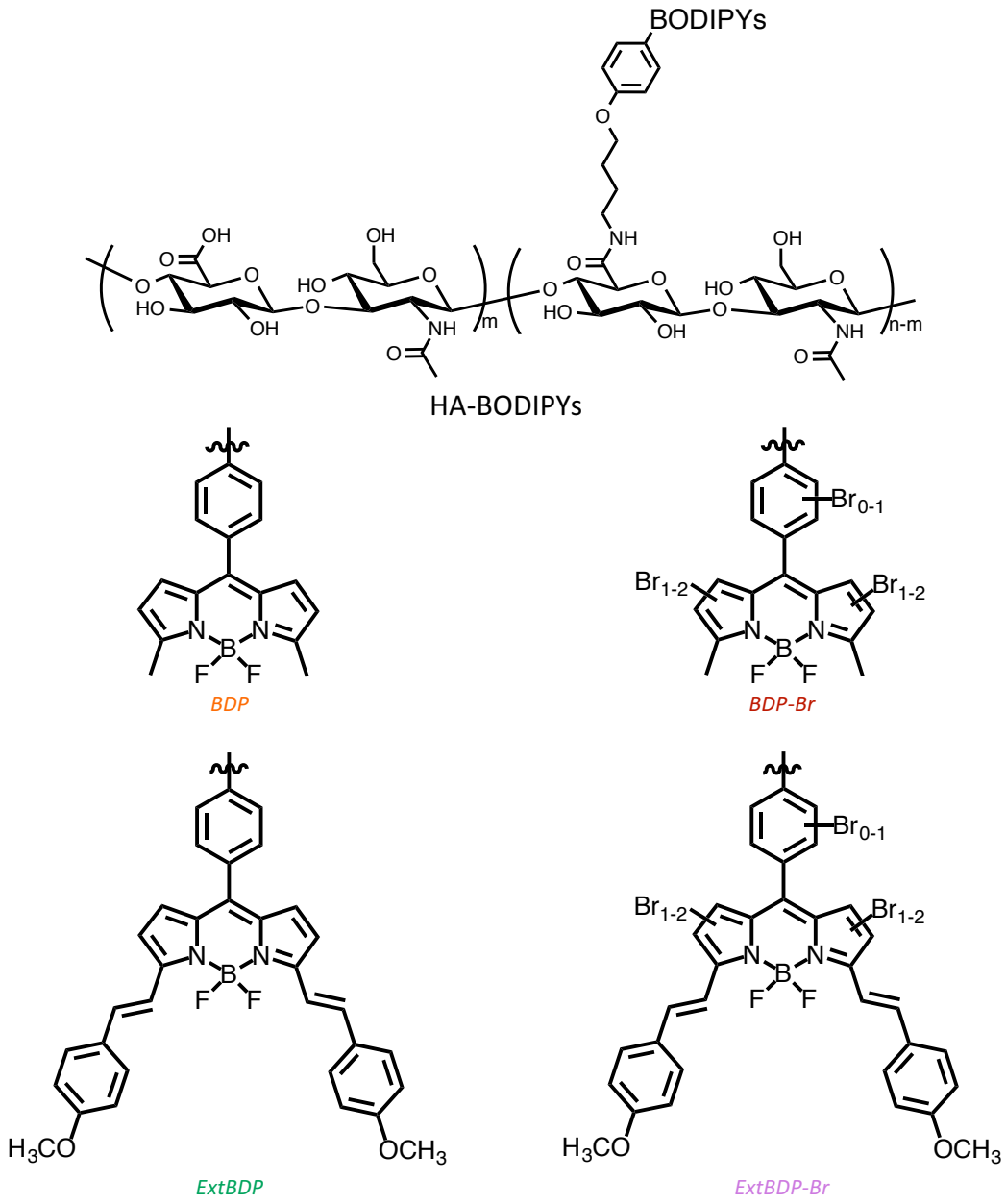

Figure 2.2 Molecular design of BODIPY-functionalized hyaluronic acids as photosensitizers for photodynamic therapy applications.

2.3. Results and Discussion

2.3.1. Synthesis

The synthetic route for the preparation of target BODIPY derivatives is shown in Scheme 1. BDP was obtained in 34 % yield *via* in situ reactions, which include a DDQ reaction followed by difluoroboration on pyrroles. BDP-Br was easily achieved through bromination of BDP with NBS in 1,1,1,3,3,3-hexafluoro-2-propanol. The various number of bromine substitution on BOIDPY were achieved within 5 min reaction. The combination of various degree of bromine substitution was used as it is because BODIPY substitution on HA is very low as well. Methyl group incorporation at the *alpha* position of BDP and BDP-Br were achieved by reaction with aldehyde in the presence of piperidine and acetic acid to extend conjugation on BODIPY using Knoevenagel condensation reaction, providing ExtBDP and ExtBDP-Br, respectively. Prepared BODIPY-derivatives were reduced in the presence of hydrazine monohydrate to produce a free amine functionality, which was conjugated to HA using the polymer's carboxylate groups by EDC coupling.

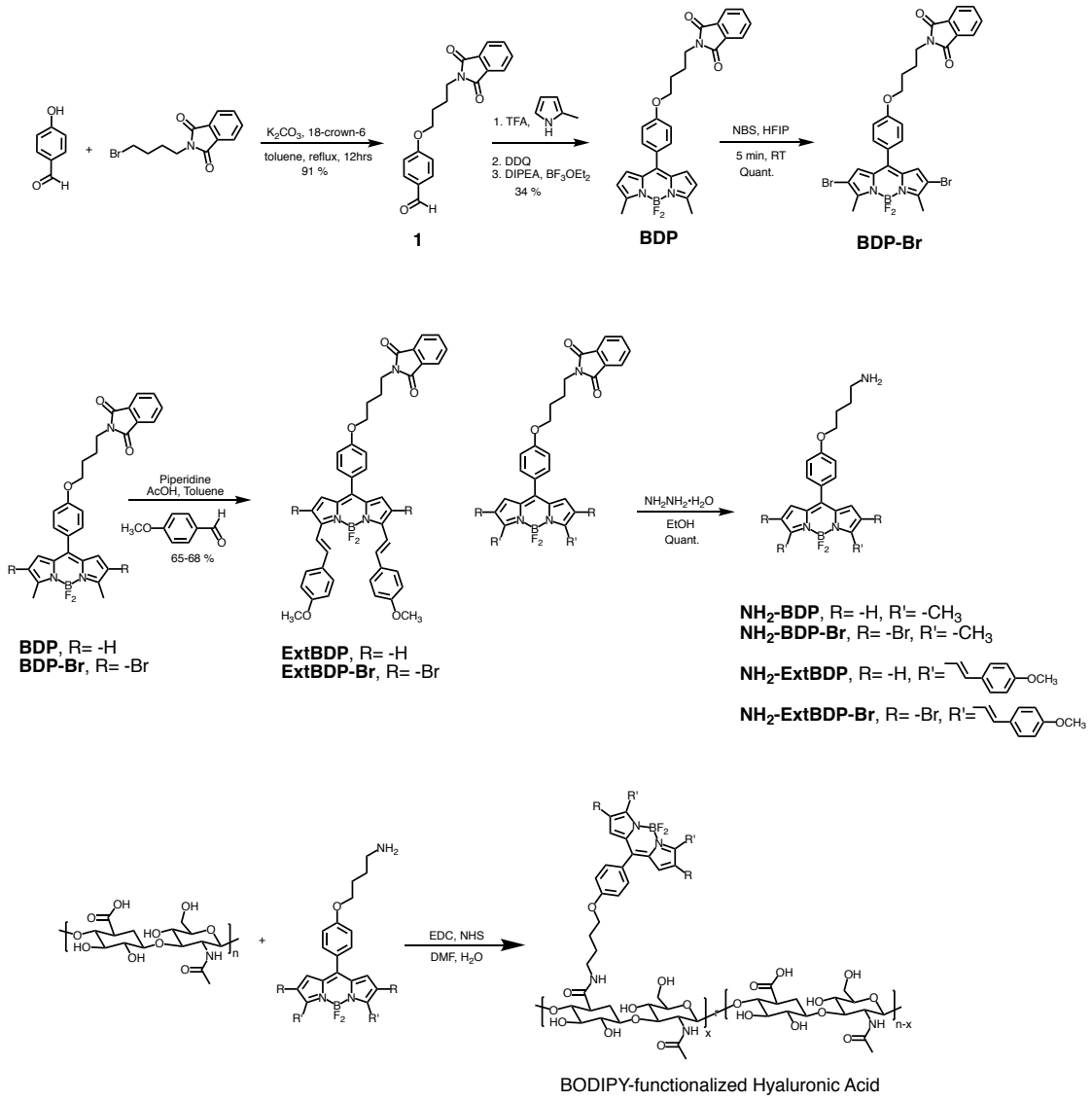

Scheme 2.1 Synthetic routes for a series of BODIPY derivatives and their functionalization on hyaluronic acid.

2.3.2. Optical Properties

Fundamental properties of the BOIDPY moieties were investigated prior to HA conjugation due to the decrease in solubility upon the attachment. The UV/vis absorption spectra of BODIPY in dichloromethane are shown in Figure 1 and the optoelectronic properties are summarized in Table 1. All BODIPY moieties show a strong $^{0}S \rightarrow {}^{1}S^{*}$ transition between 508 and 655 nm. BDP shows a strong and sharp peak at 508 nm,

which is characteristic of BODIPY Q-bands. As expected, upon extending the conjugation of the BDP core, the absorption spectra show a dramatic bathochromic shift, leading to an onset wavelength for ExtBDP and ExtBDP-Br into the therapeutic window of the light spectrum between 600 and 800 nm. Upon bromination of the BDP core, however, the spectra showed an overall band broadening, as well as a decrease in the absorption coefficient by about 10-fold. More interestingly, it is noted that the $\boldsymbol{\lambda}_{max}$ of brominated BODIPY moieties were slightly blue-shifted, although their onset wavelength were red-shifted or remained relatively similar.

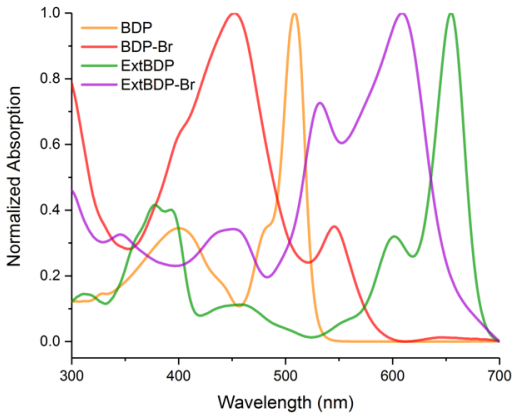

Figure 2.3 UV/vis absorption spectra of synthesized *alpha*-conjugation extended BODIPY molecules.

Table 2.1 Summary of optical properties of synthesized BODIPY derivatives.

BODIPYs	BDP	BDP-Br	ExtBDP	ExtBDP-Br
$\boldsymbol{\lambda}_{max}$ (nm)	508	452	660	609
$\boldsymbol{\lambda}_{onset}$ (nm)	540	600	700	700

Figure 2.4 shows UV/vis absorption spectra of the BODIPY series as a function of concentration. The concentration-dependent of absorption strength was plotted by Beer's law shown in Figure 2.5. Absorption coefficients of the series of BODIPY at valid peaks was extracted from the plot are summarized in Figure 2.5. It is observed that the BODIPY series exhibits high extinction coefficients (about $10^4 \sim 10^5$ M^{-1} cm^{-1}), which would allow for a better chance of light absorption and accordingly generation of singlet oxygen, making these BODIPY-based molecules great candidates for efficient light-harvesting photosensitizers in photodynamic therapy.

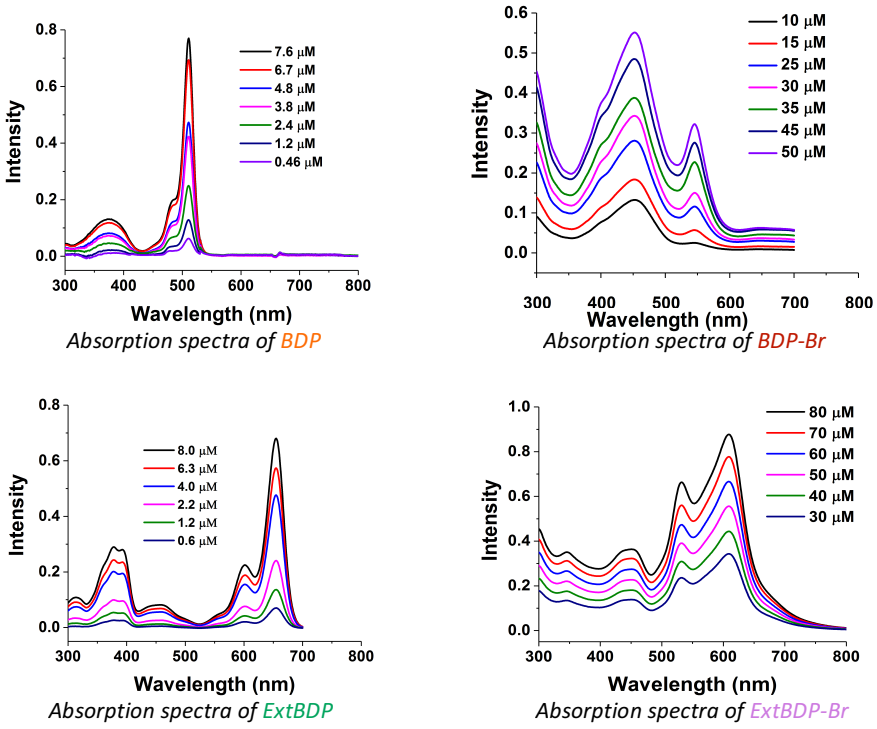

Figure 2.4 Absorption spectra of BODIPYs at various concentrations in DCM.

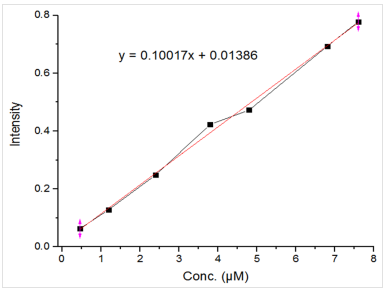

ε of BDP at 508 nm = 1.0 x 10^5 M^{-1} cm^{-1}

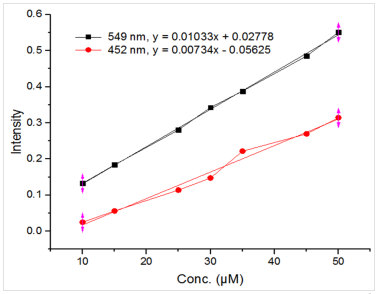

ε of ExtBDP-Br at 452 nm = 1.0 x 10^4 M^{-1} cm^{-1}
at 549 nm = 7.3 x 10^3 M^{-1} cm^{-1}

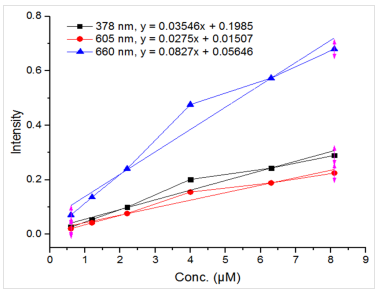

ε of ExtBDP at 378 nm = 3.5 x 10^4 M^{-1} cm^{-1}
at 605 nm = 2.8 x 10^4 M^{-1} cm^{-1}
at 660 nm = 8.3 x 10^4 M^{-1} cm^{-1}

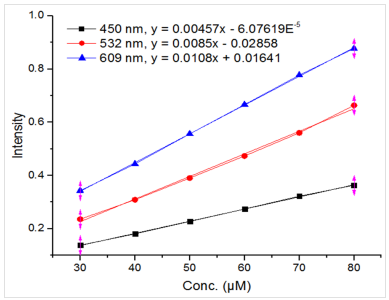

ε of ExtBDP-Br at 450 nm = 4.5 x 10^3 M^{-1} cm^{-1}
at 532 nm = 8.5 x 10^3 M^{-1} cm^{-1}
at 609 nm = 1.1 x 10^4 M^{-1} cm^{-1}

Figure 2.5 Plotted absorption coefficients at valid peaks of BDP (top left), BDP-Br (top right), ExtBDP (bottom left), and ExtBDP-Br (bottom right).

The fluorescence emission spectrum of each BODIPY is compared with UV/vis absorption spectrum in Figure 2.6. Since it is confirmed that fluorescence spectra profile of BODIPYs remained very similar shapes independent to excitation wavelength, excitation at 480 nm were selected report to avoid overlap with fluorescence profiles. It is observed that BDP and ExtBDP exhibit very little bathochromic shift whereas brominated ones, BDP-Br and ExtBDP-Br, show more distinctive shift by 100 ~ 150 nm. In addition, the little shoulder peaks at slightly lower energy than maximum peak in BDP and ExtBDP lost its pattern in fluorescence profiles while BDP exhibit typical absorption-emission relation, where fluorescence of BDP resemble UV/vis absorption spectrum profile, but simply red shifted. More interestingly, in ExtBDP-Br, it is noted

that maximum UV/vis absorption peak lose its majority in fluorescence emission, whereas shoulder peak in absorption at 532 nm dominantly emits fluorescence.

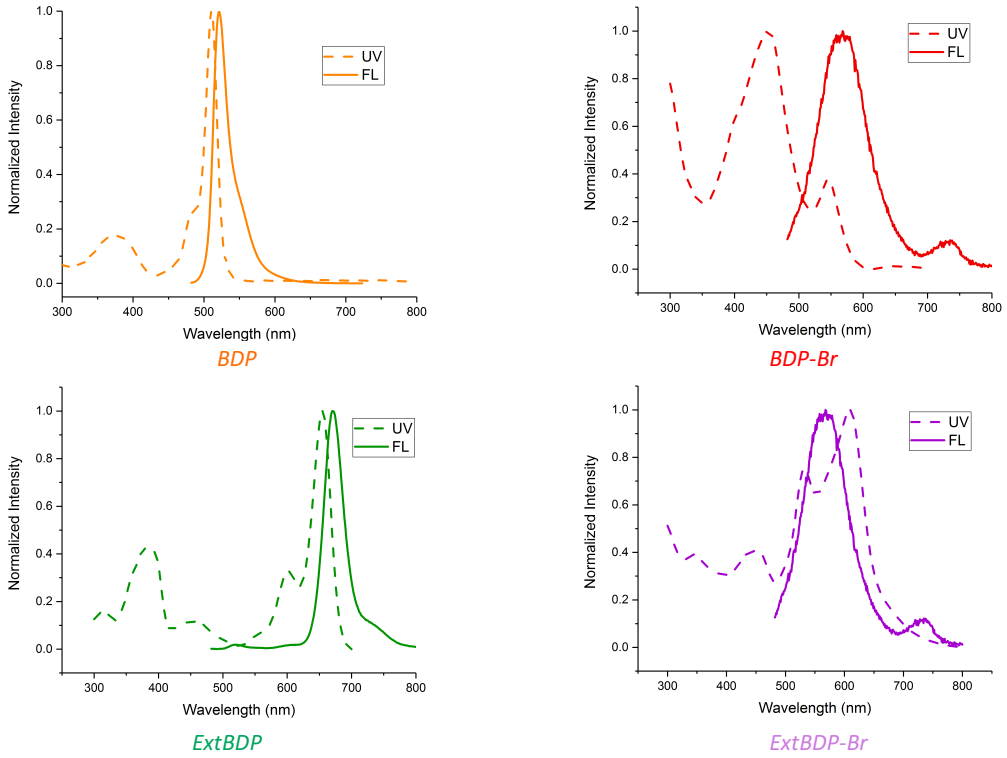

Figure 2.6 Fluorescence (FL) and UV/vis absorption (UV) spectra of synthesized BODIPY derivatives.

Fluorescence spectra of BODIPY molecules and fluorescein are shown in Figure 2.7. Fluorescence quantum yields of the series of BODIPY is estimated by using the quantum yield of fluorescein as a standard based on equation below, where fluorescence quantum yields of BODIPY samples (Q_R) is inversely proportional to optical density (OD) and directly proportional to integrated fluorescence intensity (I). The quantum yield of fluorescein standard (Q_S) in 1M NaOH is reported as 0.95. Also, it is noted that quantum yield is directly proportional to square of reflective index (n) of used solvent.

$$Q_{FL} = Q_R \times \frac{I_S}{I_R} \times \frac{OD_R}{OD_S} \times \left(\frac{n_S}{n_R}\right)^2$$

Table 2.2 Summarized fluorescence quantum yields of BODIPY compounds, measured against fluorescein standard in 1N NaOH solution.

BODIPYs	BDP	BDP-Br	ExtBDP	ExtBDP-Br
Q_{FL}	0.424	0.00493	0.526	0.00545

The calculated quantum yields of BODIPY compounds, compared with fluorescein standard are summarized in Table 2.2. It is found that bromonation scarifices fluoresecence quantum yield by hundred times, whereas conjugation extension of BODIPY through *alpha*-position does not have a significant impact. The decrease in the quantum yield upon bromination is consistent with expected results if heavy atom effect does exist in the BODIPYs. Specifically, induced ISC process upon bromination *via* heavy atom effect would possibly increase possibility of competitive process, phosphorescence emission, resulting in decrease in fluorescence quantum yield.

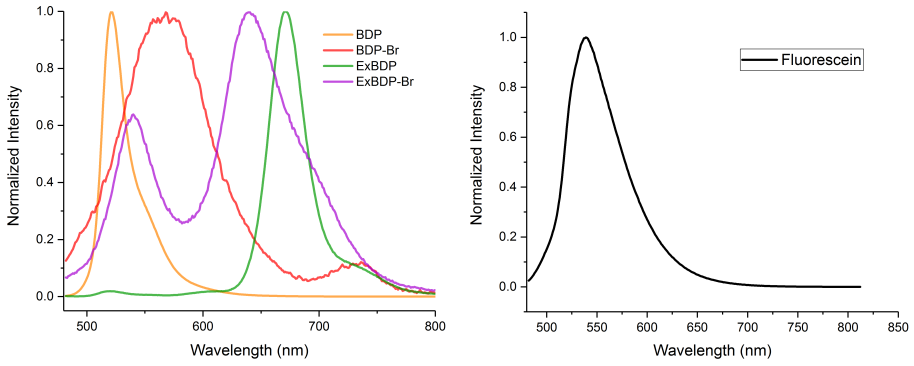

Figure 2.7 Fluorescence spectra of the BODIPY compounds (left) and fluorescein standard (right)

2.3.3. Transient Absorption Spectroscopy

TA spectroscopy was used to identify the formation of singlet and triplet excited states of each moiety, as well as to investigate the lifetimes of excited states accessed by the molecule. Single-wavelength kinetic fitting results are summarized in Tables in each corresponding Figures (Figure 2.8-11). In the simplest structure, BDP, a clear ground-state bleach (512 nm, $^{0}S \rightarrow {}^{1}S$) was observed with a lifetime of 3.2 ns. A small singlet growth was seen to the blue of 450 nm that is typical of BODIPY singlet excited states[55]. The growth occurs near the limit of the spectral window for the TA system used in these studies, and therefore could not be fit to produce a reliable lifetime. In the case of BDP-Br, other than the ground-state absorption bleach (550 nm), both the singlet (blue of 500 nm) and the triplet (650 – 750 nm) growths were observed. A singlet peak at 500 nm that turns into a triplet peak at 450 nm was also observed. Additionally, a broad triplet peak at 688 nm arises with similar dynamics to the peak at 450 nm. Single wavelength kinetics were used to extract lifetimes for BDP-Br of 332 ps and 176 μs for the singlet and triplet states, respectively.

Extension of the BODIPY core for ExtBDP and ExtBDP-Br dramatically modified the BODIPY core absorption spectrum, as well as the transient absorption spectra, observed upon excitation. The red-shift of the steady-state spectra in these moieties allowed for more features of the singlet excited states to be observed blue-shifted to the ground-state bleach. For ExtBDP, the ground state bleach was observed as expected at 664 nm. Several positive peaks that correspond to the ExtBDP singlet excited state were observed at wavelengths below 640 nm and above 780 nm. Single wavelength decays of peaks at 480 nm and 564 nm well matched the recovery of the ground state

bleach with lifetimes of approximately 4.3 ns. The spectra of ExtBDP also revealed a small unexpected bleach at 740 nm. This shoulder peak does not correspond to a ground-state bleach or stimulated emission and therefore its origin is unclear. Work is currently underway in our laboratory to identify the source of this bleach, which has been observed in several other BODIPY-based chromophores. No evidence of triplet formation was observed in the TA spectra of ExtBDP. However, ExtBDP-Br exhibited clear formation of a triplet state. The features of the ExtBDP-Br spectrum are generally broader than the other three BDP moieties presented above, meaning that features of the singlet, triplet and ground-state bleach bleed into each other and make single wavelength fitting in the TA data more challenging. The ground-state bleach was observed at 680 nm and appears to shift as the result of triplet absorptions developing at 553 nm and 754 nm over the first 5 ns. A peak corresponding to the singlet excited state was observed at 472 nm. The singlet decay at 472 nm was analyzed as a biexponential decay with lifetimes of 106 ps (75%) and 1.1 ps. The triplet peak at 750 nm was fit to a lifetime of 51 ns representing the formation of the triplet state, and 10 μs that represents the decay of that triplet state. On the nanosecond TA data, the ground state bleach (at 664 nm) was fit to similar lifetimes (67 ns and 10.45 ns), confirming that the triplet state was feeding directly back to the ground state. These TA results support the heavy atom effect, showing clearly that bromination stimulates the ISC transition, and thus increases the probability of accessing the triplet state. Although the triplet state was not observed in BDP and ExtBDP in our TA measurement conditions, it did not completely exclude the possibility of a very small triplet state population. However, observance of brominated PS BODIPYs with 10-100 μs lifetime confirmed the existence of their long-lived triplet state.

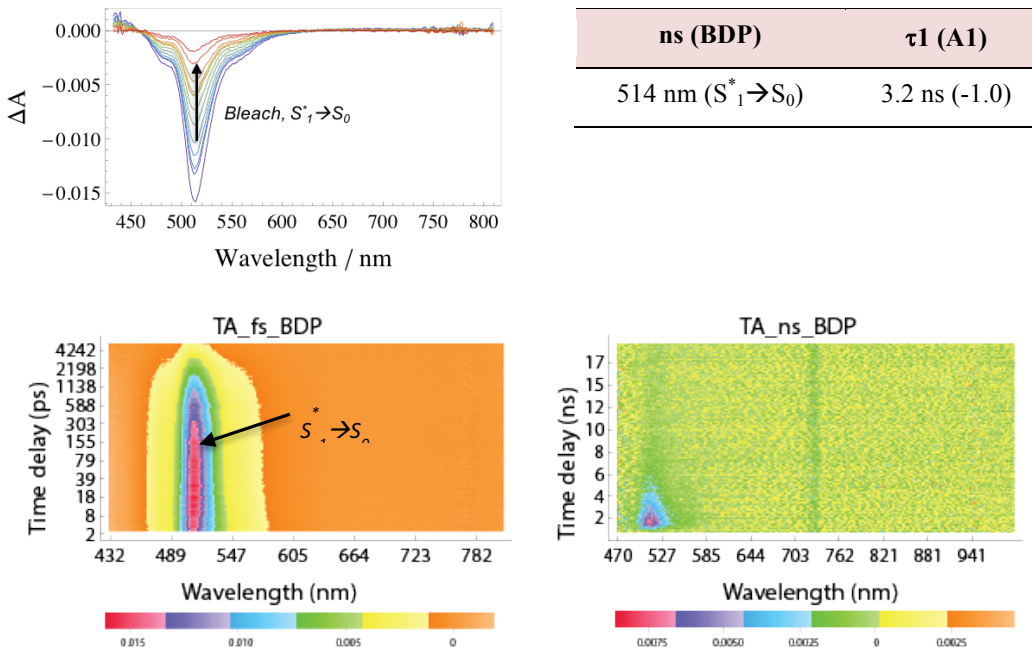

ns (BDP)	τ1 (A1)
514 nm ($S^*_1 \rightarrow S_0$)	3.2 ns (-1.0)

Figure 2.8 Transient absorption spectra (left top), heat maps of femtosecond (left bottom) and nanosecond (right bottom) measurements of BDP in argon-purged dichloromethane (DCM) solution. Valid life times at each wavelength are summarized in the included table (right top).

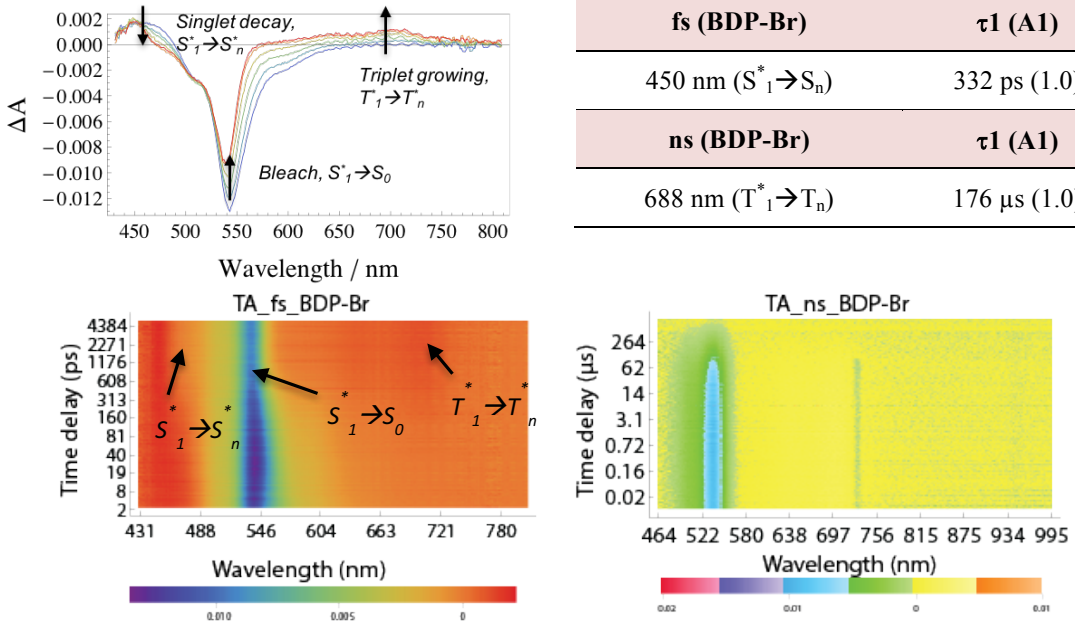

fs (BDP-Br)	τ1 (A1)
450 nm ($S^*_1 \rightarrow S_n$)	332 ps (1.0)
ns (BDP-Br)	**τ1 (A1)**
688 nm ($T^*_1 \rightarrow T_n$)	176 µs (1.0)

Figure 2.9 Transient absorption spectra (left top), heat maps of femtosecond (left bottom) and nanosecond (right bottom) measurements of BDP-Br in argon-purged dichloromethane (DCM) solution. Valid life times at each wavelength are summarized in the included table (right top).

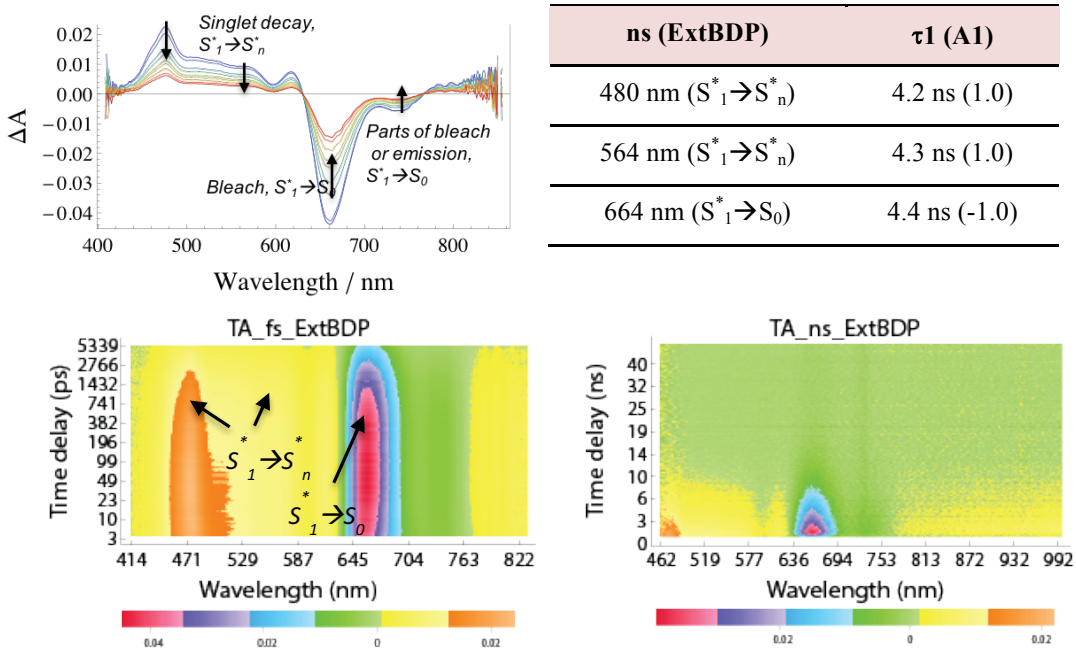

ns (ExtBDP)	τ1 (A1)
480 nm ($S^*_1 \rightarrow S^*_n$)	4.2 ns (1.0)
564 nm ($S^*_1 \rightarrow S^*_n$)	4.3 ns (1.0)
664 nm ($S^*_1 \rightarrow S_0$)	4.4 ns (-1.0)

Figure 2.10 Transient absorption spectra (left top), heat maps of femtosecond (left bottom) and nanosecond (right bottom) measurements of ExtBDP in argon-purged dichloromethane (DCM) solution. Valid life times at each wavelength are summarized in the included table (right top).

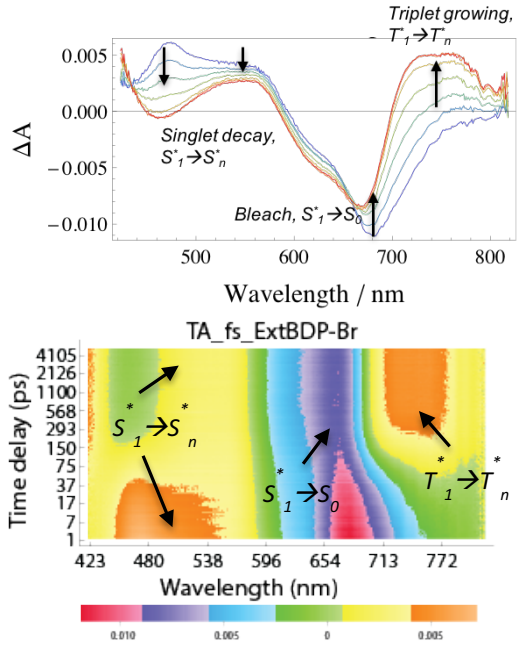

fs (ExtBDP-Br)	τ1 (A1)	τ2 (A2)
472 nm ($S^*_1 \rightarrow S^*_n$)	106 ps (0.75)	1.1 ps (0.21)
ns (ExtBDP-Br)	**τ1 (A1)**	**τ2 (A2)**
553 nm ($S^*_1 \rightarrow S^*_n$)	0.38 μs (-0.085)	11.14 μs (0.91)
664 nm ($S^*_1 \rightarrow S_0$)	0.067 μs (0.045)	10.45 μs (-0.95)
754 nm ($T^*_1 \rightarrow T^*_n$)	10.19 μs (0.87)	0.051 μs (-0.13)

Figure 2.11 Transient absorption spectra (left top), heat maps of femtosecond (left bottom) measurement of ExtBDP-Br in argon-purged dichloromethane (DCM) solution. Valid life times at each wavelength are summarized in the included table (right).

Table 2.3 Summary of singlet and triplet lifetimes, measured from transient absorption spectroscopy

BODIPYs	BDP	BDP-Br	ExtBDP	ExtBDP-Br
Singlet Lifetime	3.2 ns	332 ps	4.3 ns	106 ps, (11 μs)
Triplet Lifetime	-	176 μs	-	10 μs

2.3.4. Evaluation of Singlet Oxygen Generation

Singlet oxygen generation of each BODIPY PS molecule was measured in an organic solvent environment by using a well-known singlet oxygen chemical trap, 1,3-diphenylisobenzofuran (DPBF)[56,57]. Since DPBF undergoes a [4+2] cycloaddition with $^1O_2$ to form *o*-dibenzoylbenzene, the disappearance of DPBF in the presence of a BODIPY PS implies generation of $^1O_2$ in a controlled experimental system. DPBF is a good $^1O_2$ trap in various organic solvents because it rapidly reacts with $^1O_2$, but is insensitive to $^3O_2$ or superoxide anion. The disappearance of DPBF is monitored by UV/vis absorption spectroscopy at its maximum intensity, 410 nm, over time with light exposure. The concentrations of DPBF and relevant BODIPY PS in dichloromethane solution were determined, so that $^1O_2$ generation could be monitored effectively throughout the time of light exposure. 10 μM solutions of each PS molecule in dichloromethane were prepared containing 10 μM of DPBF and were irradiated with a NIR LED. UV/vis absorbance of the solution was measured every 2 min over the course of 1 hour. As a control, 10 μM DPBF solution was tested in the same condition without the presence of a PS molecule. The absorbance spectra of DPBF over time are shown in Figure 2.14 and calculated initial rates are summarized in Table 1.3. It is noted that both conjugation extension and bromination promote the initial rate of DPBF depletion by

twice and seven-times, respectively. It is also observed that brominated PS molecules (BDP-Br and ExtBDP-Br) are more efficient at depletion of DPBF than by non-brominated PS molecules. After 20 min of light exposure, BDP-Br generated much more singlet oxygen than non-brominated BDP. This heavy atom effect observation is consistent with observations from the TA measurements. Specifically, even though bromination resulted in a ten-fold decrease in the extinction coefficient, the increase in ISC from the heavy atom effect generated a larger triplet yield that results in substantial generation of $^1O_2$.

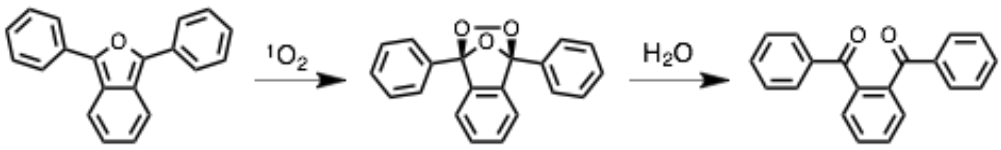

1,3-diphenylisobenzofuran (DPBF)

o-dibenzoylbenzene

Figure 2.12 Chemical structure of 1,3-diphenylisobenzofuran (DPBF) and its reaction with singlet oxygen, yielding *o*-dibenzoylbenzene byproduct.

Theoretically, because singlet oxygen generation from a PS molecule is a cyclic process, where the PS can be regenerated by returning to its original stable ground state, the PS should not be consumed. However, in the reality, the cycle stops if the PS reacts with other species or is decomposed. The observation of a plateau in DPBF depletion from BDP-Br and ExtBDP-Br following rapid generation of singlet oxygen indicates degradation of PS could occur. Greater consumption of DPBF at the plateau in BDP-Br than in ExtBDP-Br consistently supports the TA measurement results of a 17-times longer lifetime of triplet state for BDP-Br.

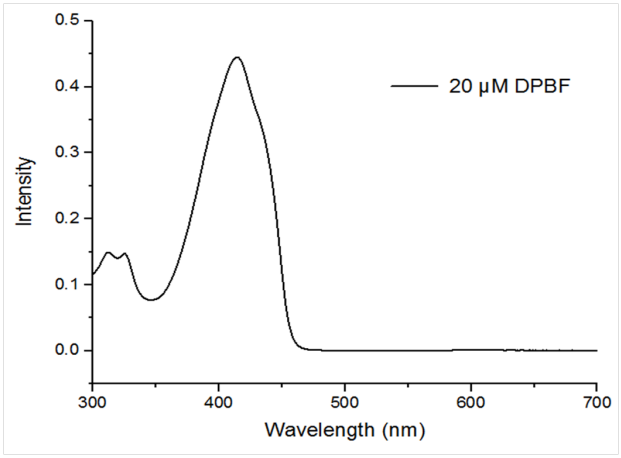

Figure 2.13 UV/vis spectrum of 20 μM of DPBF in dichloromethane (CH_2Cl_2) solution. The maximum peak of DPBF at 410 nm is chosen to monitor DPBF consumption.

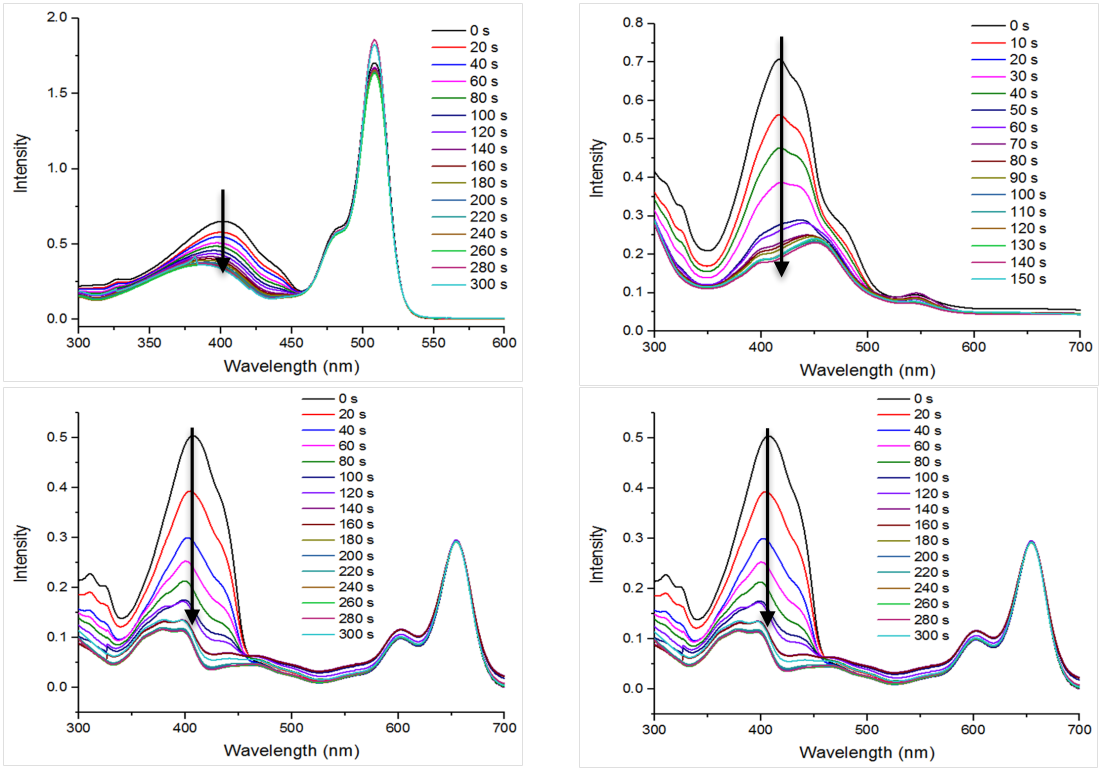

Figure 2.14 UV/vis spectra of DPBF and BODIPY derivative solutions as a function of light exposure time: BDP (top left), BDP-Br (top right), ExtBDP (left bottom) and ExtBDP-Br (right bottom)

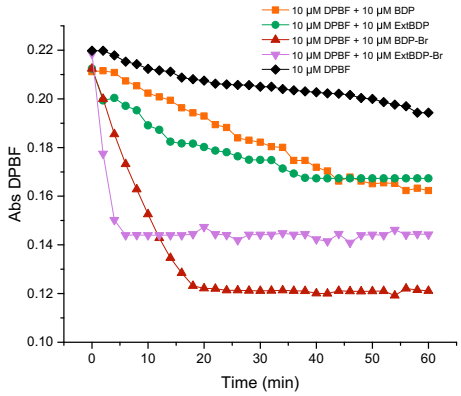

Figure 2.15 Singlet oxygen generation implied by DPBF consumption as a function of NIR LED light exposure time. The DPBF consumption was monitored by UV/vis spectrum. The slop of graphs means the rate of singlet oxygen generation.

Table 1.3 Summarized initial rate of the singlet oxygen generation of synthesized BODIPY derivatives

BODIPYs (10 μM)	BDP	ExtBDP	BDP-Br	ExtBDP-Br
Initial rate (min^{-1})	0.001	0.002	0.007	0.014

2.3.5. Synthesis of BODIPY-functionalized Hyaluronic Acids

BODIPY derivatives are functionalized on HA polymer backbone through EDC coupling reaction between a carboxylic acid on HA chain and primary amine on BODIPY molecules, the primary amines of which were obtained by deprotection of phthalimide in the presence of hydrazine mono hydrate. BODIPYs were added to HA solutions with a 10 or 20 % feed ratio respective to the carboxylate moieties on the HA backbone. Following purification, the degree of substitution was esitimated based on the calculated absorption coefficient of each BODIPY. Although low conjugation extents were achieved in all cases due to solvent compatibility with HA, this was not of concern for PDT applications due to the efficient $^1O_2$ capability of these PS molecules. A 0.01% of degree of substitution was achieved for HA-BDP-Br and HA-ExtBDP, while less than

0.005% was obtained in case of ExtBDP-Br. Because ExtBDP and ExtBDP-Br are the PSs that absorbs the light within the appropriate therapeutic range, they were selected for further cytotoxicity studies.

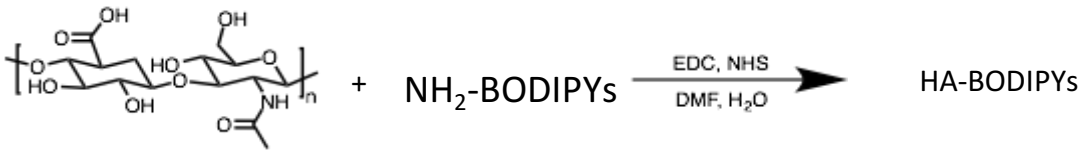

Scheme 2.2 Simplified synthetic scheme of BODIPY functionalization on hyaluronic acids through EDC coupling reaction in water solution: the reaction occurs between carboxylic acid on hyaluronic acid and primary amine on BODIPY. 10 and 20 % of feed ratio was used.

Table 2.4 Degree of BODIPY substitution on hyaluronic acids, estimated from absorption-based calibration curves.

Feed ratio	HA-BDP	HA-BDP-Br	HA-ExtBDP	HA-ExtBDP-Br
10 %	0.02	0.01	0.01	< 0.005
20 %	-	-	0.03	0.01

2.3.6. Cytotoxicity with CD44+ HeLa cell line due to their appropriate absorption

HA modified with ExtBDP and ExtBDP-Br were chosen for cytotoxicity studies with CD44+ HeLa cell line due to their appropriate absorption within the therapeutic range of the light spectrum. HA-ExtBDP and HA-ExtBDP-Br that were synthesized with 10 % feed ratio was used with a variation of their concentration (0.1, 0.5 and 1 mg/mL) and LED NIR light exposure time (0, 15 and 30 min) after 3 hours of photosensitizer incubation, following the remove of free photosensitizers that did not internalized or anchored on the cell. MTT assay was used to detect cell viability after 24 hours. In addition, since test with trypan blue shows mitochondria death, the same condition was

tested with trypan blue to confirm that the cell viability results from MTT assay is driven by actual cell death. As a negative control, PBS buffer without photosensitizer incubated was tested at different light exposure time.

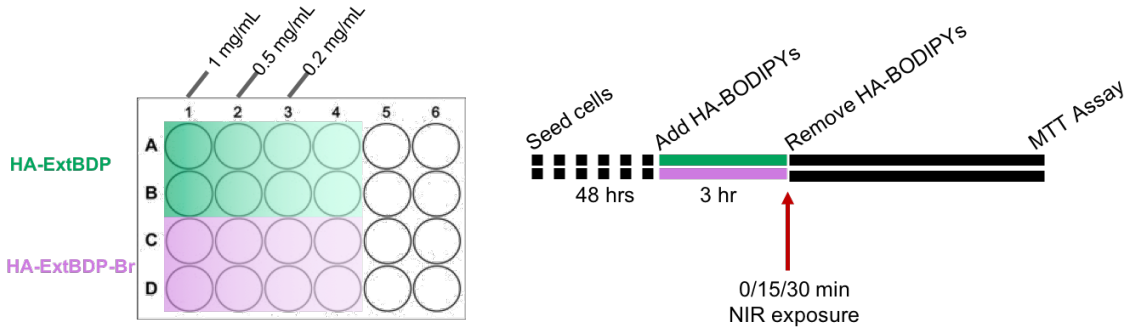

Figure 2.16 Illustration of procedure of cytotoxicity study

Figure 2.17 shows the cell viability results from the described condition above: 3 hours of PS incubation, light treatment for 15 and 30 min, and 10 % feed ratio of BODIPYs. Above 75 % of cell viability is found in negative controls: 1) where NIR light is treated, but no PS is incubated and 2) where PS was incubated, but no NIR light was treated. Overall, HA-ExtBDP-Br shows higher cytotoxicity compared to HA-ExtBDP following light treatment. This data is consistent with expectations from singlet oxygen generation measurements by DPBF, where ExtBDP-Br showed greater and faster initial rate of $^1O_2$ generation than ExtBDP. Further, when 0.2 mg/mL of HA-ExtBDP-Br was used, a very controlled and gradual increase of cytotoxicity up to 75 % was achieved as light exposure time increased. When the concentration increased above 0.5 mg/mL, rapid toxicity up to 90 % was observed after just 15 min of light treatment. Meanwhile, HA-ExtBDP showed only slight cell death upon light treatment. At the highest concentration tested (1 mg/mL) HA-ExtBDP showed about 50 % cell death with 15 min of light exposure, however, in the dark it also showed about 25 % cell death. The toxicity of HA-

ExtBDP in dark observed possibly because of the toxicity of ExtBDP itself on HA unit. The toxicity of ExtBDP-Br could be covered due to its lower degree of substitution of less than 0.05 % on HA backbone.

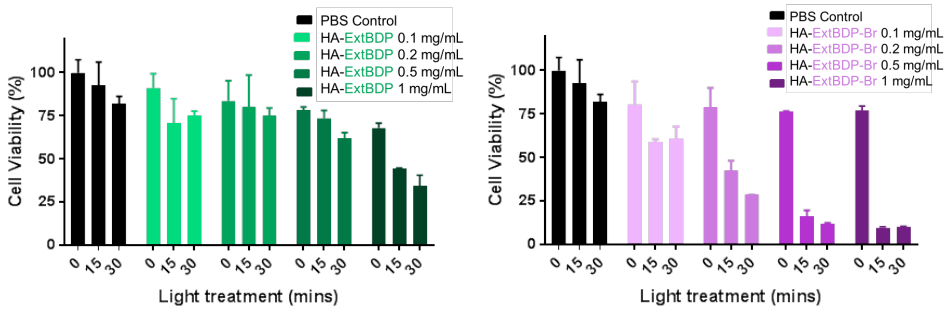

Figure 2.17 Cell viability of HA-ExtBDP (left) and HA-ExtBDP-Br (right) at various concentrations as a function of LED NIR light exposure time after 3 hours of incubation. 10 % feed ratio.

Separately, HA-ExtBDP and HA-ExtBDP-Br with 20 % of feed ratio were tested with a variety of conditions: various LED NIR light exposure time (0, 30, 90, 180 min) and concentrations of PS (0.1, 0.5 and 1.0 mg/mL) incubated. The results are shown in Figure 2.18. HA-ExtBDP exhibits saturated toxicity even in dark was observed at the concentration of 0.5 mg/mL, which is understood as HA-ExtBDP-Br with 10 % feed ratio showed toxicity in dark. Furthermore, HA-ExtBDP-Br with 20 % feed ratio at the concentration of 0.5 mg/mL has 65 %, which is much higher than 25 % cell death by HA-BDP-Br at 1.0 mg/mL concentration in dark.

Surprisingly, HA-ExtBDP showed cytotoxicity with gradual controls as a function of all of factors: incubation time, time of exposure to LED NIR light, and concentration of HA-ExtBDP incubated. For example, 1.0 mg/mL of HA-ExtBDP, treated with LED NIR for 15 min can finely control viability of HeLa cells from 100 to 50 or 20 %,

depending on incubation time from 30 to 90 or 180 min, respectively. Also, cytotoxicity of HA-ExtBDP can be finely controlled as a function of light exposure time to LED NIR. For instance, 1 mg/mL of HA-ExtBDP with 90 min of incubation time displays a gradual cell death from 25 % to 50 or 90 % as a function of light treatment time from 0 to 15 or 30 min, respectively. Lastly, gradually controlled cell death also can be achieved depending on the use of concentration of HA-ExtBDP as PS. For example, HA-ExtBDP incubated for 90 min with 30 min of LED NIR light treatment shows a gradual cell death from 0 to 50, or 90 % as its concentration during incubation varied from 0.1 to 0.5, or 1.0 mg/mL. The similar control with a variation of PS concentration (0.1, 0.5, or 1.0 mg/mL) is possible with HA-ExtBDP incubated for 180 min with 15 min light treatment, where 100, 75, or 20 % of cell viability can be achieved. This finely manageable cytotoxicity is significantly worthwhile with its high biocompatibility in dark (~100 %), making HA-ExtBDP as a strong candidate as a photosensitizer in photodynamic therapy application. Moreover, it is observed that slight increase in cell viability over 100 % in the mildest condition: HA-ExtBDP of 20% feed ratio with 30 min of incubation at low concentration (0.1 and 0.5 mg/mL). Increased cell viability regardless LED NIR treatment is the consistent evidence of low toxicity in dark as well as with light because HeLa possibly grow faster than ExtBDP-induced or photodynamically-induced cell death occurs.

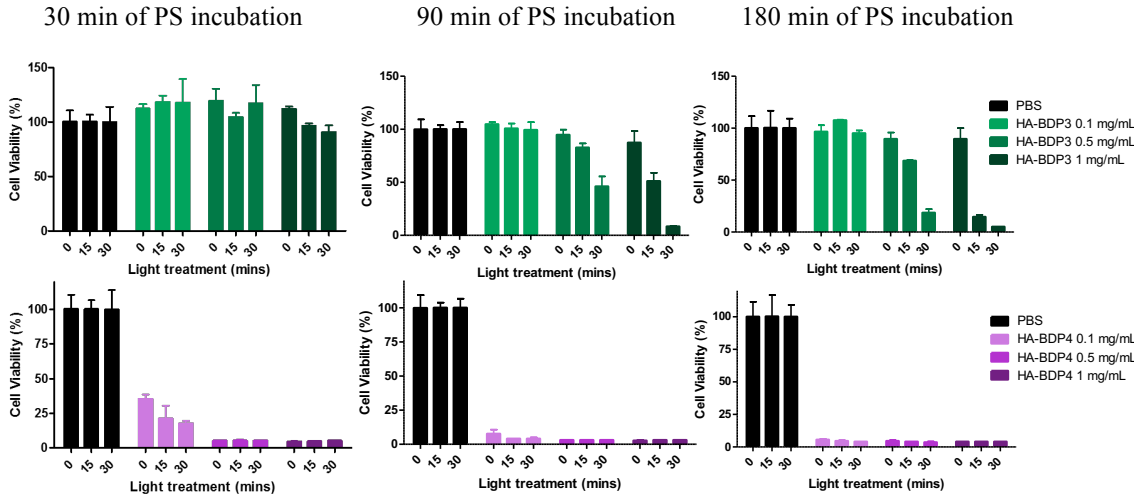

Figure 2.18 Cell viability of HA-ExtBDP (top) and HA-ExtBDP-Br (bottom) with variations of incubation time of 30 min (left), 90 min (middle), and 180 min (right) at three different concentrations as a function of LED NIR light exposure time. 20% feed ratio

HA-ExtBDP is further investigated to study its preference property towards CD44+ cell over CD44- cell lines, originated from hyaluronic acid. Cell viability of HA-ExtBDP in HeLa (CD44+) and HepG2 (CD44-) are researched separately. Also, the blend of HeLa and HepG2 is examined to verify our hypothesis that HA-ExtBDP preferably interact with CD44 receptor through its HA backbone, as illustrated in chapter 1.

Figure 2.19 shows cell viability result of HA-ExtBDP at the concentration of 1 mg/mL as a function of LED NIR light exposure time. Specific condition was chosen (3 hours of incubation, 1 mg/mL of PS) based on previously discussed results above to expect gradual cell death with a variation control, minimizing the possibility of saturation of cytotoxicity results. Figure 2.19 explains the result where HepG2 cell lines are more endured the light treatment, whereas HeLa cell lines are more vulnerable. In CD44

receptor bearing HeLa cell lines. To the details in Figure 2.19, it is discovered that cell viability drops dramatically after 15 min of NIR irradiation to 75 %, which can further decline until 10 % over the course of light exposure for 30 min. Also, it is noted that HA-ExtBDP possess slight toxicity in dark by 25 % at the given conditions in HeLa cell lines. Contrast to the HeLa cell viability, HepG2 exhibits less dramatic cell death of 25 and 40 % upon 15 and 30 min of light treatment with a high viability of 100 % in dark. This is a significant cytotoxicity, considering HepG2 is CD44 negative. It is possible to understood that HA-ExtBDP can be internalized into HepG2 during the incubation with an aid of hydrophobic property of ExtBDP functionality, which would allow easier pathway into the cells through its lipid layers. This internalization of HA-ExtBDP into HepG2 could be even easier in the absence of competitive cells, HeLa.

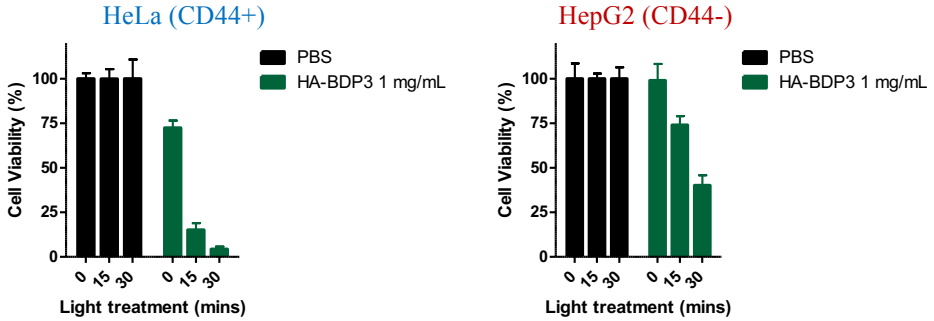

Figure 2.19 Cell viability of HA-ExtBDP in CD44+ HeLa cells (left) and CD44- HepG2 cells (right), separately, at the concentration of 1 mg/mL as a function of LED NIR light exposure time.

On the other hand, the experimental conditions with a mixture of HeLa and HepG2 likely provide a better understanding on the selectivity of HA-ExtBDP. Illustration of procedure is shown in Figure 2.20. HA-ExtBDP is incubated in the mixture of two cell lines for 3 hours. After washing free PS, the light exposure is repeated every

12 hours of incubation for 30 min at each time, followed by flow cytometry for the detection of HepG2 and HeLa as violet positive and negative cells under 405 nm laser. The concentration HA-ExtBDP is varied to be 0.5 and 1.0 mg/mL throughout the study.

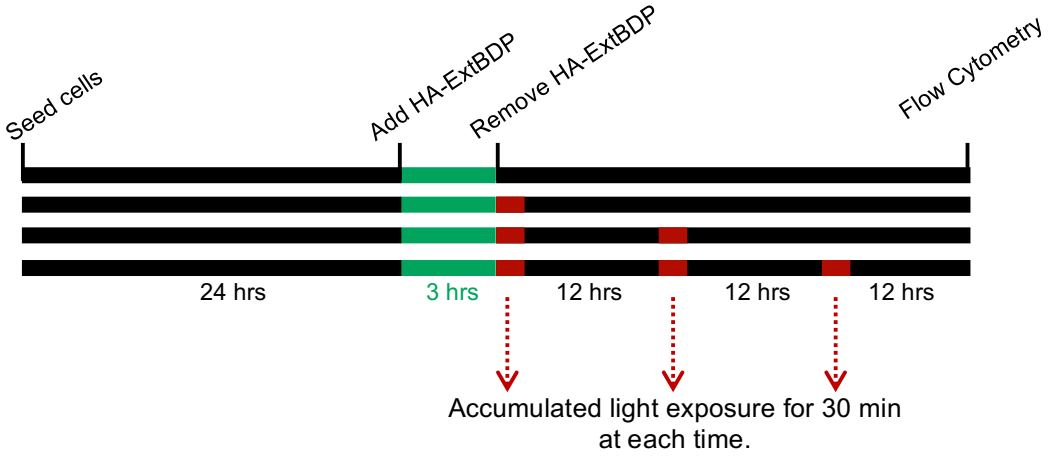

Figure 2.20 Illustration of procedure for cytotoxicity studies in the mixture of HeLa and HepG2 system.

Our hypothesis of the selectivity of HA-containing PS towards CD44+ cell lines is consistently supported by the results in Figure 2.21, where facilitated cell death of HeLa over HepG2 is observed in co-existing system. This is because dominant interaction of HA on HA-ExtBDP with CD44 receptor on HeLa could limit the competitive interaction between HA-ExtBDP and HepG2, making HepG2 more endurable in photodynamic condition with HA-ExtBDP. Figure 2.21 shows the ratio of HepG2/HeLa obtained after LED NIR light treatment in the mixture of HeLa and HepG2 system. The result is also expressed in live cell percentage in Figure 2.21 at the bottom. It is noticed that the light treatment affects on the viability of both HeLa and HepG2 lines, lowering live cell percentage of both. However, the diminish in viability is more dramatic

in HeLa cell lines, which is consistently supporting selectivity of HA-ExtBDP towards CD44 positive HeLa over CD44 negative HepG2.

The initial HepG2/HeLa ratio is varied to be 0.1, 0.2, and 0.4. In addition, HA-ExtBDP at the concentration of 0.5 or 1.0 mg/mL were treated with NIR light for 30 min, repeated two more cycles with 12 hours of incubation. In case of 1 mg/mL of HA-ExtBDP at all three initial ratios, it is observed that the ratio of HepG2/HeLa increases as light treatment cycle proceed. However, although HepG2/HeLa ratio increases when 0.5 mg/mL of HA-ExtBDP was tested, it is noted that the increase in HepG2/HeLa ratio becomes saturated after the first light exposure for 30 min.

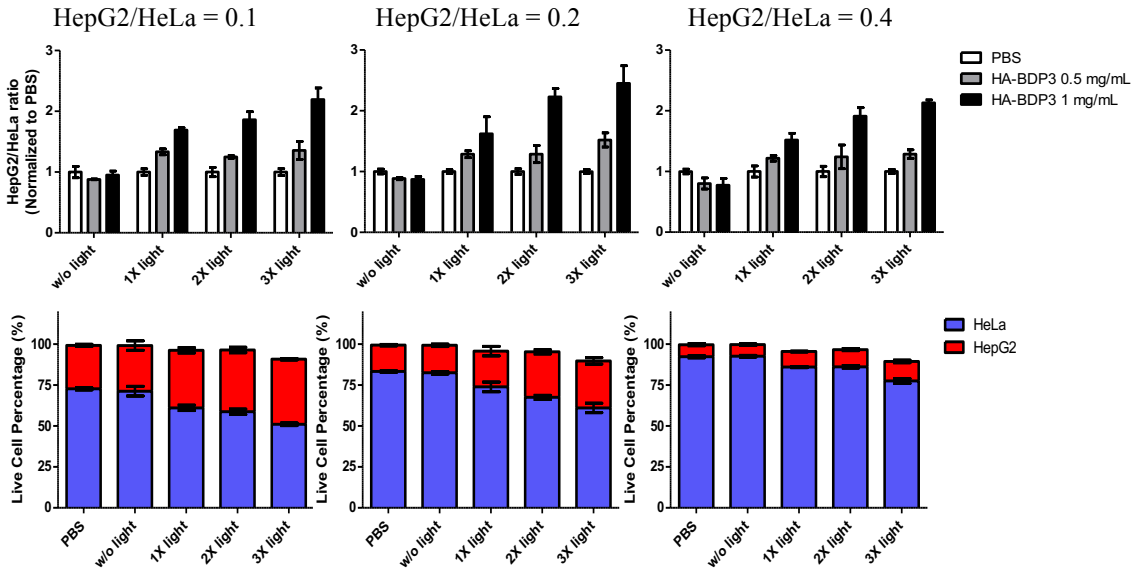

Figure 2.21 The preference of HA-ExtBDP towards HeLa (CD44+) over HepG2 (CD44-). HA-ExtBDP is tested in the mixture of HeLa and HepG2 cells with a variation of HepG2/HeLa ratio to be 0.1 (left), 0.2 (middle), or 0.4 (right). The results are expressed in two ways: HepG2/HeLa ratio (top) and percentage of live cell (bottom, 1mg/mL). Conditions: HA-ExtBDP (20 % feed ratio) was incubated at the concentration of 0.5 or 1 mg/mL for 3 hours and irradiated by LED NIR light for 30, 60 and 90 min.

Control experiment with HA backbone in the absence of BODIPY functionality were designed in order to verify HA itself is biocompatible to both HeLa and HepG2, which would not affect on cytotoxicity observed previously. The concentration of HA is varied to be 0.1 or 1.0 mg/mL. Figure 2.22 shows the expected result that HA is non-toxic to neither of HeLa nor HepG2 cells. Over the course of light exposure for 30 min, cell viability remains intact in both cell lines. This is result that further confirms that previously described cytotoxicity results are attributed from the photodynamic property of BODIPY-functionalities.

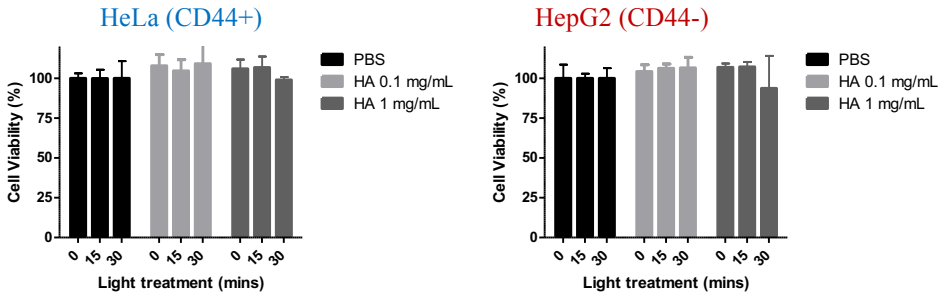

Figure 2.22 Cell viability of HA without BODIPY conjugation in CD44+ HeLa cells (left) and CD44- HepG2 cells (right) at three different concentrations as a function of LED NIR light exposure time.

2.4. Summary

In summary, a series of BODIPY-functionalized hyaluronic acids are synthesized for PDT application as PS. The BODIPY structures were designed with a variation of heavy atom functionality and π-conjugation extension through alpha position: HA-BDP, HA-BDP-Br, HA-ExtBDP, and HA-ExtBDP-Br.

These molecules exhibited good absorption coefficients ($10^4 \sim 10^5$ M^{-1} cm^{-1}). BDP and exhibits a typical sharp π-π* transition of BODIPY moiety at 508. As alpha

extension introduced to BDP, producing ExtBDP, the peak red shifted to 660 nm. On the other hand, bromination on BODIPY showed UV/vis peak broadening. Considering HA-ExtBDP and HA-ExtBDP-Br exhibit absorption profiles within therapeutic window of light, they are further discussed for cytotoxicity characterization.

Singlet oxygen generation was examined by monitoring DPBF consumption as a function of LED NIR light exposure time. Ones with bromination showed seven times faster initial rate of DPBF consumption, compared to their corresponding BODIPY analogues without bromine. Extension of alpha-conjugation also showed increased initial rate by two times. This is consistent with their fluorescence quantum yield, calculated as compared to fluorescein standard. Moreover, the existence of triplet in brominated compounds, BDP-Br and BDP-ExtBr, was characterized by transient absorption spectroscopy to be 10 and 176 μs, respectively.

In cytotoxicity study, HA-ExtBDP and HA-ExtBDP-Br were examined due to their light absorption profile within therapeutic window, which would be essiential for PDT applications. Both HA-ExtBDP and HA-ExtBDP-Br are able to show optimistic conditions where cell death through PDT effect is gradually controllable as a function of factors such as light exposure time, concentration of PS, incubation duration, and etc. Specifically, HA-ExtBDP in selected conditions where they exhibit various degree of cell death depends on factors (1mg/mL of PS, at 3 hours of incubation time) is further tested to study selectivity of PS towards CD44+ cell lines over CD44- cells, which is one of the important PS requirement in PDT application to avoid normal cell damages. In their cytotoxicity test in the mixture of HeLa and HepG2, preferred cell toxicity, driven by HA-ExtBDP, was successfully observed. Combination of its selectivity towards CD44+

cells, a favorable light absorption property with efficient and manageable cell death upon light exposure as well as its good biocompatibility in the dark makes HA-ExtBDP as a strong PS candidate for PDT applications.

2.5. Experimental Section

2.5.1. Materials and Instrumentation

All reagents were purchased from commercial sources and used as received, unless otherwise described. Analytical techniques: ^{1}H NMR spectra were recorded on a 400 MHz Bruker NMR spectrometer using the residual proton resonance of the solvent as the internal standard. Chemical shifts are reported in parts per million (ppm). When peak multiplicities are given, the following abbreviations are used: s, singlet; bs, broad singlet; d, doublet; t, triplet; m, multiplet. ^{13}C NMR spectra were proton decoupled and recorded on a 100 MHz Bruker spectrometer using carbon signal of the deuterated solvent as the internal standard. Cary 100 Scan UV-Visible Spectrophotometer was used for UV/vis absorption experiments. Fluorescence spectra were recorded using a JASCO FP-6500 spectrofluorimeter. FAB-MS spectra were measured on a JEOL JMS700. MALDI-TOF spectra were measured on a Bruker OmnifleX.

2.5.2. Transient Absorption Spectroscopy

Femtosecond and nanosecond transient absorption (TA) measurements were performed using a Coherent Libra amplifier with a TOPAS-C optical parametric amplifier as the excitation source, and an Ultrafast system's Helios/EOS system was used for detection as described previously[55]. In summary, excitation pulses for TA were generated by an optical parametric amplifier (TOPAS-C, Light Conversion) pumped by

96% of a Coherent Libra Ti:Sapphire system (~1.0 W at 800 nm). The Libra produces a 1 kHz pulse train with 100 fs pulse duration. The resulting pump beam was attenuated to 0.5-2 mW for TA experiments. An excitation wavelength of 365 nm was used for all BODIPY molecules with pump powers of 0.5 mW (for ExtBDP and ExtBDP-Br) or 1 mW (for BDP and BDP-Br) to prevent photobleaching. Samples were prepared in dichloromethane in an inert glovebox environment with absorption intensities at the excitation wavelength about 0.3 AU. Throughout the experiment, the excitation pulse and the probe pulse were overlapped onto the sample with constant stirring. UV/vis absorption spectra were taken before and after each TA measurement to exclude the possibility of photo-bleaching during the TA experiment. Lifetimes at a specific wavelength were extracted from kinetic fitting by using Surface Xplorer software from Ultrafast Systems.

2.5.3. Cytotoxicity Study

For cytotoxicity studies, HeLa (human cervical adenocarcinoma) and HepG2 (human liver hepatocellular carcinoma) were obtained from the American Type Culture Collection (ATCC ID: CCL-2 and HB-8065, respectively). HeLa cells were cultured in Dulbecco's Modified Eagles Medium (DMEM) and HepG2 cells were cultured in Minimum Essential Medium (MEM). Media were supplemented with 2 mM *L*-glutamine, 10 μg/mL streptomycin, 100 U/mL penicillin and 10% (v/v) fetal bovine serum (FBS) for both cell cultures. Cells were kept at 37 °C in a humid atmosphere of 10% CO_2. When cells were grown to 90 % confluency, cells were trypsinized for 5 mins in PBS and passaged 1:10 into a new tissue culture plate. Maximum number of passage was limited to no more than 10. Media and supplements were obtained from ThermoFisher.

2.5.3.1. *In vitro* Photodynamic Therapy Treatment

The photodynamic activity of the BODIPY was investigated by assaying the photo-induced cytotoxicity of hyaluronic acid (HA) conjugated BDP on HeLa cells.

HeLa cells were trypsinized to be detached from the cell culture plate. Cells were suspended in the medium, counted and seeded on flat bottom 96-well tissue culture plates at a density of 7,000 cells/well and rested for 24 to 48 hours at 37 °C in 10 % CO_2. HA-ExtBDP solution prepared fresh before each experiment. 10 mg of HA-ExtBDP was dissolved in 2 mL of PBS and filtered through 0.22 μm PES membrane to prepare sterile 5 mg/mL solution. After cells reached 70 % confluency on 96-well plate, the culture medium was removed and cells were treated with HA-ExtBDP or PBS at different concentrations in complete medium for 90 minutes or 180 minutes at 37 °C in 10 % CO_2 at dark conditions. After treatments, cells were washed with PBS at least twice to remove excess HA-ExtBDP. For photo-induced cytotoxicity assay, 100 μL of PBS buffer was added to the wells and one third of the plate was covered with aluminum foil as a control group. Rest of the plate were irradiated using a 10 W Red LED Lamp as a light source with an intensity of 14.2 mW cm^{-2} for 15 or 30 mins at room temperature. After irradiation, PBS buffer was removed from the wells and cells were incubated with a fresh medium for further 24 hours at dark conditions. After 24 hours, medium was replaced with 3-(4,5-dimethylthiazol-2-yl) 2,5-diphenyltetrazolium solution (MTT) (prepared as 1 mg/mL in medium) and cells were incubated for 3-4 hours at 37 °C to allow the formation of the MTT formazan. 96-well plate was spinned for 5 minutes to let the formazan settle at the bottom of the plate. MTT medium was discarded and formazan is

dissolved in 100 μL of DMSO. Purple color formation was observed and recorded using a plate reader at 540 nm.

2.5.3.2. *In vitro* Hyaluronic Acid Targeting Assay

HepG2 (CD44-) and HeLa (CD44+) cells trypsinized to be detached from the cell culture plate. HepG2 cells were labeled with 1μM of CellTracker Violet BMQC Dye (ThermoFisher) in PBS at RT for 15 mins. Fluorescently labeled HpeG2 cells washed with 10 excess volume of PBS and resuspended in fresh media. HepG2 and HeLa cells were mixed at different ratios and seeded on flat bottom 96-well tissue culture plates at a density of 15,000 cells/well. After 24 hours, cells were treated with HA-ExtBDP or PBS at different concentrations for 180 minutes at 37 °C in 10 % CO_2 at dark conditions. Treatment and the photo irradiation of the cells were carried out as described above. The next day, cells were trpsinized and transferred to a V-bottom 96-well plate to be analyzed by BD-FACS LSRFortessa- High Throughput Sampler (HTS) cell analyzer. Around 4,000 events were collected from each well. These events were gated for live cell population by forward scatter (FSC) and side scatter (SSC). Fluorescence of the HepG2 cells were measured with a 405nm laser and a 420LP emission filter. Thus, percentage of HepG2 was determined from the data as Violet positive cell population, whereas percentage of HeLa cells were determined as Violet negative. FlowJo V10 was used as the analysis platform for flow cytometry analysis.

2.5.4. Synthesis

2.5.4.1. Synthesis of Compound 1

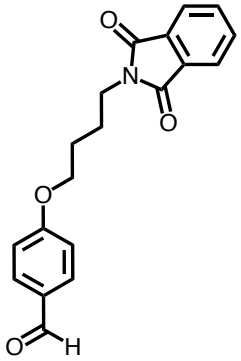

1

To a 2-neck 250 mL round bottom flask, 4-hydroxyaldehyde (5 g, 40.94 mmol), *N*-(4-bromobutyl)phthalimide (15 g, 53.23 mmol), potassium carbonate (14.15 g, 102.36 mmol) and 18-crown-6 (0.325 g, 1.23 mmol) were added. Argon was purged for a 10 min, followed by addition of toluene (160 mL). The reaction mixture was stirred at refluxing temperature for overnight. The solvent was evaporated in vacuo and the crude mixture was purified by silica gel column chromatography using ethyl acetate and hexane as eluents to yield 12.0 g (91%) of pure compound 1. ^{1}H-NMR (400 MHz; $CDCl_3$): δ 9.85 (s, 1H), 7.84-7.78 (m, 4H), 7.71-7.69 (m, 2H), 4.07 (t, J = 5.3 Hz, 2H), 3.76 (t, J = 6.3 Hz, 2H), 1.88-1.86 (m, 4H). ^{13}C-NMR (100 MHz, $CDCl_3$) δ 190.81, 168.60, 164.54, 160.74, 157.05, 144.72, 131.98, 129.72, 114.76, 37.63, 26.68, 25.36, 15.01

2.5.4.2. Synthesis of BDP

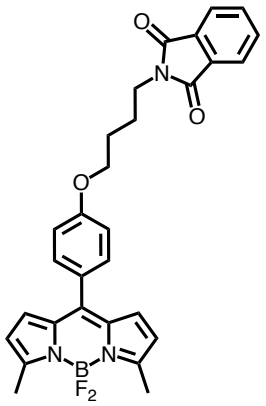

BDP

Compound 1 (0.8 g, 2.47 mmol) and methylpyrrole (0.4 g, 4.94 mmol) were dissolved in DCM (100 mL) under argon. 3 drops of TFA was added by syringe. The reaction was stirred for 3 hours. DDQ (1.09 g, 4.82 mmol) was added at once. The mixture was stirred for an additional hour. DIPEA (6.1 mL) was added, and after 5 min, BF_3OEt_2 (6.1 mL) was added. After 1 hour, the reaction mixture was washed with 1 N NaOH and brine. Organic solvents were evaporated and dried with sodium sulfate. The crude product was purified with automated flash chromatography by using ethyl acetate/hexane solvent system to yield 0.43 g (34%) of yellow crystal BDP. ^{1}H-NMR (400 MHz, $CDCl_3$): δ 7.88-7.86 (m, 2H), 7.75-7.73 (m, 2H) 7.44-7.42 (d, J = 9.1 Hz, 2H), 6.99-6.97 (d, J = 9.1 Hz, 2H), 6.76-6.75 (d, J = 6.2 Hz, 2H), 6.28-6.27 (d, J = 6.2 Hz, 2H), 4.09 (t, J = 7.5 Hz, 2H), 3.81 (t, J = 7.0 Hz, 2H), 2.66 (s, 6H) 1.94-1.90 (m, 4H). ^{13}C NMR (100 MHz, $CDCl_3$) δ 168.61, 160.77, 157.02, 142.81, 134.64, 134.14, 132.24, 132.16, 130.42, 126.66, 123.40, 119.28, 114.35, 67.49, 37.73, 26.66, 25.46, 15.00

2.5.4.3. Synthesis of BDP-Br

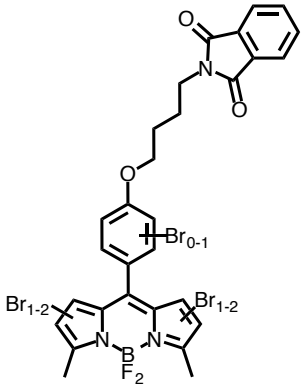

BDP-Br

A mixture of the BDP (200 mg, 0.38 mmol) and NBS (165 mg, 0.93 mmol) in hexafluoro-2-propanol (6.2 mL) was stirred at room temperature for 5 minutes. After reaction, the solvent was removed by evaporation. The residue was extracted with dichloromethane, washed with water, dried over sodium sulfate, and concentrated under reduced pressure. The crude product was further purified using column chromatography by using DCM and hexanes to afford the product mixture with various degree of bromine substitution from disubstitute to pentasubstitute. The mixture of brominated products were used as it is for further reactions. (Yield : 63%). ^{1}H-NMR (400 MHz, $CDCl_3$): δ 7.88-7.86 (m, 2H), 7.75-7.73 (m, 2H) 7.44-7.42 (d, *J* = 9.1 Hz, 2H), 6.99-6.97 (d, *J* = 9.1 Hz, 2H), 6.76-6.75 (d, *J* = 6.2 Hz, 2H), 6.28-6.27 (d, *J* = 6.2 Hz, 2H), 4.09 (t, *J* = 7.5 Hz, 2H), 3.81 (t, *J* = 7.0 Hz, 2H), 2.66 (s, 6H) 1.94-1.90 (m, 4H). ^{13}C-NMR (100 MHz, $CDCl_3$) δ 168.61, 160.63, 156.93, 155.39, 134.14, 132.26, 130.40, 124.16, 123.42, 122.95, 115.36, 113.40, 112.88, 67.47, 37.81, 26.74, 25.55, 14.49.

2.5.4.4. Synthesis of ExtBDP

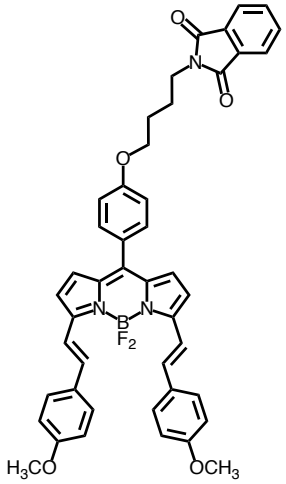

ExtBDP

BDP (0.4 g, 0.78 mmol) and 4-methoxybenzaldehyde (0.38 ml, 3.12 mmol) were dissolved in benzene (40 mL). Piperidine (0.6 mL) and glacial acetic acid (0.6 mL) were added. The solution was refluxed using Dean-Stark apparatus. When the solution was concentrated, the reaction was monitored by TLC until green-colored product became the major product. 20% ethyl acetate in hexanes was used for TLC monitoring. Benzene was evaporated by air blow. It was extracted with $CHCl_3$ and water. Organic layer was dried with sodium sulfate and evaporated under reduced pressure. The product was purified by silica gel column chromatography using ethyl acetate : hexane (20 %→40 %) as mobile phase. Fraction containing the product was collected then the solvent was removed under reduced pressure to yield 380 mg (65%) of ExtBDP. ^{1}H-NMR (400 MHz, $CDCl_3$): δ 7.80-7.78 (m, 2H), 7.67-7.65 (m, 2H) 7.61-7.52 (m, 6H), 7.39-7.37 (d, J = 9.1 Hz, 2H), 7.23-7.21 (d, J = 9.1 Hz, 2H), 6.93-6.86 (m, 6H) 6.83-6.82 (d, J = 8.4Hz, 2H), 6.75-6.74 (d, J = 8.4 Hz, 2H), 4.02 (t, J = 7.5 Hz, 2H), 3.79 (s, 6H), 3.74 (t, J= 7.0 Hz, 2H), 1.94-1.80 (m, 4H). ^{13}C-NMR (100 MHz, $CDCl_3$): δ 168.63, 160.62, 158.34, 154.60, 148.04, 136.02, 134.14,

132.25, 132.12, 129.90, 129.66, 129.23, 123.40, 117.58, 115.90, 114.45, 114.42, 114.19, 113.77, 67.50, 55.54, 37.75, 26.69, 25.48

2.5.4.5. Synthesis of ExtBDP-Br

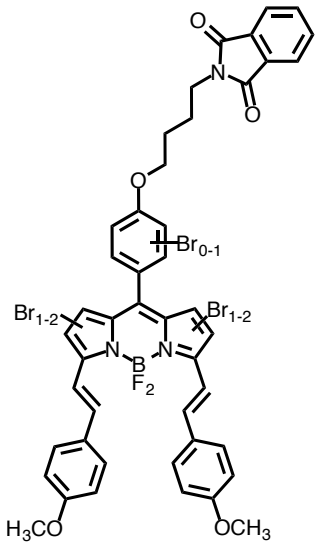

ExtBDP-Br

BDP-Br (200 mg, 0.324 mmol) and 4-methoxybenzaldehyde (0.16 mL, 1.296 mmol) were dissolved in toluene (32 mL). Piperidine (0.24 mL) and glacial AcOH (0.24 mL) were added. The solution was refluxed with Dean-Stark apparatus. When the solution was concentrated, the reaction was monitored by TLC until the product spot becomes major spot. Ethyl acetate/hexanes (40 %) was used to monitor TLC. Toluene was evaporated and dissolved in chloroform again. Organic layer is washed with water. Organic layers were collected and dried with sodium sulfate, and evaporated under reduced pressure. Crude is purified with column chromatography to yield 183 mg (68%)

of ExtBDP-Br. ^{1}H-NMR (400 MHz, $CDCl_3$): δ 7.90-7.85 (m, 2H), 7.74-7.71 (m, 2H) 7.62-7.54 (m, 4H), 7.52-7.43 (m, 2H), 7.16-7.14 (d, J = 9.1 Hz, 2H), 7.01-6.88 (m, 6H) , 6.75-6.74 (d, J = 8.4 Hz, 2H), 4.18-4.07 (m, 2H), 3.85 (s, 6H), 3.82 (m, 2H), 2.01-1.80 (m, 4H). ^{13}C-NMR (100 MHz, $CDCl_3$): δ 168.60, 161.34, 161.23, 160.71, 160.55, 159.84, 134.14, 132.27, 131.39, 129.76, 129.69, 129.24, 129.12, 123.41, 115.29, 114.56, 114.53, 114.41, 114.37, 55.54, 51.63, 37.78, 26.00, 25.50.

2.5.4.6. General Procedure for Deprotection of Phthalimide on BDP Derivatives

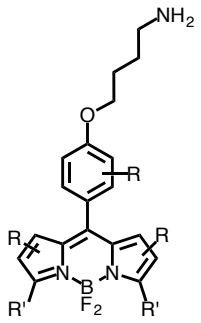

NH_2-BDP, R= -H, R'= $-CH_3$
NH_2-BDP-Br, R= $-Br_{2-5}$, R'= $-CH_3$

NH_2-ExtBDP, R= -H, R'= 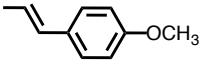

NH_2-ExtBDP-Br, R= $-Br_{2-5}$, R'= 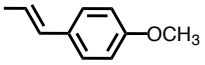

Hydrazine monohydrate (0.7 mL, 14.43 mmol) was added to a desired BDP compound (0.29 mmol) in ethanol, and the mixture was refluxed for 3.5 hours. Upon cooling to room temperature, a precipitate formed. The precipitate was filtered and the filtrate was concentrated. After sample purification on TLC, successful deprotection of

phthalimide group was confirmed by ^{1}H-NMR spectrum of NH_2-BDP. For other BODIPYs, residual water was evaporated completely using lyophilizer and the reaction crude was used for next step without further purification. NH_2-BDP ^{1}H-NMR (400 MHz, CD_3OD): δ 7.53-7.51 (ddd, *J* = 8.9, 1.9, 0.5 Hz 2H), 7.12-7.10 (ddd, *J* = 8.9, 1.9, 0.5 Hz, 2H), 6.81-6.80 (d, *J* = 6.2 Hz, 2H), 6.38-6.37 (d, *J* = 6.2 Hz, 2H), 3.04 (t, *J* = 7.3 Hz, 2H), 3.81 (t, *J*= 7.0 Hz, 2H), 2.66 (s, 6H) 2.00-1.86 (m, 6H). ^{13}C-NMR (100 MHz, $(CD_3)_2SO$): δ 161.01, 156.62, 142.79, 133.99, 132.89, 132.62, 130.89, 120.18, 114.99, 67.89, 55.89, 31.26, 26.31, 14.73.

2.5.4.7. General Procedure for BODIPY-functionalized Hyaluronic Acid

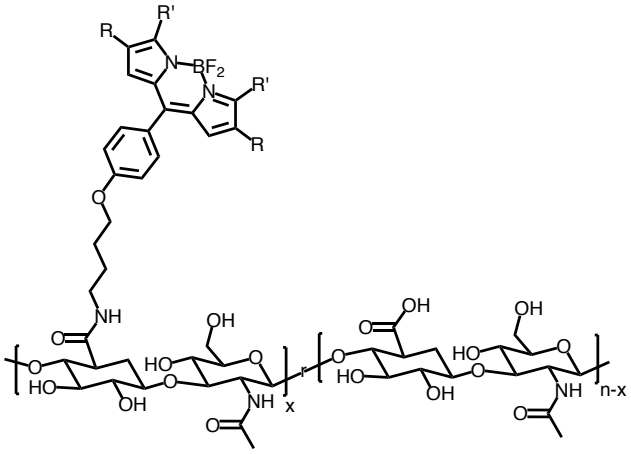

BODIPY-functionalized Hyaluronic Acid

Hyaluronic acid (HA) (0.46 mmol) was dissolved in deionized water at concentration 8 mg/mL. NH_2- BDP (0.046 mmol) was dissolved in 4 mL of acetonitrile:water (1:1) to the HA solution. Obtained mixture was stirred until complete dissolution of the reagent. *N*-hydroxybenzotriazole (HOBt) (0.46 mmol) was separately

dissolved in 13 mL of a 1:1 (v/v) mixture of acetonitrile-water (0.2 M) and added to the reaction mixture. HOBt is insoluble in 0.2 M of acetonitrile-water (1:1) mixture. The pH of the resultant solution was adjusted to 4.7 after, which the coupling reaction was initiated by addition of solid EDC (0.138 mmol) to the reaction mixture. The mixture was stirred overnight. The pH of the reaction solution was slightly increasing during this time, which evidenced the coupling of the reagents to HA carboxylates. After 24 hours of reaction, the reaction mixture was concentrated. Unreacted free BODIPY and reagents are dialyzed against organic solvent mixture of dichloromethane, acetonitrile and acetone for 3 days. The degree of BODIPY substitution was determined by UV absorption spectroscopy.

2.6. Reference

(1) Gorman, A.; Killoran, J.; O'Shea, C.; Kenna, T.; Gallagher, W. M.; O'Shea, D. F. In Vitro Demonstration of the Heavy-Atom Effect for Photodynamic Therapy. *J. Am. Chem. Soc.* **2004**, *126* (34), 10619–10631.

(2) Kochevar, I. E.; Redmond, R. W. Photosensitized Production of Single Oxygen. *Methods Enzymol.* **2000**, *319*, 20–28.

(3) Chen, X.; Li, Y.; Wang, A.; Zhou, L.; Lu, S.; Zhou, J.; Lin, Y.; Wei, S. Protonation Salt Derivative with Heavy-Atom Effect on Phthalocyanine for Enhanced in Vitro Photodynamic Therapy. *Dye. Pigment.* **2015**, *114* (C), 93–104.

(4) Yogo, T.; Urano, Y.; Ishitsuka, Y.; Maniwa, F.; Nagano, T. Highly Efficient and Photostable Photosensitizer Based on BODIPY Chromophore. *J. Am. Chem. Soc.* **2005**, *127* (35), 12162–12163.

(5) Rodriguez-Serrano, A.; Rai-Constapel, V.; Daza, M. C.; Doerr, M.; Marian, C. M.

Internal Heavy Atom Effects in Phenothiazinium Dyes: Enhancement of Intersystem Crossing via Vibronic Spin-Orbit Coupling. *Phys. Chem. Chem. Phys.* **2015**, *17* (17), 11350–11358.

(6) Cui, G.; Fang, W. H. State-Specific Heavy-Atom Effect on Intersystem Crossing Processes in 2-Thiothymine: A Potential Photodynamic Therapy Photosensitizer. *J. Chem. Phys.* **2013**, *138* (4).

(7) Turro, N. J. The Triplet State. *J. Chem. Educ.* **1966**, *46* (1), 2–6.

(8) McClure, D. S. Spin-Orbit Interaction in Aromatic Molecules. *J. Chem. Phys.* **1952**, *20* (4), 682.

(9) Lower, S.; El-Sayed, M. The Triplet State and Molecular Electronic Processes in Organic Molecules. *Chem. Rev.* **1966**, *66* (2), 199–241.

(10) Levine, I. N. Quantum Chemistry; Allyn and Bacon: Boston, 1970; pp 306–310.

(11) McClure, D. S. Triplet-Singlet Transitions in Organic Molecules. Lifetime Measurements of the Triplet State. *J. Chem. Phys.* **1949**, *17* (10), 905.

(12) Ermolaev, V. L.; Svitasbev, K. K. Quantum Yields of Phosphorescence and Fluorescence of Some 1-Derivatives of Naphthalene in Solutions at -196˚C.pdf. *Opt. Spectrosc.* **1959**, *1*, 399.

(13) Cowan, D. O. Elements of Organic Photochemistry. In *Elements of Organic Photochemistry*; Plenum Press: New York, N.Y., 1976; pp 250–262.

(14) Chock, P. B.; Stadtman, E. R. Superiority of Interconvertible Enzyme Cascades in Metabolite Regulation: Analysis of Multicyclic Systems. *Proc Natl Acad Sci U S A* **1977**, *74* (7), 2766–2770.

(15) Koshland, D. E.; Goldbeter, A.; Stock, J. B. Amplification and Adaptation in

Regulatory and Sensory Systems Author (S): Daniel E . Koshland , Albert Goldbeter and Jeffry B . Stock Published by : American Association for the Advancement of Science Stable URL : http://www.jstor.org/stable/1689499 JS. **2017**, *217* (4556), 220–225.

(16) Chock, P. B.; Rhee, S. G.; Stadtman, E. R. Interconvertible Enzyme Cascades in Cellular-Regulation. *Annu. Rev. Biochem.* **1980**, *49*, 813–843.

(17) Bhalla and Ravi Iyengar, U. S. Emergent Properties of Networks of Biological Signaling Pathways. *Science (80-.).* **1999**, *283* (5400), 381–387.

(18) Weng, G. Complexity in Biological Signaling Systems. *Science (80-.).* **1999**, *284* (5411), 92–96.

(19) Jordan, J. D.; Landau, E. M.; Iyengar, R. Signaling Networks: The Origins of Cellular Multitasking. *Cell* **2000**, *103* (2), 193–200.

(20) Levine, S. N. Enzyme Amplifier Kinetics. *Science (80-.).* **1966**, *152* (3722), 651–653.

(21) Wald, G. Visual Excitation and Blood Clotting. *Science* **1965**, *150* (3699), 1028–1030.

(22) Brown, G. C.; Hoek, J. B.; Kholodenko, B. N. Why Do Protein Kinase Cascades Have More than One Level? *Trends Biochem. Sci.* **1997**, *22*, 288.

(23) Fozooni, T.; Ravan, H.; Sasan, H. Signal Amplification Technologies for the Detection of Nucleic Acids: From Cell-Free Analysis to Live-Cell Imaging. *Appl. Biochem. Biotechnol.* **2017**, 1–30.

(24) Wu, W.; Bazan, G. C.; Liu, B. Conjugated-Polymer-Amplified Sensing, Imaging, and Therapy. *Chem* **2017**, *2* (6), 760–790.

(25) Mittal, S.; Kaur, H.; Gautam, N.; Mantha, A. K. Biosensors for Breast Cancer Diagnosis: A Review of Bioreceptors, Biotransducers and Signal Amplification Strategies. *Biosens. Bioelectron.* **2017**, *88*, 217–231.

(26) Dewit, M. A.; Nazemi, A.; Karamdoust, S.; Beaton, A.; Gillies, E. R. Design, Synthesis and Assembly of Self-Immolative Linear Block Copolymers. *Non-Coventional Funct. Block Copolym.* **2011**, 9–21.

(27) Li, Y.; Liu, G.; Wang, X.; Hu, J.; Liu, S. Enzyme-Responsive Polymeric Vesicles for Bacterial-Strain-Selective Delivery of Antimicrobial Agents. *Angew. Chemie - Int. Ed.* **2016**, *55* (5), 1760–1764.

(28) Liu, G.; Wang, X.; Hu, J.; Zhang, G.; Liu, S. Self-Immolative Polymersomes for High-Efficiency Triggered Release and Programmed Enzymatic Reactions. *J. Am. Chem. Soc.* **2014**, *136* (20), 7492–7497.

(29) Sauer, M.; Haefele, T.; Graff, a; Nardin, C.; Meier, W. Ion-Carrier Controlled Precipitation of Calcium Phosphate in Giant ABA Triblock Copolymer Vesicles. *Chem. Commun. (Camb).* **2001**, No. 23, 2452–2453.

(30) Sceince, P. Polymer Vesicles. *Science (80-.).* **2005**, *297* (17), 967–974.

(31) Wu, J.; Eisenberg, A. Proton Diffusion across Membranes of Vesicles of Poly(styrene-B-Acrylic Acid) Diblock Copolymers. *J. Am. Chem. Soc.* **2006**, *128* (9), 2880–2884.

(32) Gabrielli, L.; Mancin, F. Minimal Self-Immolative Probe for Multimodal Fluoride Detection. *J. Org. Chem.* **2016**, *81* (22), 10715–10720.

(33) Amir, R. J.; Pessah, N.; Shamis, M.; Shabat, D. Self-Immolative Dendrimers. *Angew. Chemie - Int. Ed.* **2003**, *42* (37), 4494–4499.

(34) Shamis, M.; Shabat, D. Single-Triggered AB6 Self-Immolative Dendritic Amplifiers. *Chemistry* **2007**, *13* (16), 4523–4528.

(35) Tan, X.; Li, B. B.; Lu, X.; Jia, F.; Santori, C.; Menon, P.; Li, H.; Zhang, B.; Zhao, J. J.; Zhang, K. Light-Triggered, Self-Immolative Nucleic Acid-Drug Nanostructures. *J. Am. Chem. Soc.* **2015**, *137* (19), 6112–6115.

(36) Niculescu-Duvaz, I.; Niculescu-Duvaz, D.; Friedlos, F.; Spooner, R.; Martin, J.; Marais, R.; Springer, C. J. Self-Immolative Nitrogen Mustard Prodrugs for Suicide Gene Therapy. *J. Med. Chem.* **1998**, *41* (13), 5297–5309.

(37) De Groot, F. M. H.; Albrecht, C.; Koekkoek, R.; Beusker, P. H.; Scheeren, H. W. "Cascade-Release Dendrimers" liberate All End Groups upon a Single Triggering Event in the Dendritic Core. *Angew. Chemie - Int. Ed.* **2003**, *42* (37), 4490–4494.

(38) Shamis, M.; Lode, H. N.; Shabat, D. Bioactivation of Self-Immolative Dendritic Prodrugs by Catalytic Antibody 38C2. *J. Am. Chem. Soc.* **2004**, *126* (6), 1726–1731.

(39) Dresselhaus, M.S.; Thomas, I. . Alternative Energy Technologies. *Nature* **2001**, *414* (November), 332–337.

(40) Gregg, B. A.; Hanna, M. C. Comparing Organic to Inorganic Photovoltaic Cells: Theory, Experiment, and Simulation. *J. Appl. Phys.* **2003**, *93* (6), 3605–3614.

(41) https://energy.gov/eere/solar/downloads/research-cell-efficiency-records.

(42) Potscavage, W. J.; Sharma, a; Kippelen, B. Critical Interfaces in Organic Solar Cells and Their Influence on the Open-Circuit Voltage. *Acc. Chem. Res.* **2009**, *42* (11), 1758–1767.

(43) Carsten, B.; Szarko, J. M.; Son, H. J.; Wang, W.; Lu, L.; He, F.; Rolczynski, B. S.;

Lou, S. J.; Chen, L. X.; Yu, L. Examining the Effect of the Dipole Moment on Charge Separation in Donor-Acceptor Polymers for Organic Photovoltaic Applications. *J. Am. Chem. Soc.* **2011**, *133* (50), 20468–20475.

(44) Yao, K.; Intemann, J. J.; Yip, H.-L.; Liang, P.-W.; Chang, C.-Y.; Zang, Y.; Li, Z.; Chen, Y.; Jen, A. K.-Y. Efficient All Polymer Solar Cells from Layer-Evolved Processing of a Bilayer Inverted Structure. *J. Mater. Chem. C* **2014**, *2* (3), 416.

(45) Takacs, C. J.; Sun, Y.; Welch, G. C.; Perez, L. A.; Liu, X.; Wen, W.; Bazan, G. C.; Heeger, A. J. Solar Cell Efficiency, Self-Assembly, and Dipole-Dipole Interactions of Isomorphic Narrow-Band-Gap Molecules. *J. Am. Chem. Soc.* **2012**, *134* (40), 16597–16606.

(46) Beaujuge, P. M.; Fréchet, J. M. J. Molecular Design and Ordering Effects in π-Functional Materials for Transistor and Solar Cell Applications. *J. Am. Chem. Soc.* **2011**, *133* (50), 20009–20029.

(47) Kallmann, H.; Pope, M. Photovoltaic Effect in Organic Crystals. *J. Chem. Phys.* **1959**, *30* (2), 585–586.

(48) Benanti, T. L.; Venkataraman, D. Organic Solar Cells: An Overview Focusing on Active Layer Morphology. *Photosynth. Res.* **2006**, *87* (1), 73–81.

(49) Yu, G.; Pakbaz, K.; Heeger, A. J. Semiconducting Polymer Diodes: Large Size, Low Cost Photodetectors with Excellent Visible-Ultraviolet Sensitivity. *Appl. Phys. Lett.* **1994**, *64* (25), 3422–3424.

(50) Dang, M. T.; Hirsch, L.; Wantz, G. P3HT:PCBM, Best Seller in Polymer Photovoltaic Research. *Adv. Mater.* **2011**, *23* (31), 3597–3602.

(51) Wu, P. T.; Xin, H.; Kim, F. S.; Ren, G.; Jenekhe, S. A. Regioregular poly(3-

Pentylthiophene): Synthesis, Self-Assembly of Nanowires, High-Mobility Field-Effect Transistors, and Efficient Photovoltaic Cells. *Macromolecules* **2009**, *42* (22), 8817–8826.

(52) Gabe, Y.; Ueno, T.; Urano, Y.; Kojima, H.; Nagano, T. Tunable Design Strategy for Fluorescence Probes Based on 4-Substituted BODIPY Chromophore: Improvement of Highly Sensitive Fluorescence Probe for Nitric Oxide. *Anal. Bioanal. Chem.* **2006**, *386* (3), 621–626.

(53) Li, Y.; Wang, J.; Zhang, X.; Guo, W.; Li, F.; Yu, M.; Kong, X.; Wu, W.; Hong, Z. Highly Water-Soluble and Tumor-Targeted Photosensitizers for Photodynamic Therapy. *Org. Biomol. Chem.* **2015**, *13* (28), 7681–7694.

(54) Gee, K. R.; Archer, E. A.; Kang, H. C. 4-Sulfotetrafluorophenyl (STP) Esters: New Water-Soluble Amine-Reactive Reagents for Labeling Biomolecules. *Tetrahedron Lett.* **1999**, *40* (8), 1471–1474.

(55) Hendel, S. J.; Poe, A. M.; Khomein, P.; Bae, Y.; Thayumanavan, S.; Young, E. R. Photophysical and Electrochemical Characterization of BODIPY-Containing Dyads Comparing the Influence of an A–D–A versus D–A Motif on Excited-State Photophysics. *J. Phys. Chem. A* **2016**, *120*, 8794–8803.

(56) Gollnick, K.; Griesbeck, A. Singlet Oxygen Photooxygenation of Furans. *Tetrahedron* **1985**, *41* (11), 2057–2068.

(57) Morone, M.; Beverina, L.; Abbotto, A.; Silvestri, F.; Collini, E.; Ferrante, C.; Bozio, R.; Pagani, G. A. Enhancement of Two-Photon Absorption Cross-Section and Singlet-Oxygen Generation in Porphyrins upon ??-Functionalization with Donor-Acceptor Substituents. *Org. Lett.* **2006**, *8* (13), 2719–2722.

(58) Deng, P.; Zhang, Q. Recent Developments on Isoindigo-Based Conjugated Polymers. *Polym. Chem.* **2014**, *5* (10), 3298–3305.

(59) Lin, Y.; Li, Y.; Zhan, X. Small Molecule Semiconductors for High-Efficiency Organic Photovoltaics. *Chem. Soc. Rev.* **2012**, *41* (11), 4245.

(60) Zhang, Z.; Wang, J. Structures and Properties of Conjugated Donor–Acceptor Copolymers for Solar Cell Applications. *J. Mater. Chem.* **2012**, *22* (10), 4178.

(61) Zhou, H.; Yang, L.; You, W. Rational Design of High Performance Conjugated Polymers for Organic Solar Cells. *Macromolecules* **2012**, *45* (2), 607–632.

(62) Hou, J.; Huo, L.; He, C.; Yang, C.; Li, Y. Synthesis and Absorption Spectra of poly(3-(Phenylenevinyl)thiophene)s with Conjugated Side Chains. *Macromolecules* **2006**, *39* (2), 594–603.

(63) Hou, J.; Tan, Z.; Yan, Y.; He, Y.; Yang, C.; Li, Y. Synthesis and Photovoltaic Properties of Two-Dimensional Conjugated Polythiophenes with Bi(thienylenevinylene) Side Chains. *J. Am. Chem. Soc.* **2006**, *128* (14), 4911–4916.

(64) He, G.; Li, Z.; Wan, X.; Liu, Y.; Zhou, J.; Long, G.; Zhang, M.; Chen, Y. Impact of Dye End Groups on Acceptor–donor–acceptor Type Molecules for Solution-Processed Photovoltaic Cells. *J. Mater. Chem.* **2012**, *22* (18), 9173.

(65) Liu, J.; Walker, B.; Tamayo, A.; Zhang, Y.; Nguyen, T. Q. Effects of Heteroatom Substitutions on the Crystal Structure, Film Formation, and Optoelectronic Properties of Diketopyrrolopyrrole-Based Materials. *Adv. Funct. Mater.* **2013**, *23* (1), 47–56.

(66) Yuan, J.; Huang, X.; Zhang, F.; Lu, J.; Zhai, Z.; Di, C.; Jiang, Z.; Ma, W. Design

of Benzodithiophene-Diketopyrrolopyrrole Based Donor–acceptor Copolymers for Efficient Organic Field Effect Transistors and Polymer Solar Cells. *J. Mater. Chem.* **2012**, *22* (42), 22734.

(67) Sonar, P.; Ng, G.-M.; Lin, T. T.; Dodabalapur, A.; Chen, Z.-K. Solution Processable Low Bandgap Diketopyrrolopyrrole (DPP) Based Derivatives: Novel Acceptors for Organic Solar Cells. *J. Mater. Chem.* **2010**, *20* (18), 3626.

(68) Della Pelle, A. M.; Homnick, P. J.; Bae, Y.; Lahti, P. M.; Thayumanavan, S. Effect of Substituents on Optical Properties and Charge-Carrier Polarity of Squaraine Dyes. *J. Phys. Chem. C* **2014**, *118* (4), 1793–1799.

(69) Huang, X.; Zhu, C.; Zhang, S.; Li, W.; Guo, Y.; Zhan, X.; Liu, Y.; Bo, Z. Porphyrin-Dithienothiophene π-Conjugated Copolymers: Synthesis and Their Applications in Field-Effect Transistors and Solar Cells. *Macromolecules* **2008**, *41* (19), 6895–6902.

(70) Benniston, A. C.; Copley, G. Lighting the Way Ahead with Boron Dipyrromethene (Bodipy) Dyes. *Phys. Chem. Chem. Phys.* **2009**, *11* (21), 4124.

(71) Oosterhout, S. D.; Savikhin, V.; Zhang, J.; Zhang, Y.; Burgers, M. A.; Marder, S. R.; Bazan, G. C.; Toney, M. F. Mixing Behavior in Small Molecule:Fullerene Organic Photovoltaics. *Chem. Mater.* **2017**, *29* (7), 3062–3069.

(72) Carlé, J. E. Polymers for Organic Photovoltaics Based on 1,5-bis(2-Hexyldecyloxy)-Naphthalene, Thiophene, and Benzothiadiazole. *J. Photonics Energy* **2011**, *1* (1), 11111.

(73) Guo, X.; Watson, M. D. Conjugated Polymers from Napthalene Bisimide. *Org. Lett.* **2008**, *10* (23), 5333–5336.

(74) Eggert Carlé, J.; Wenzel Andreasen, J.; Jørgensen, M.; Christian Krebs, F. Low Band Gap Polymers Based on 1,4-Dialkoxybenzene, Thiophene, Bithiophene Donors and the Benzothiadiazole Acceptor. *Sol. Energy Mater. Sol. Cells* **2010**, *94* (5), 774–780.

(75) Poe, A. M.; Della Pelle, A. M.; Subrahmanyam, A. V.; White, W.; Wantz, G.; Thayumanavan, S. Small Molecule BODIPY Dyes as Non-Fullerene Acceptors in Bulk Heterojunction Organic Photovoltaics. *Chem. Commun.* **2014**, *50* (22), 2913–2915.

(76) Matsumura, S.; Hlil, A. R.; Lepiller, C.; Gaudet, J.; Guay, D.; Shi, Z.; Holdcroft, S.; Hay, A. S. Ionomers for Proton Exchange Membrane Fuel Cells with Sulfonic Acid Groups on the End-Groups: Novel Branched Poly(ether-Ketone)s. *Am. Chem. Soc. Polym. Prepr. Div. Polym. Chem.* **2008**, *49* (1), 511–512.

(77) Wakim, S.; Beaupré, S.; Blouin, N.; Aich, B.-R.; Rodman, S.; Gaudiana, R.; Tao, Y.; Leclerc, M. Highly Efficient Organic Solar Cells Based on a poly(2,7-Carbazole) Derivative. *J. Mater. Chem.* **2009**, *19* (30), 5351.

(78) Goud, T. V.; Tutar, A.; Biellmann, J. F. Synthesis of 8-Heteroatom-Substituted 4,4-Difluoro-4-Bora-3a,4a-Diaza-S-Indacene Dyes (BODIPY). *Tetrahedron* **2006**, *62* (21), 5084–5091.

(79) Rakstys, K.; Paek, S.; Gao, P.; Gratia, P.; Marszalek, T.; Grancini, G.; Cho, K. T.; Genevicius, K.; Jankauskas, V.; Pisula, W.; et al. Molecular Engineering of Face-on Oriented Dopant-Free Hole Transporting Material for Perovskite Solar Cells with 19% PCE. *J. Mater. Chem. A* **2017**, *5* (17), 7811–7815.

CHAPTER 3

BENZYL CARBAMATE-BASED SELF-IMMOLATIVE POLYMERS FOR SIGNAL AMPLIFICATION

3.1. Introduction

In the field of molecular amplification, self-immolative materials have been widely used for various applications including drug delivery systems, biomarker detections, imaging and sensing in biological applications. The traditional molecular structures of self-immolative materials are focused on either linear polymers with reporter unit on each monomeric molecules or dendritic molecules with reporters on its periphery functionality. Common strategy to improve signal amplification on these systems include synthetic changes: high degree of polymerization and synthesis of high generation of dendritic systems are necessary to achieve more reporter groups released upon triggering stimuli. This linear amplification depends on degree of polymerization or dendrimer generation often limit the development towards rapid and reliable molecular signal amplification. To achieve reliable amplification, the system is required to have rapid respond with dramatic signal output upon molecular level of stimuli. A signal amplification system, consisting of two different polymers with counter ionic functionality, where one of them possesses self-degradation property upon triggering stimuli, could demonstrate gel-to-sol transition upon stimuli trigger, resulting a morphological change as a read-out signal.

3.2. Design and Hypothesis

In this project, non-linearly amplified signal amplification was designed by combination of self-immolative polymer with previously unexplored strategy, where molecular-scale signal is amplified into macroscopic phase transition. The designed system produces a gel-like morphology under given conditions, then is capable of degradation upon application of a specific stimuli, inducing a macroscale morphological change to a solution-like state. The design of the self-immolative polymer includes a carbamate backbone with a light-sensitive trigger at one terminus of the polymer. Once the moiety of the light-sensitive trigger is cleaved, one end of the polymer backbone gets deprotected revealing its self-degradable functional group. Deprotection promotes depolymerization of backbone into monomers and carbon dioxide byproducts (Figure 3.1).

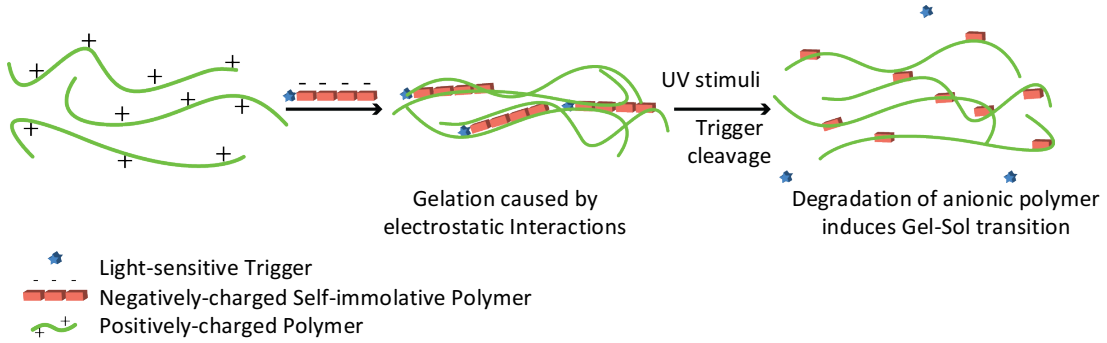

Figure 3.1 Illustration of supramolecular design of signal amplification through self-immolative degradation of electrostatic gels upon stimuli of UV light.

The polymer structure was designed with the aim of demonstrating a stimuli-induced morphological read out, where the molecular level signal and self-immolation is amplified into macroscopic level. The initial gelation of these materials is achieved by mixing positively charged molecules with the negatively charged functional group

introduced on the self-immolative polymer chains. The blending of two polymers with opposite charges can form a gel-like morphology, induced by electrostatic interactions. Once the negatively-charged polymer, undergoes light-induced degradation, the morphology of the mixture could go back to solution-like morphology, which produce gel-sol transition as a read out (Figure 3.2).

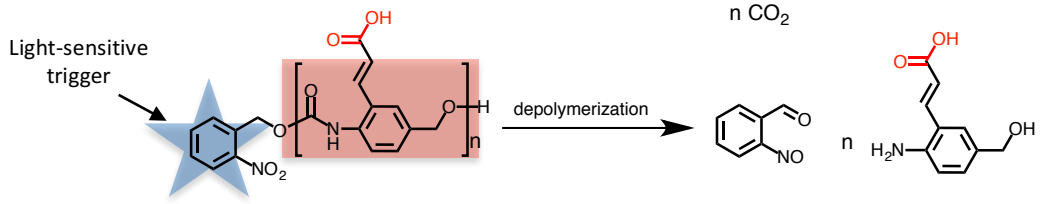

Figure 3.2 Chemical scheme of depolymerization of carbamate-based polymers, bearing light-sensitive trigger, upon UV light exposure. The degradation process generates CO_2, small molecular derivative of degraded polymer backbone and aldehyde byproduct from cleaved endcap trigger moiety.

3.3. Results and Discussion

3.3.1. Synthesis

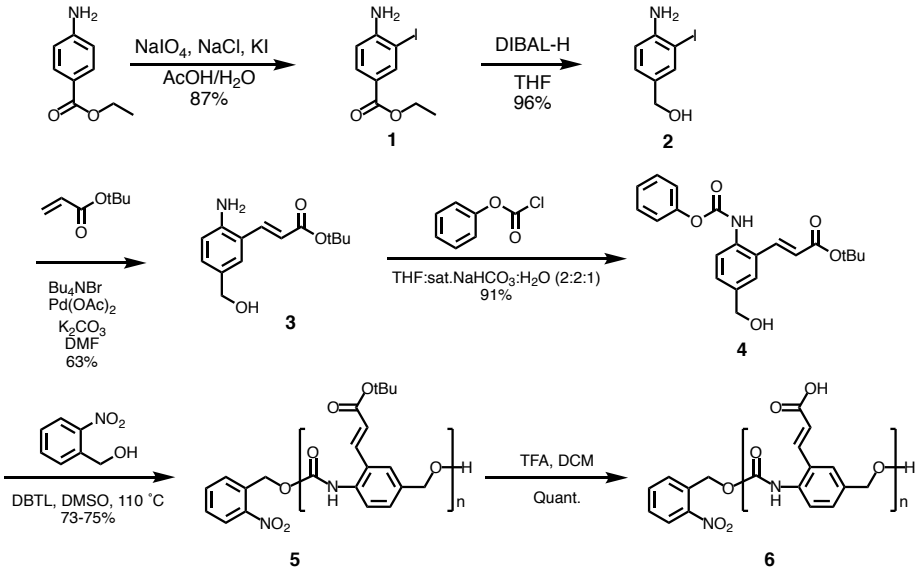

Scheme 3.1 Synthetic scheme of carbamate-based self-immolative polymer (P-).

Synthesis of the self-immolative polymer started from 4-amino ethyl benzoate, which was iodonated by reaction with sodium iodate to form **1**, then ethyl benzoate was reduced using DIBAL-H to produce **2** (Scheme 3.1). At this step, the side chain functionality of interest was installed using the Heck coupling reaction to produce monomer precursor **3**. Then, reaction with free amine and chloroformate produced monomer **4**. The monomer was highly purified for polymerization to avoid introducing impurity in the middle of polymer backbone, which could potentially stop the depolymerization process and thus impact the signal amplification properties. The side-chain protected polymer **5** was achieved by using DBTL and end-capped with *o*-nitrobenzylalcohol. Finally, the designed polymer **6** was obtained after deprotection of *tert*-butyl group in the presence of acid, generating a carboxylate-functionalized self-immolative polymer.

3.3.2. Characterization of Degradation by ^{1}H NMR and UV/vis Absorption Spectroscopy

^{1}H NMR spectroscopy was used to analyze the degradation of the synthesized polymer as a function of UV treatment time. Because *tert*-butyl protected carboxylate polymer **5** provided a clear NMR spectrum, this precursor was used for ^{1}H NMR studies. We assumed this would reasonable to characterize light-induced degradation, as the depolymerization occurs through the backbone of the polymer, and side chains are not expected to participate and therefore should not impact this characterization. The polymer was characterized by ^{1}H NMR prior to UV treatment, and the degree of polymerization and trigger capping percentile of the polymer chains were found to be seven and 100 %, respectively. THF-*d*8 was used as a standard solvent. Upon UV light

exposure, all peaks of the polymer except the side chain *tert*-butyl peak show modifications such as shifts and splits, which indicates successful degradation of the polymer.

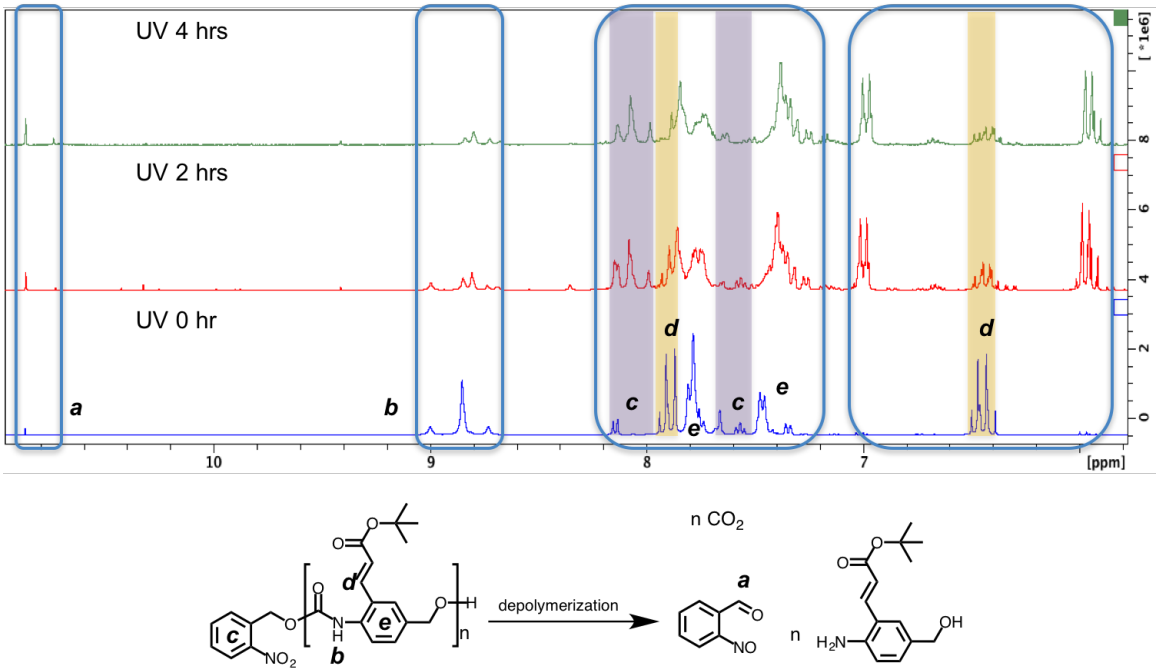

Figure 3.3 Characterization of degradation by ^{1}H NMR spectra (magnified 11 ~ 6 ppm) of carbamate-based self-immolative polymer upon UV light exposure. Before any treatment (bottom), UV treatment for 2 hours (middle), and 4 hours (top) are shown here.

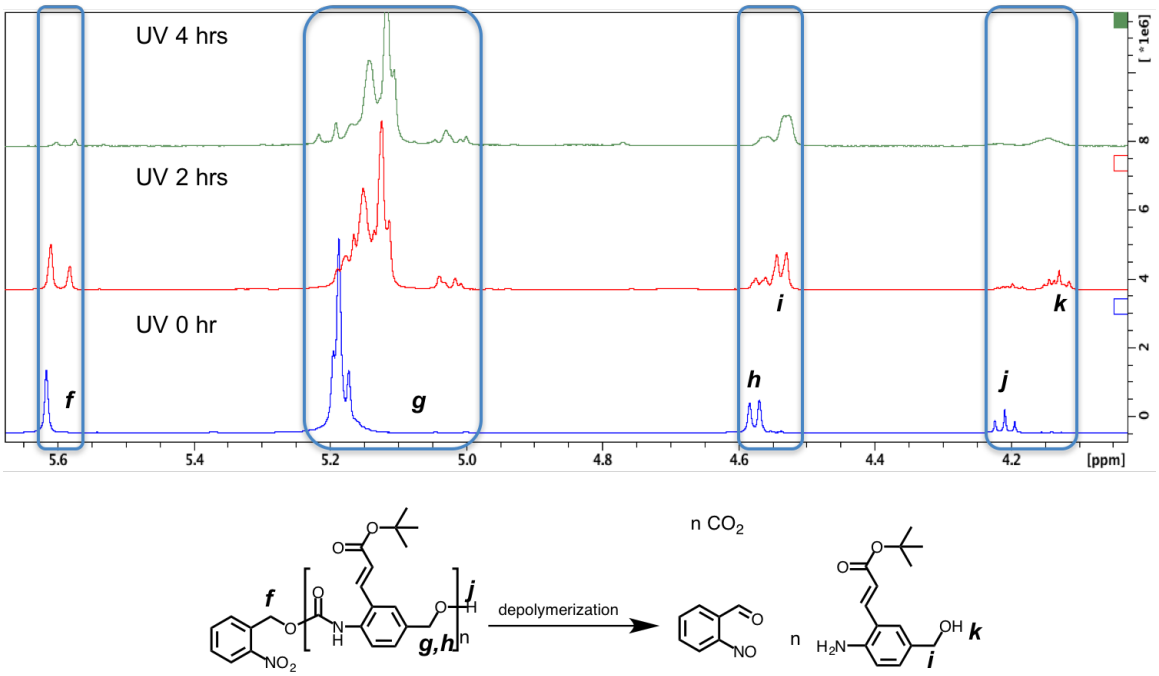

Figure 3.4 Characterization of degradation by ^{1}H NMR spectra (magnified 5.6 ~ 4.3 ppm) of carbamate-based self-immolative polymer upon UV light exposure over time. Before any treatment (bottom), UV treatment for 2 hours (middle), and 4 hours (top) are shown here.

Detailed spectra before and after UV treatment are shown in Figure 3.3 and Figure 3.4. As UV treatment time increases, a small new peak (***a***) appears at 10.9 ppm, which corresponds to the aldehyde byproduct formed from the cleaved light sensitive end cap units. This result supports the expectation that light sensitive *o*-nitrobenzyl functionality is cleaved under UV irradiation, initiating the self-immolative cascade reaction. Furthermore, most of polymer peaks showed dramatic changes in their multiplicity and chemical shift with time of UV light exposure. The peak corresponding to carbamate (8.9 ppm, ***b***) starts to lose its clear splitting pattern and eventually disappears. Aromatic protons of *o*-nitrobenzylcarbamate (***c***) are marked with a purple region in Figure 3.3. They show a complex change as it produces another set of aromatic peaks that belong to the *o*-nitrobenzaldehyde byproduct upon degradation. A similar

trend was observed in the aromatic protons (***e***) that belong to the polymer backbone. In both cases, deformation of splitting patterns as well as changes in chemical shift were observed. Alkene peaks at 6.5 ppm (***d***) exhibited dramatic changes with a new set of alkene peaks, corresponding to p-aminobenzylalcohol, appearing at 7.0 and 6.0 ppm, while its original peaks disappear. The terminal benzylic proton (***f***), which is associated with light sensitive trigger moiety, decreased and eventually disappeared after 7 hours of UV exposure (data not shown). This justified the assumption that the light sensitive trigger moieties at the polymer terminus could be cleaved completely. Benzylic protons display two distinctive peaks at 4.6 ppm corresponding to the terminal benzylic proton (***h***) next to alcohol and at 5.2 ppm corresponding to all other benzylic protons (***g***) on the polymer backbone. Upon UV exposure, benzylic protons on the polymer backbone (***g***) showed not only change in chemical shift, but also a widening of peak range with complex multiplicity as the polymer solution contained a random mixture of oligomers of various lengths during the depolymerization process. The terminal benzylic proton (***h***) next to alcohol gradually broadened and eventually disappeared, generating an adjacent new peak (***i***) positioned slightly up-field, which is associated with benzylic proton of byproduct small molecules. In addition, since these two peaks (***h*** and ***i***) can provide molecular ratio between polymer chain and generated small molecule byproduct, the change in integration ratio was used to calculate the degree of degradation over UV exposure time. Lastly, the terminal alcohol peak (***j***) on the polymer chain disappeared over UV irradiation time, creating a new alcohol peak (***k***) that belongs to benzylalcohol of the monomer. Since benzylalcohol peaks are very distinctive depending on whether they are on a small molecule or polymer, it is possible to confirm the concurrent

disappearance of peak ***j*** and appearance of peak ***k***, which implies complete transition of polymer chains into small monomers upon UV treatment.

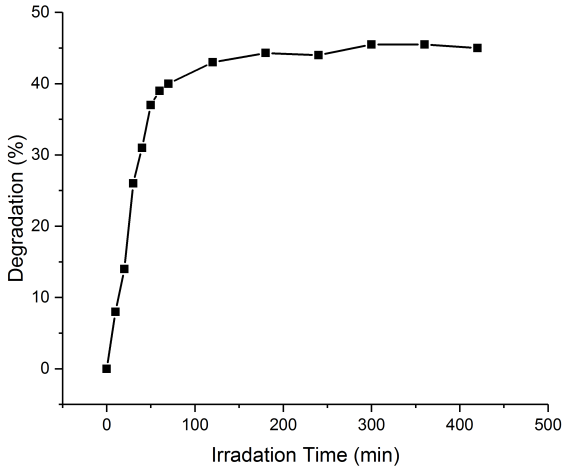

$$\text{Degree of degradation (\%)} = \frac{\int 4.50\ ppm}{\int 4.54\ ppm} \text{ x } \frac{1}{7} \text{x } 100$$

Figure 3.5 Plotted degree of degradation based on ^{1}H NMR analysis as a function of UV irradiation time.

It is possible to calculate degree of degradation based on analysis of ^{1}H NMR spectra due to the integration of distinctive peaks that provide the number of monomer molecules that are detached from polymer backbone at any given time. The integration of terminal benzyl (***h***) next to alcohol on polymer backbone was assigned as one proton. Then, the integration of benzylic proton (***i***) of produced aminobenzylalcohol can be considered as the relative number of monomers that are released from the polymer backbone upon degradation. Considering the degree of polymer is seven, dividing number of generated aminobenzylalcohol monomer by seven at each time of measurement will be degradation percent. The degree of degradation over seven hours is plotted and shown in Figure 3.5. It is noticeable that the degradation reaches about 40% after 1hour of UV exposure. Then, it reaches a saturated plateau of 45% over 7 hours.

Degradation of the polymer was also confirmed by using UV/vis absorption spectroscopy. As a reference, *o*-nitrobenzylalcohol was tested separately to evaluate its degradation. Figure 3.6 shows the absorption spectra of *o*-nitrobenzylalcohol small molecule before and after UV treatment. As expected, the benzylalcohol peak at 250 nm diminishes as with time of irradiation, whereas the peak at 350 nm grows that corresponds to the benzaldehyde byproduct that results from UV degradation. The synthesized polymer was also evaluated in the same manner. As expected, the peak corresponding to benzaldehyde at 350 nm appears slightly when depolymerization has occurred (after 2 hours) and increases to 7 hours of UV irradiation. In addition, development of a peak at 275 nm was observed. This peak can be attributed to the generation of monomers and resultant aromatic byproduct mixture upon UV degradation. These results consistently support our hypothesis that the synthesized polymer can undergo cleavage of the light-sensitive trigger under UV irradiation, which is the first step to successful cascade of self-immolation through polymer back bone.

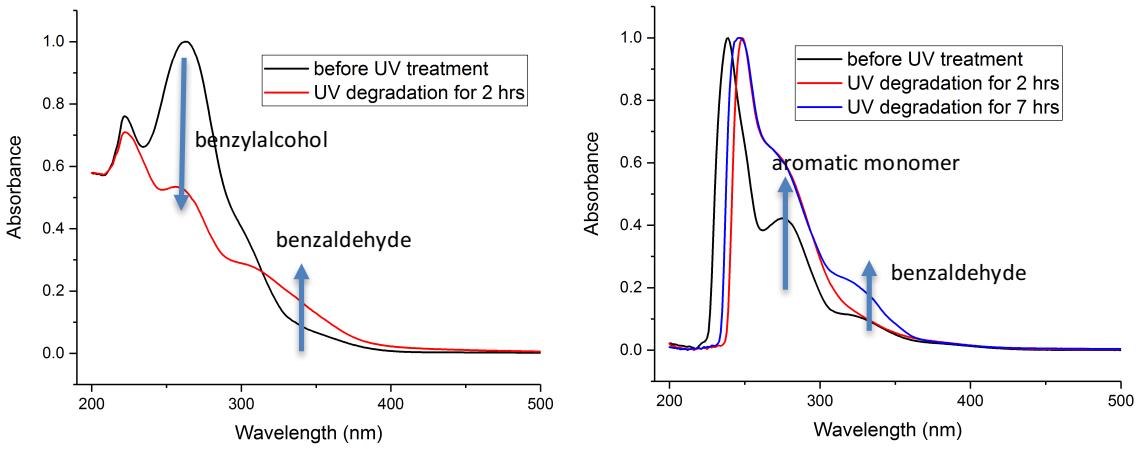

Figure 3.6 UV/vis spectra of benzylalcohol before and after 2 hours of UV treatment (left) and UV/vis spectra of synthesized carbamate-based self-immolative polymer before and after UV degradation over 7 hours (right), supporting the generation of benzaldehyde byproduct.

3.3.3. Optimization of Gelation

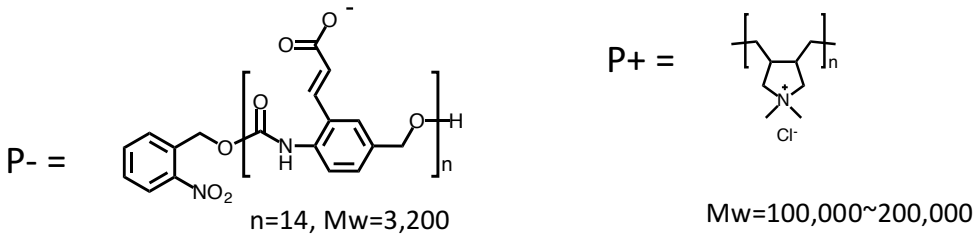

Figure 3.7 Chemical structures of synthesized P- and commercially available P+. The molecular weight and degree of polymerization were analyzed based on ^{1}H NMR spectroscopy.

The stimuli-responsive gel was prepared by mixing two polymers with charge complementarity in aqueous solution. Commercially available poly(diallyldimethyl)ammonium chloride (PDADMAC, 100,000 ~ 200,000 g/mol) was used as the positively charged polymer component (P+). Serial dilution of the stock (200 mg/mL) P+ solution provides desired concentration of the cationic polymer. After testing wide range of P+ concentrations (10 ~ 250 mg/mL), four different concentrations between 100 ~ 250 mg/mL were selected for further investigation due to obvious morphological changes that were visually observable when mixed with P- . Because the synthesized negatively-charged self-immolative polymer (P-) is insoluble in neutral or acidic aqueous media, the polymer was dissolved in slightly basic conditions. Potassium carbonate and sodium hydroxide were used as bases to solubilize P-. The concentration of P- was fixed to 18 mg/mL as it is the maximum soluble concentration under the conditions used. We expect that the maximum compatible P- composition would result in the most dramatic morphological transition during degradation of the gel. Complete solubility of 18 mg/mL P- was achieved after 24 hours of stirring at room temperature. In all cases, a 1:1 volume ratio of two solutions were blended for gelation test so that P+

concentration would be varied (100, 150, 200, and 250 mg/mL) at constant P- concentration (18 mg/mL). Although both of potassium carbonate and sodium hydroxide aid in formation of the gel morphology upon blending the P- and P+ solutions, P- in potassium carbonate was chosen for further morphology experiment since it is observed that potassium carbonate solution provides more homogenous gelation, whereas sodium hydroxide solution makes formed gel that was visibly heterogeneous in density, which makes viscosity characterization by rheology difficult. With these optimized gelation conditions, the blend was then irradiated with UV for 30 min for observations in morphology. As expected, it was visually apparent that the morphology of the gel was disrupted by this UV treatment to cause a gel-sol transition (Figure 3.8).

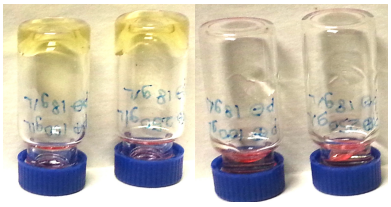

Figure 3.8 Demonstration of gelation by blending P- and P+ mixtures in different concentrations (left) and their degradation upon light exposure for 30 min (right).

3.3.4. Characterization of Degradation by Rheology

The optimized gels were further investigated by rheology, to measure the melt flow rate of these viscous materials. The instrument applies a physical stress to the samples, providing a modulus or viscosity in response to the stress. Specifically, rigidity is measured as a form of the complex modulus, G*, as a function of frequency sweep. In addition, reliable viscosity was obtained by inspecting constant viscosity regardless of shear rate verifies reliable viscosity measurement.

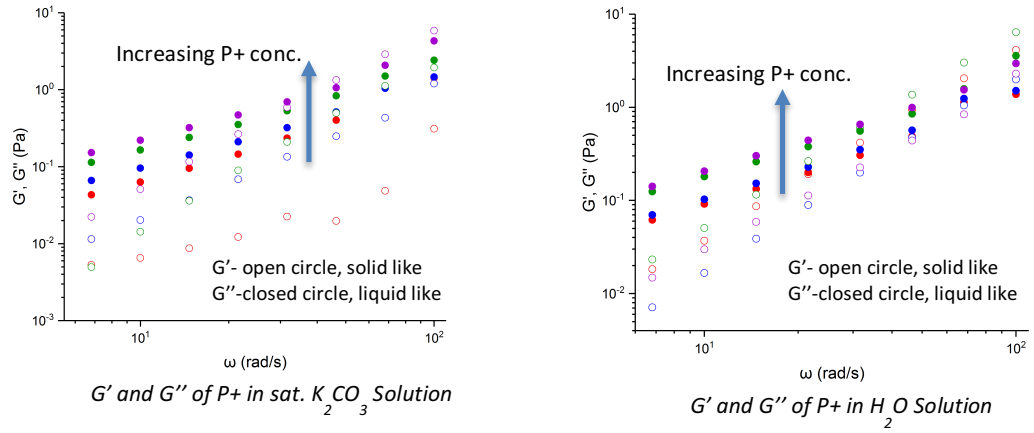

Figure 3.9 Modulus measurement of P+ polymer in various concentrations in sat. K_2CO_3 solution (left) or water solution (right). modulus increases as P+ concentration increases.

P+ aqueous solutions with and without saturated potassium carbonate were evaluated prior to blending with the P- solution and UV treatment. (Figure 3.9) In both solvents, the same trend in modulus was obtained, with an increase in the complex modulus (G*) of P+ solution as the concentration of P+ was increased. This is a result of an increase in rigidity of solution with increase in concentration of the high molecular weight (100,000 ~ 200,000 g/mol) polymer. The viscosity measurement also demonstrated a consistent result, with values reliable throughout a shear rate range of 1 ~ 10 s^{-1}. Viscosity results of P+ solutions in saturated potassium carbonate show that they are similar to those in water at the concentration between 150 ~ 250 mg/mL (Figure 3.10). At a lower concentration of 100 mg/mL, the viscosity is lower in saturated potassium carbonate than water solution. Based on this result, we can rule out the influence of potassium carbonate on rigidity of solution and it is possible to ensure that no overestimated impact on viscosity is falsely attributed to the use of this solvent condition.

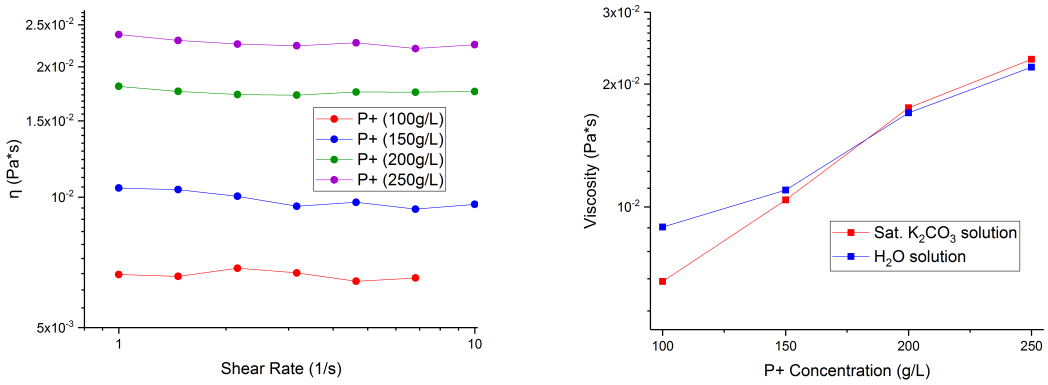

Viscosity of P+ in sat. K_2CO_3 Solution

Viscosity of P+ in sat K_2CO_3 (red) and H_2O (blue)

Figure 3.10 Viscosity Measurement of P+ Polymer in Saturated K_2CO_3 Solution as a Function of Shear Rate (Left) and Comparison with One in Water Solution.

Then, the G* modulus of P-/P+ blends was investigated at various concentrations of P+, while P- concentration was kept constant to be 18 mg/mL. Figure 3.11 indicates that the viscosity of P-/P+ blends becomes higher than that of P+ solution at each concentration of P+ evaluated. The comparison of viscosity of the mixture and their corresponding P+ pre-blends indicates that addition of P- into P+ solution, which is followed by homogenous stirring, induces rigidity in the entire solution. This is consistent with our expectation that the positively charged, long polymer chain could get cross linked via columbic interaction with a relatively small polymer, bearing polyvalent counter ionic functionality.

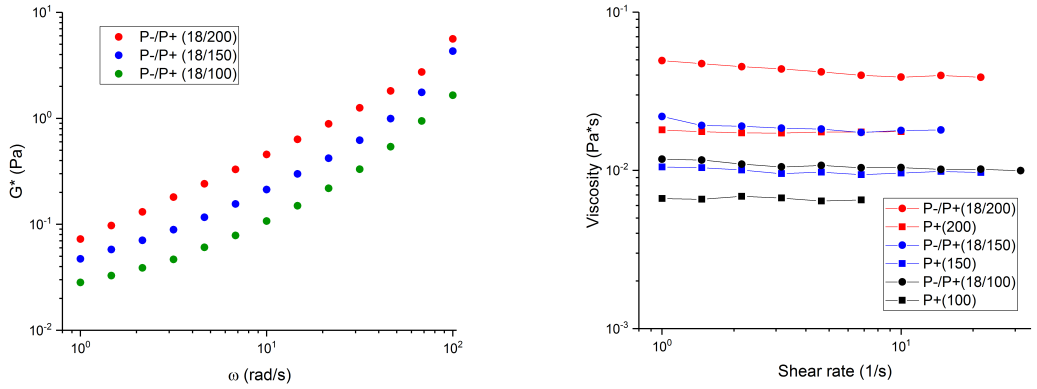

Figure 3.11 Complex modulus (G*) of P-/P+ blends in sat. K_2CO_3 solutions in various concentrations (left) and viscosity of P+ before and after blending with P- (right).

First, when 1:1 ratio of 18 g/L P- solution and 200 g/L of P+ solution was blended, their homogeneous gel-like mixture shows 0.4554 Pa of complex rigidity (Figure 3.12). This G* very slightly increases during UV light exposure over 30 min. During the first 30 min of UV light treatment, G* modulus reached to 0.4643 Pa, which is followed by drastic drop to 0.3812 Pa during the following 30 min. Then, G* gradually decreased over the next 3 hours, where it reached a value of 0.3106 Pa. Although G* declined after 4 hours of UV light treatment, it is noted that the decrease in the rigidity of P-/P+ blend after 4 hours of UV exposure did not recover a G* value as low as that of P+ pre-blend solution of the same concentration. This phenomenon could suggest the possibilities of incomplete degradation of P- polymer, which is consistent with degradation study based on ^{1}H NMR analysis. By NMR, degradation of P- solution reached 40 % and saturated at 45 % after UV light treatment for 1 hour and 4 hours, respectively.

Similarly, in case of 150 g/L of P+ solution mixed with 18 g/L of P- solution, G* diminishes from 0.213 to 0.155 Pa with time of UV light exposure, with the exception of

the first 30 min of the exposure, where an even slighter increase from 0.213 to 0.214 Pa in G* was observed (Figure 3.12). Furthermore, it is noted that although the changes in G* showed similar trend in both P+ concentrations (200 and 150 g/L), a more dramatic difference in G* was found for 200 g/L P+, with a larger change in G* observed upon blending with P-.

Lastly, the blend of P+ solution at 100 g/L with P- was investigated for their degradation characteristics. Similar to the higher concentrations of P+, it was observed that the first 30 min of UV treatment induced slight increase in G* from 0.1073 to 0.1245 Pa. This slight increase in G* is followed by a surprisingly dramatic spike during the following 30 min of degradation, reaching 0.1665 Pa at 1 hour, which then showed a gradual decrease over the next 3 hours. It is noted that in this case, the G* at the end of 4 hours of degradation remained as high as 0.1324 Pa, which is even higher rigidity than obtained prior to blending.

In all cases, unexpected G* modulus increases were observed at the beginning of the degradation. This could be a result of released monomeric byproduct upon the initiation of P- self-immolation, for which the negatively charged small molecules could behave similar to the P- cross-linker in the P+ containing blending system. Since P- polymer with multiple monomer units is more rigid and brittle compared to monomeric analog, elastic monomers could make better contact with P+ polymers, leading to increase in G*. In other words, it is possible that the negatively charged monomeric analog of P- maintains coulombic interactions with the P+ chain, contributing to entanglement of the gel in addition to the remaining P- polymer backbone that had not yet degraded.

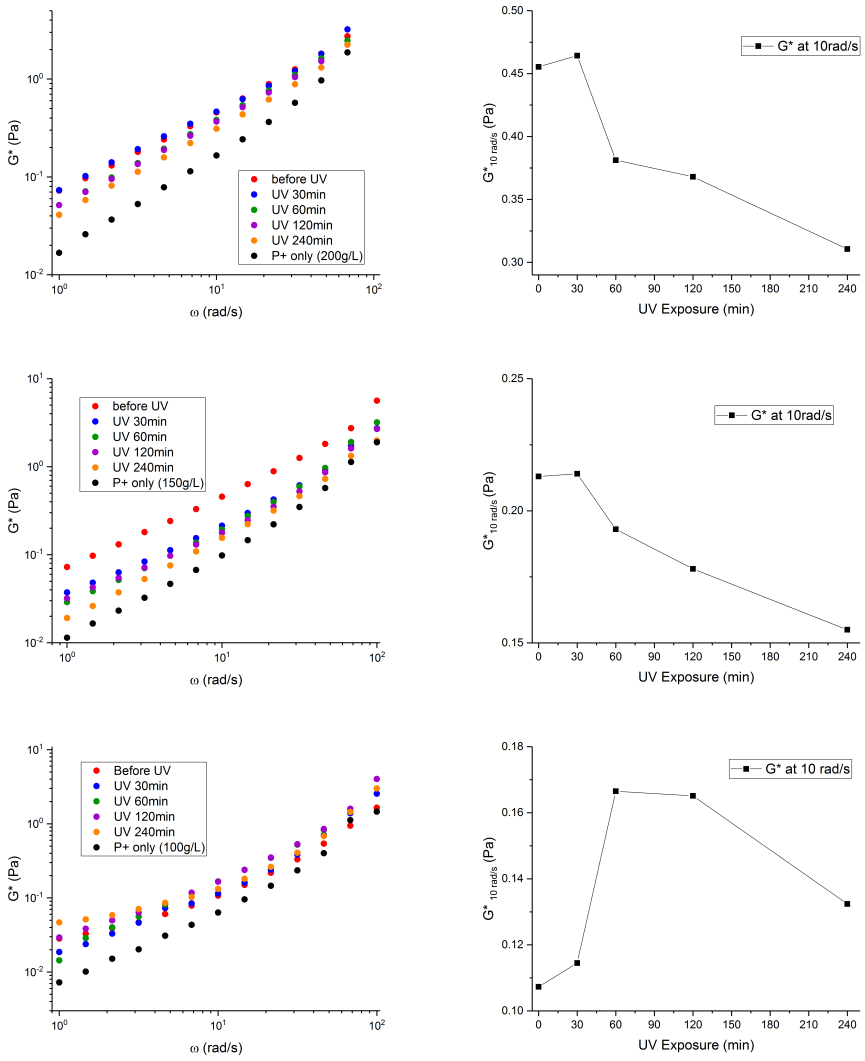

Figure 3.12 Complex modulus (G*) changes as a function of a frequency sweep at different UV light exposure times (left). G* at 10 rad/s plotted as a function of UV exposure time (right). The concentrations were selected to be 200 (top), 150 (middle), and 100 g/L (bottom).

G' and G" changes over the course of degradation was plotted in Figure 3.13. Although G' does not show a consistent trend over time, G" nicely increases as a function of frequency sweep over the degradation. Specifically, although it is unreliable to discuss G' values at the early time of degradation, it is noted that gels are reached to well-defined homogenous status after 1~3 hours of UV light treatment. Considering that there was 10 mins of stirring between each UV treatment and measurements, it is concluded that it is

necessary to wait this long time to obtain a well-defined gel formation after mixing two polymers as well as after degradations.

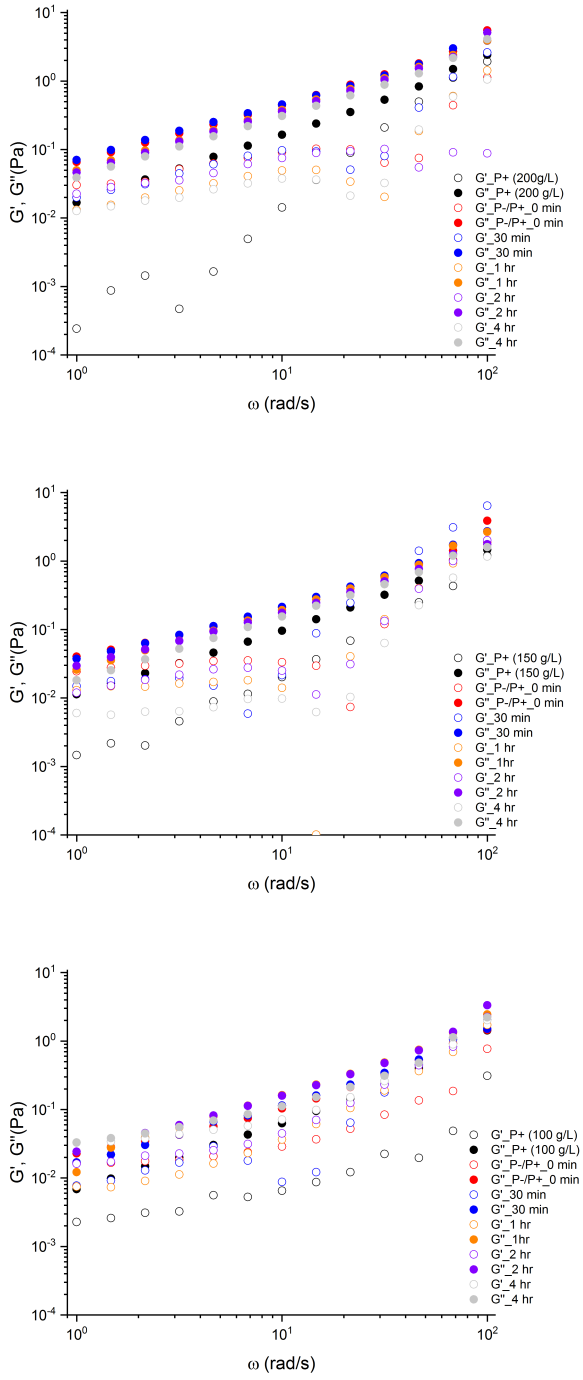

Figure 3.13 G' and G" modulus changes as a function of a frequency sweep at different UV light exposure times. P+ concentrations are 200 (top), 150 (middle), 100 (bottom) g/L, respectively.

3.4. Summary

The naturally evolved highly efficient biological mechanism of signal amplification has inspired man-developed amplification technologies for various scientific applications. In order to demonstrate signal amplification that can amplify molecular scale inputs into macro scale phase transitions, self-immolative polymeric (P-/P+) gel blends were designed and investigated. Prior to gel formation, the cleavage of light sensitive endcap trigger *o*-nitrobenzylalcohol on self-immolative P- was confirmed using UV/vis spectroscopy. In addition, the degradation of P- as a result of light treatment was fully confirmed by ^{1}H NMR spectroscopy. Upon UV irradiation, the degree of P1 degradation saturated at 45 % over 7 hours of irradiation with initial fast degradation up to 40% for 1 hour.

Optimization of gelation conditions prior to degradation studies was conducted, providing a range of concentration that the mixture formed a homogenous gel that could be measured with reliability. Considering the fact that P- polymer is short, more like an oligomer (seven monomers per chain) compared to P+, and the addition of P- does increase rigidity of the P+ solutions (100 g/L) by two-fold, it is possible to hypothesize that P- columbically cross-links the P+ polymer chain by multivalent charge complimentary interactions.

Three concentration variations of P+ were selected for the further investigation of gel-sol transitions from self-immolation. Upon UV degradation, unexpected spikes in rigidity were observed in all cases at the first 30 ~ 60 min of light treatment, which could be induced by released small molecules of monomeric P-, still bearing carboxylate functionality. These negatively charged small molecules could entangle the P-/P+ gel in

addition to the dominant cross-link by remaining intact P-. This inspires further studies on the kinetics of these rigidity changes during the initial phase of degradation. It is possible that the increase in Pa was induced by a swelling of the gel with the initiation of self-immolation, prior to the morphological equilibrium. Further ^{1}H NMR and rheology studies during this first 1 hour may provide deeper insight to this process.

3.5. Experimental Section

3.5.1. Materials and Instrumentation

All chemicals and solvents were purchased from commercial sources and were used as received, unless otherwise described. Analytical techniques: ^{1}H NMR spectra were recorded on a 400 MHz Bruker NMR spectrometer using the residual proton resonance of the solvent as the internal standard. Chemical shifts are reported in parts per million (ppm). When peak multiplicities are given, the following abbreviations are used: s, singlet; bs, broad singlet; d, doublet; t, triplet; m, multiplet. ^{13}C NMR spectra were proton decoupled and recorded on a 100 MHz Bruker spectrometer using carbon signal of the deuterated solvent as the internal standard. FAB-MS spectra were measured on a JEOL JMS700. MALDI-TOF spectra were measured on a Bruker OmnifleX. Cary 100 Scan UV-Visible Spectrophotometer was used for UV/vis absorption experiments. For rheology measurement, a stress-controlled rotational rheometer (Malvern Kinexus Pro+), with a couette geometry, was used to achieve uniform shear. Both steady-shear and small amplitude oscillatory shear (SAOS) measurements were performed. Steady-shear measurements were carried out using shear rates between 1 ~ 50 s^{-1} taking 6 samples per decade. SAOS measurements were carried out at 0.5 % strain with frequency

measurements between 1 ~ 100 rad/s.

3.5.2. Synthesis

3.5.2.1. Synthesis of compound 1

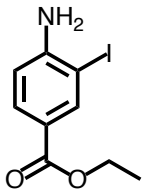

1

To a 2-neck 250 mL round bottom flask, Ethyl-4-aminobenzoate (10 g, 60.54 mmol), sodium periodoate (12.94 g, 60.94 mmol), potassium chloride (7.08 g, 121.07 mmol) and potassium iodide (10.05 g, 60.54 mmol) were added. Argon was purged for a 10 min, followed by addition of $AcOH/H_2O$ (120 mL/13 mL). The reaction mixture was stirred for 30 h. After the reaction, water, sodium thiosulfate, and sodium bicarbonate solutions were used once each for extraction. Following evaporation of organic solvent, there was a significant amount of acetic acid remaining. Several extractions with sodium bicarbonate and water should be performed in the future. Residual solid was recrystallized with Ethyl acetate/Hexane combination to yield 15.3 g (87%) of pure compound 1 ^{1}H NMR (400 MHz, $CDCl_3$) δ 8.20 (d, J = 15.9 Hz, 2H), 8.05 (s, 1H), 4.99(s, 2H), 4.30 (q, *J* = 7.1 Hz, 2H), 1.36 (t, *J* = 7.1 Hz, 3H). ^{13}C NMR (100 MHz, $CDCl_3$) δ 164.52, 145.70, 133.33, 121.31, 107.41, 61.09, 14.38.

3.5.2.2. Synthesis of compound 2

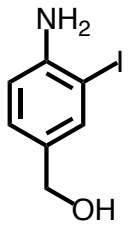

2

Compound 1 (6.4 g, 22.2 mmol) was dissolved in dry THF (100.0 mL), cooled to –78 ºC under argon, and 50ml of DIBAL-H (1M solution in dichloromethane or hexanes) was added. The mixture was stirred for two hours, then warmed to room-temperature and EtOAc (25 mL) was added, followed by 3N HCl (0.3 mL) and water (5.0 mL). The mixture was extracted with EtOAc (3 x 50 mL). The organic phase was separated, washed with brine (3 x 50mL), dried (Na_2SO_4), and the solvent was removed under vacuum. The product was obtained as a white precipitate and was isolated by filtration (5.03 g, 91%) ^{1}H NMR (400 MHz, $CDCl_3$): δ 8.09 (d, J = 2.0, 1H), 7.63 (dd, J = 8.4, 2.0 Hz, 1H), 6.73 (d, J = 8.4 Hz, 1H), 5.97 (br, 2H, NH_2) ^{13}C NMR (100 MHz, $CDCl_3$): δ 166.14, 152.63, 140.54, 130.71, 119.40, 112.89, 81.10.

3.5.2.3. Synthesis of compound 3

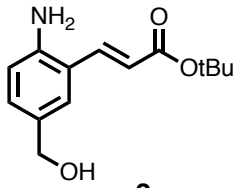

3

Compound 2 (2 g, 8.03 mmol) was dissolved in 15 mL dry DMF under Ar atmosphere. $Pd(OAc)_2$ (0.09g, 0.402 mmol), K_2CO_3 (5.55 g, 40.15 mmol), Bu_4NBr (3.24 g, 10.04 mmol), and *t*-butylacrylate (1.54 g, 12.05 mmol) were added. The reaction mixture was heated to 60 ˚C, stirred for 2 hours, and monitored to completion by TLC. The reaction mixture was extracted with ethyl acetate and water, dried by sodium sulfate and vacuuo. And then it was purified by column chromatography on silica gel (EtOAc:Hex 30:70) to yield compound 3 (1.26 g, 63%) ^{1}H-NMR (400 MHz, $CDCl_3$): δ = 7.61 (d, *J* = 15.8 Hz, 1H), 7.28 (s, 1H), 7.04 (d, *J* = 8.3 Hz, 1H), 6.58 (d, *J* = 8.3 Hz, 1H), 6.19 (d, *J* = 15.8 Hz, 1H), 4.43 (d, *J* = 8.6 Hz, 2H), 3.98 (s, 2H), 1.46 (s, 9H). ^{13}C NMR (100 MHz, $CDCl_3$): δ = 28.1, 64.7, 80.5, 116.7, 119.7, 126.9, 128.6, 130.3, 131.2, 138.8, 144.9, 166.8. MS (FAB+): calc. for $C_{14}H_{19}NO_3$: 249.1; found: 249.1.

3.5.2.4. Synthesis of compound 4

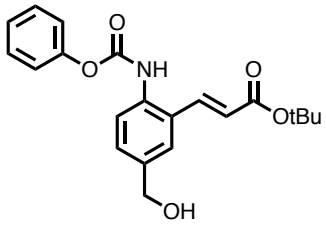

4

Compound 4 (1.0 g, 4.0 mmol) was suspended in a mixture of THF:sat. $NaHCO_3$:H_2O (ratio 2:2:1) and phenylchloroformate (0.51 mL, 4.10 mmol) was added drop wise over 5 min. The reaction was monitored to completion (10 min) by TLC (EA70). EA was then added and the organic phase was washed twice with saturated NH_4Cl solution. The solvent was removed under reduced pressure and the crude product

was purified by column chromatography on silica gel (EA 20%) to give product as a yellow solid (1.34 g, 91 %). ^{1}H-NMR (400 MHz, $CDCl_3$): δ = 7.76 (d, *J* = 15.7 Hz, 1H), 7.27 (m, 8H), 6.34 (d, *J* = 15.7 Hz, 1H), 4.63 (d, *J* = 5.1 Hz, 2H), 1.46 (s, 9H). ^{13}C NMR (100 MHz, $CDCl_3$): δ = 28.1, 64.7, 80.5, 116.7, 119.7, 126.9, 128.6, 130.3, 131.2, 138.8, 144.9, 166.8. MS (FAB+): calc. for $C_{21}H_{23}NO_5$: 369.1; found: 369.1.

3.5.2.5. Synthesis of compound 5

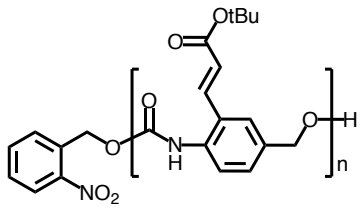

5

A small vial was prepared and purged with Ar gas for a 10 min. Dried DMSO and compound 4 (70 mg, 0.189 mmol) were added to the vial, then the solution was submerged into a 110 ˚C oil bath for pre-heating. After 5 min, DBTL (5.61 μL, 9.47 μmol) was added to the vial to initiate the reaction. After 15 min of stirring, *o*-nitrobenzylalcohol (5.8 mg, 37.8 μmol) in DMSO was added to the reaction mixture to quench the polymerization, and left at 110 ˚C for additional 1 hour. The reaction mixture was then cooled to room temperature and the organic solvent was evaporated. The resultant polymer was washed with MeOH and collected by centrifugation four times. ^{1}H-NMR (400 MHz, THF-d_8): δ 10.81 (s, 1H), 8.80 (s, 16H) 7.86-7.73 (m, 48H), 7.43-7.7.40 (m, 16H), 6.42-6.38 (d, *J* = 15.9 Hz, 16H), 5.57 (d, *J* = 15.9 Hz, 1H), 5.14 (s, 30H), 4.53 (s, 2H), 1.48 (s, 144H).

3.5.2.6. Synthesis of compound 6

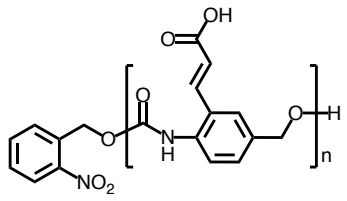

6

Compound 5 (100 mg) was dissolved in a mixture of TFA/DCM, stirred for 15 mins, then an aliquot was taken for NMR after quickly drying under vacuum. Once completion of the reaction was confirmed, the mixture was dried under reduced pressure. ^{1}H-NMR (400 MHz, THF-d_8): δ 10.81 (s, 1H), 8.80 (s, 16H) 7.86-7.73 (m, 48H), 7.43-7.40 (m, 16H), 6.42-6.38 (d, J = 15.9 Hz, 16H), 5.57 (d, J = 15.9 Hz, 1H), 5.14 (s, 30H), 4.53 (s, 2H).

3.6. Reference

(1) Gorman, A.; Killoran, J.; O'Shea, C.; Kenna, T.; Gallagher, W. M.; O'Shea, D. F. In Vitro Demonstration of the Heavy-Atom Effect for Photodynamic Therapy. *J. Am. Chem. Soc.* **2004**, *126* (34), 10619–10631.

(2) Kochevar, I. E.; Redmond, R. W. Photosensitized Production of Single Oxygen. *Methods Enzymol.* **2000**, *319*, 20–28.

(3) Chen, X.; Li, Y.; Wang, A.; Zhou, L.; Lu, S.; Zhou, J.; Lin, Y.; Wei, S. Protonation Salt Derivative with Heavy-Atom Effect on Phthalocyanine for Enhanced in Vitro Photodynamic Therapy. *Dye. Pigment.* **2015**, *114* (C), 93–104.

(4) Yogo, T.; Urano, Y.; Ishitsuka, Y.; Maniwa, F.; Nagano, T. Highly Efficient and Photostable Photosensitizer Based on BODIPY Chromophore. *J. Am. Chem. Soc.* **2005**, *127* (35), 12162–12163.

(5) Rodriguez-Serrano, A.; Rai-Constapel, V.; Daza, M. C.; Doerr, M.; Marian, C. M. Internal Heavy Atom Effects in Phenothiazinium Dyes: Enhancement of Intersystem Crossing via Vibronic Spin-Orbit Coupling. *Phys. Chem. Chem. Phys.* **2015**, *17* (17), 11350–11358.

(6) Cui, G.; Fang, W. H. State-Specific Heavy-Atom Effect on Intersystem Crossing Processes in 2-Thiothymine: A Potential Photodynamic Therapy Photosensitizer. *J. Chem. Phys.* **2013**, *138* (4).

(7) Turro, N. J. The Triplet State. *J. Chem. Educ.* **1966**, *46* (1), 2–6.

(8) McClure, D. S. Spin-Orbit Interaction in Aromatic Molecules. *J. Chem. Phys.* **1952**, *20* (4), 682.

(9) Lower, S.; El-Sayed, M. The Triplet State and Molecular Electronic Processes in

Organic Molecules. *Chem. Rev.* **1966**, *66* (2), 199–241.

(10) Levine, I. N. Quantum Chemistry; Allyn and Bacon: Boston, 1970; pp 306–310.

(11) McClure, D. S. Triplet-Singlet Transitions in Organic Molecules. Lifetime Measurements of the Triplet State. *J. Chem. Phys.* **1949**, *17* (10), 905.

(12) Ermolaev, V. L.; Svitasbev, K. K. Quantum Yields of Phosphorescence and Fluorescence of Some 1-Derivatives of Naphthalene in Solutions at -196˚C.pdf. *Opt. Spectrosc.* **1959**, *1*, 399.

(13) Cowan, D. O. Elements of Organic Photochemistry. In *Elements of Organic Photochemistry*; Plenum Press: New York, N.Y., 1976; pp 250–262.

(14) Chock, P. B.; Stadtman, E. R. Superiority of Interconvertible Enzyme Cascades in Metabolite Regulation: Analysis of Multicyclic Systems. *Proc Natl Acad Sci U S A* **1977**, *74* (7), 2766–2770.

(15) Koshland, D. E.; Goldbeter, A.; Stock, J. B. Amplification and Adaptation in Regulatory and Sensory Systems Author (S): Daniel E . Koshland , Albert Goldbeter and Jeffry B . Stock Published by : American Association for the Advancement of Science Stable URL : http://www.jstor.org/stable/1689499 JS. **2017**, *217* (4556), 220–225.

(16) Chock, P. B.; Rhee, S. G.; Stadtman, E. R. Interconvertible Enzyme Cascades in Cellular-Regulation. *Annu. Rev. Biochem.* **1980**, *49*, 813–843.

(17) Bhalla and Ravi Iyengar, U. S. Emergent Properties of Networks of Biological Signaling Pathways. *Science (80-.).* **1999**, *283* (5400), 381–387.

(18) Weng, G. Complexity in Biological Signaling Systems. *Science (80-.).* **1999**, *284* (5411), 92–96.

(19) Jordan, J. D.; Landau, E. M.; Iyengar, R. Signaling Networks: The Origins of Cellular Multitasking. *Cell* **2000**, *103* (2), 193–200.

(20) Levine, S. N. Enzyme Amplifier Kinetics. *Science (80-.).* **1966**, *152* (3722), 651–653.

(21) Wald, G. Visual Excitation and Blood Clotting. *Science* **1965**, *150* (3699), 1028–1030.

(22) Brown, G. C.; Hoek, J. B.; Kholodenko, B. N. Why Do Protein Kinase Cascades Have More than One Level? *Trends Biochem. Sci.* **1997**, *22*, 288.

(23) Fozooni, T.; Ravan, H.; Sasan, H. Signal Amplification Technologies for the Detection of Nucleic Acids: From Cell-Free Analysis to Live-Cell Imaging. *Appl. Biochem. Biotechnol.* **2017**, 1–30.

(24) Wu, W.; Bazan, G. C.; Liu, B. Conjugated-Polymer-Amplified Sensing, Imaging, and Therapy. *Chem* **2017**, *2* (6), 760–790.

(25) Mittal, S.; Kaur, H.; Gautam, N.; Mantha, A. K. Biosensors for Breast Cancer Diagnosis: A Review of Bioreceptors, Biotransducers and Signal Amplification Strategies. *Biosens. Bioelectron.* **2017**, *88*, 217–231.

(26) Dewit, M. A.; Nazemi, A.; Karamdoust, S.; Beaton, A.; Gillies, E. R. Design, Synthesis and Assembly of Self-Immolative Linear Block Copolymers. *Non-Coventional Funct. Block Copolym.* **2011**, 9–21.

(27) Li, Y.; Liu, G.; Wang, X.; Hu, J.; Liu, S. Enzyme-Responsive Polymeric Vesicles for Bacterial-Strain-Selective Delivery of Antimicrobial Agents. *Angew. Chemie - Int. Ed.* **2016**, *55* (5), 1760–1764.

(28) Liu, G.; Wang, X.; Hu, J.; Zhang, G.; Liu, S. Self-Immolative Polymersomes for

High-Efficiency Triggered Release and Programmed Enzymatic Reactions. *J. Am. Chem. Soc.* **2014**, *136* (20), 7492–7497.

(29) Sauer, M.; Haefele, T.; Graff, a; Nardin, C.; Meier, W. Ion-Carrier Controlled Precipitation of Calcium Phosphate in Giant ABA Triblock Copolymer Vesicles. *Chem. Commun. (Camb).* **2001**, No. 23, 2452–2453.

(30) Sceince, P. Polymer Vesicles. *Science (80-.).* **2005**, *297* (17), 967–974.

(31) Wu, J.; Eisenberg, A. Proton Diffusion across Membranes of Vesicles of Poly(styrene-B-Acrylic Acid) Diblock Copolymers. *J. Am. Chem. Soc.* **2006**, *128* (9), 2880–2884.

(32) Gabrielli, L.; Mancin, F. Minimal Self-Immolative Probe for Multimodal Fluoride Detection. *J. Org. Chem.* **2016**, *81* (22), 10715–10720.

(33) Amir, R. J.; Pessah, N.; Shamis, M.; Shabat, D. Self-Immolative Dendrimers. *Angew. Chemie - Int. Ed.* **2003**, *42* (37), 4494–4499.

(34) Shamis, M.; Shabat, D. Single-Triggered AB6 Self-Immolative Dendritic Amplifiers. *Chemistry* **2007**, *13* (16), 4523–4528.

(35) Tan, X.; Li, B. B.; Lu, X.; Jia, F.; Santori, C.; Menon, P.; Li, H.; Zhang, B.; Zhao, J. J.; Zhang, K. Light-Triggered, Self-Immolative Nucleic Acid-Drug Nanostructures. *J. Am. Chem. Soc.* **2015**, *137* (19), 6112–6115.

(36) Niculescu-Duvaz, I.; Niculescu-Duvaz, D.; Friedlos, F.; Spooner, R.; Martin, J.; Marais, R.; Springer, C. J. Self-Immolative Nitrogen Mustard Prodrugs for Suicide Gene Therapy. *J. Med. Chem.* **1998**, *41* (13), 5297–5309.

(37) De Groot, F. M. H.; Albrecht, C.; Koekkoek, R.; Beusker, P. H.; Scheeren, H. W. "Cascade-Release Dendrimers" liberate All End Groups upon a Single Triggering

Event in the Dendritic Core. *Angew. Chemie - Int. Ed.* **2003**, *42* (37), 4490–4494.

(38) Shamis, M.; Lode, H. N.; Shabat, D. Bioactivation of Self-Immolative Dendritic Prodrugs by Catalytic Antibody 38C2. *J. Am. Chem. Soc.* **2004**, *126* (6), 1726–1731.

(39) Dresselhaus, M.S.; Thomas, I. . Alternative Energy Technologies. *Nature* **2001**, *414* (November), 332–337.

(40) Gregg, B. A.; Hanna, M. C. Comparing Organic to Inorganic Photovoltaic Cells: Theory, Experiment, and Simulation. *J. Appl. Phys.* **2003**, *93* (6), 3605–3614.

(41) https://energy.gov/eere/solar/downloads/research-cell-efficiency-records.

(42) Potscavage, W. J.; Sharma, a; Kippelen, B. Critical Interfaces in Organic Solar Cells and Their Influence on the Open-Circuit Voltage. *Acc. Chem. Res.* **2009**, *42* (11), 1758–1767.

(43) Carsten, B.; Szarko, J. M.; Son, H. J.; Wang, W.; Lu, L.; He, F.; Rolczynski, B. S.; Lou, S. J.; Chen, L. X.; Yu, L. Examining the Effect of the Dipole Moment on Charge Separation in Donor-Acceptor Polymers for Organic Photovoltaic Applications. *J. Am. Chem. Soc.* **2011**, *133* (50), 20468–20475.

(44) Yao, K.; Intemann, J. J.; Yip, H.-L.; Liang, P.-W.; Chang, C.-Y.; Zang, Y.; Li, Z.; Chen, Y.; Jen, A. K.-Y. Efficient All Polymer Solar Cells from Layer-Evolved Processing of a Bilayer Inverted Structure. *J. Mater. Chem. C* **2014**, *2* (3), 416.

(45) Takacs, C. J.; Sun, Y.; Welch, G. C.; Perez, L. A.; Liu, X.; Wen, W.; Bazan, G. C.; Heeger, A. J. Solar Cell Efficiency, Self-Assembly, and Dipole-Dipole Interactions of Isomorphic Narrow-Band-Gap Molecules. *J. Am. Chem. Soc.* **2012**, *134* (40), 16597–16606.

(46) Beaujuge, P. M.; Fréchet, J. M. J. Molecular Design and Ordering Effects in π-Functional Materials for Transistor and Solar Cell Applications. *J. Am. Chem. Soc.* **2011**, *133* (50), 20009–20029.

(47) Kallmann, H.; Pope, M. Photovoltaic Effect in Organic Crystals. *J. Chem. Phys.* **1959**, *30* (2), 585–586.

(48) Benanti, T. L.; Venkataraman, D. Organic Solar Cells: An Overview Focusing on Active Layer Morphology. *Photosynth. Res.* **2006**, *87* (1), 73–81.

(49) Yu, G.; Pakbaz, K.; Heeger, A. J. Semiconducting Polymer Diodes: Large Size, Low Cost Photodetectors with Excellent Visible-Ultraviolet Sensitivity. *Appl. Phys. Lett.* **1994**, *64* (25), 3422–3424.

(50) Dang, M. T.; Hirsch, L.; Wantz, G. P3HT:PCBM, Best Seller in Polymer Photovoltaic Research. *Adv. Mater.* **2011**, *23* (31), 3597–3602.

(51) Wu, P. T.; Xin, H.; Kim, F. S.; Ren, G.; Jenekhe, S. A. Regioregular poly(3-Pentylthiophene): Synthesis, Self-Assembly of Nanowires, High-Mobility Field-Effect Transistors, and Efficient Photovoltaic Cells. *Macromolecules* **2009**, *42* (22), 8817–8826.

(52) Gabe, Y.; Ueno, T.; Urano, Y.; Kojima, H.; Nagano, T. Tunable Design Strategy for Fluorescence Probes Based on 4-Substituted BODIPY Chromophore: Improvement of Highly Sensitive Fluorescence Probe for Nitric Oxide. *Anal. Bioanal. Chem.* **2006**, *386* (3), 621–626.

(53) Li, Y.; Wang, J.; Zhang, X.; Guo, W.; Li, F.; Yu, M.; Kong, X.; Wu, W.; Hong, Z. Highly Water-Soluble and Tumor-Targeted Photosensitizers for Photodynamic Therapy. *Org. Biomol. Chem.* **2015**, *13* (28), 7681–7694.

(54) Gee, K. R.; Archer, E. A.; Kang, H. C. 4-Sulfotetrafluorophenyl (STP) Esters: New Water-Soluble Amine-Reactive Reagents for Labeling Biomolecules. *Tetrahedron Lett.* **1999**, *40* (8), 1471–1474.

(55) Hendel, S. J.; Poe, A. M.; Khomein, P.; Bae, Y.; Thayumanavan, S.; Young, E. R. Photophysical and Electrochemical Characterization of BODIPY-Containing Dyads Comparing the Influence of an A–D–A versus D–A Motif on Excited-State Photophysics. *J. Phys. Chem. A* **2016**, *120*, 8794–8803.

(56) Gollnick, K.; Griesbeck, A. Singlet Oxygen Photooxygenation of Furans. *Tetrahedron* **1985**, *41* (11), 2057–2068.

(57) Morone, M.; Beverina, L.; Abbotto, A.; Silvestri, F.; Collini, E.; Ferrante, C.; Bozio, R.; Pagani, G. A. Enhancement of Two-Photon Absorption Cross-Section and Singlet-Oxygen Generation in Porphyrins upon ??-Functionalization with Donor-Acceptor Substituents. *Org. Lett.* **2006**, *8* (13), 2719–2722.

(58) Deng, P.; Zhang, Q. Recent Developments on Isoindigo-Based Conjugated Polymers. *Polym. Chem.* **2014**, *5* (10), 3298–3305.

(59) Lin, Y.; Li, Y.; Zhan, X. Small Molecule Semiconductors for High-Efficiency Organic Photovoltaics. *Chem. Soc. Rev.* **2012**, *41* (11), 4245.

(60) Zhang, Z.; Wang, J. Structures and Properties of Conjugated Donor–Acceptor Copolymers for Solar Cell Applications. *J. Mater. Chem.* **2012**, *22* (10), 4178.

(61) Zhou, H.; Yang, L.; You, W. Rational Design of High Performance Conjugated Polymers for Organic Solar Cells. *Macromolecules* **2012**, *45* (2), 607–632.

(62) Hou, J.; Huo, L.; He, C.; Yang, C.; Li, Y. Synthesis and Absorption Spectra of poly(3-(Phenylenevinyl)thiophene)s with Conjugated Side Chains.

Macromolecules **2006**, *39* (2), 594–603.

(63) Hou, J.; Tan, Z.; Yan, Y.; He, Y.; Yang, C.; Li, Y. Synthesis and Photovoltaic Properties of Two-Dimensional Conjugated Polythiophenes with Bi(thienylenevinylene) Side Chains. *J. Am. Chem. Soc.* **2006**, *128* (14), 4911–4916.

(64) He, G.; Li, Z.; Wan, X.; Liu, Y.; Zhou, J.; Long, G.; Zhang, M.; Chen, Y. Impact of Dye End Groups on Acceptor–donor–acceptor Type Molecules for Solution-Processed Photovoltaic Cells. *J. Mater. Chem.* **2012**, *22* (18), 9173.

(65) Liu, J.; Walker, B.; Tamayo, A.; Zhang, Y.; Nguyen, T. Q. Effects of Heteroatom Substitutions on the Crystal Structure, Film Formation, and Optoelectronic Properties of Diketopyrrolopyrrole-Based Materials. *Adv. Funct. Mater.* **2013**, *23* (1), 47–56.

(66) Yuan, J.; Huang, X.; Zhang, F.; Lu, J.; Zhai, Z.; Di, C.; Jiang, Z.; Ma, W. Design of Benzodithiophene-Diketopyrrolopyrrole Based Donor–acceptor Copolymers for Efficient Organic Field Effect Transistors and Polymer Solar Cells. *J. Mater. Chem.* **2012**, *22* (42), 22734.

(67) Sonar, P.; Ng, G.-M.; Lin, T. T.; Dodabalapur, A.; Chen, Z.-K. Solution Processable Low Bandgap Diketopyrrolopyrrole (DPP) Based Derivatives: Novel Acceptors for Organic Solar Cells. *J. Mater. Chem.* **2010**, *20* (18), 3626.

(68) Della Pelle, A. M.; Homnick, P. J.; Bae, Y.; Lahti, P. M.; Thayumanavan, S. Effect of Substituents on Optical Properties and Charge-Carrier Polarity of Squaraine Dyes. *J. Phys. Chem. C* **2014**, *118* (4), 1793–1799.

(69) Huang, X.; Zhu, C.; Zhang, S.; Li, W.; Guo, Y.; Zhan, X.; Liu, Y.; Bo, Z.

Porphyrin-Dithienothiophene π-Conjugated Copolymers: Synthesis and Their Applications in Field-Effect Transistors and Solar Cells. *Macromolecules* **2008**, *41* (19), 6895–6902.

(70) Benniston, A. C.; Copley, G. Lighting the Way Ahead with Boron Dipyrromethene (Bodipy) Dyes. *Phys. Chem. Chem. Phys.* **2009**, *11* (21), 4124.

(71) Oosterhout, S. D.; Savikhin, V.; Zhang, J.; Zhang, Y.; Burgers, M. A.; Marder, S. R.; Bazan, G. C.; Toney, M. F. Mixing Behavior in Small Molecule:Fullerene Organic Photovoltaics. *Chem. Mater.* **2017**, *29* (7), 3062–3069.

(72) Carlé, J. E. Polymers for Organic Photovoltaics Based on 1,5-bis(2-Hexyldecyloxy)-Naphthalene, Thiophene, and Benzothiadiazole. *J. Photonics Energy* **2011**, *1* (1), 11111.

(73) Guo, X.; Watson, M. D. Conjugated Polymers from Napthalene Bisimide. *Org. Lett.* **2008**, *10* (23), 5333–5336.

(74) Eggert Carlé, J.; Wenzel Andreasen, J.; Jørgensen, M.; Christian Krebs, F. Low Band Gap Polymers Based on 1,4-Dialkoxybenzene, Thiophene, Bithiophene Donors and the Benzothiadiazole Acceptor. *Sol. Energy Mater. Sol. Cells* **2010**, *94* (5), 774–780.

(75) Poe, A. M.; Della Pelle, A. M.; Subrahmanyam, A. V.; White, W.; Wantz, G.; Thayumanavan, S. Small Molecule BODIPY Dyes as Non-Fullerene Acceptors in Bulk Heterojunction Organic Photovoltaics. *Chem. Commun.* **2014**, *50* (22), 2913–2915.

(76) Matsumura, S.; Hlil, A. R.; Lepiller, C.; Gaudet, J.; Guay, D.; Shi, Z.; Holdcroft, S.; Hay, A. S. Ionomers for Proton Exchange Membrane Fuel Cells with Sulfonic

Acid Groups on the End-Groups: Novel Branched Poly(ether-Ketone)s. *Am. Chem. Soc. Polym. Prepr. Div. Polym. Chem.* **2008**, *49* (1), 511–512.

(77) Wakim, S.; Beaupré, S.; Blouin, N.; Aich, B.-R.; Rodman, S.; Gaudiana, R.; Tao, Y.; Leclerc, M. Highly Efficient Organic Solar Cells Based on a poly(2,7-Carbazole) Derivative. *J. Mater. Chem.* **2009**, *19* (30), 5351.

(78) Goud, T. V.; Tutar, A.; Biellmann, J. F. Synthesis of 8-Heteroatom-Substituted 4,4-Difluoro-4-Bora-3a,4a-Diaza-S-Indacene Dyes (BODIPY). *Tetrahedron* **2006**, *62* (21), 5084–5091.

(79) Rakstys, K.; Paek, S.; Gao, P.; Gratia, P.; Marszalek, T.; Grancini, G.; Cho, K. T.; Genevicius, K.; Jankauskas, V.; Pisula, W.; et al. Molecular Engineering of Face-on Oriented Dopant-Free Hole Transporting Material for Perovskite Solar Cells with 19% PCE. *J. Mater. Chem. A* **2017**, *5* (17), 7811–7815.

CHAPTER 4

IMPROVING LIGHT-HARVESTING PROPERTY OF BODIPY DERIVATIVES THROUGH ALPHA-CONJUGATION EXTENSION FOR PHOTOVOLTAIC APPLICATION

4.1. Introduction

Light-harvesting is the primary process that all photovoltaic cells require. As more light is harvested, more excitons are generated, and the extent which is one of the critical factors that impact device efficiency. Although P3HT:PCBM is a promising blending system due to the high electron mobility of PCBM (10^{-3} cm^2 V^{-1} s^{-1}), high hole mobility of P3HT (10^{-4} cm^2 V^{-1} s^{-1}), as well as favorable nano-scale morphology which all facilitate charge transportation, their poor absorption profile in the vis-NIR range could be improved. Various conjugated organic compounds alternative to P3HT typically display intense and broad absorption profiles, extending into vis-NIR regions, where a large overlap with solar energy spectrum exist.[46] A wide overlap with the solar spectrum as well as a high molecular coefficient, ε, of the active layer would maximize utilization of solar energy, permitting the active layer to be fabricated into a thin film condition.

Low bandgap polymers have been extensively studied to enhance the light-harvesting property of the active layer.[58–61] A low bandgap can be conveniently achieved by extending their conjugation length through the polymer backbone.[62,63] However, synthesis of polymers involves difficulties in purification and controlling batch to batch molecular weight compared to small molecules. The inconsistency of molecular structure limits characterization of the polymer properties, and their reproducibility due to

molecular weight variability can impact device performance through altered morphology of thin film in the active layer. Alternatively, small molecules benefit from defined molecular structure and high purity without batch to batch variability. The light-harvesting ability of small molecules, however, is typically hindered by their short conjugation length.

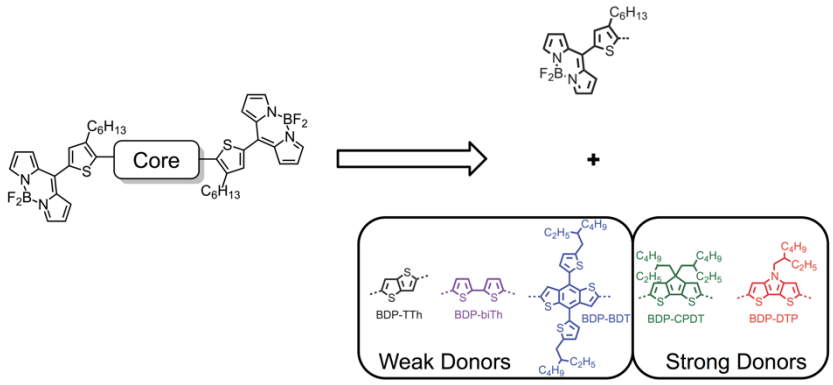

Figure 4.1 Previously reported BODIPY-based n-type small molecules for active layer materials in photovoltaic applications.

Dye molecules can provide one approach to solve this light-harvesting problem for organic photovoltaics.[64] Small molecule dyes and their polymeric derivatives have gained extensive attention due to their strong optoelectronic properties for organic semiconductors.[65–69] BODIPY (4,4-difluoro-4-bora-3a,4a-diaza-*s*-indacene) is a dye that is derived from the porphyrin structure in chlorophyll. BODIPY and its derivatives have drawn a great attention in the field of imaging, sensing, and photovoltaics due to their uniquely strong absorption and emission profiles in the visible light range with photochemical stability.[70] While it is tricky to modify porphyrin due to its symmetric macro cyclic structure, disabling selective substitution, BOIDPY can provide easier synthetic modification to either the *alpha*, *beta* and *meso*-position. The bare BODIPY structure consists of boron difluoride chelated by the amine group in a pyrrole ring.

BODIPY is capable of both oxidation and reduction, which means that they can be used as either a p-type hole transporting or n-type electron transporting material. Our group has reported a variety of BODIPY small molecules and polymers for photovoltaic applications. For example, a series of BODIPYs consisting of a thiophene-based core conjugated through the *meso*-position was reported. As an n-type material, the reported BODIPY derivatives showed a decent electron mobility of ~ 10^{-5} cm^2 V^{-1} s^{-1}, which was attributed to their low-lying LUMOs between -3.7 eV and -3.9 eV. The major inspiration of this work is that the well-known PCBM acceptor has very poor light harvesting ability towards the vis-NIR region and also has a cost-inefficient process requirement. With thiophene-modified BODIPY derivatives it was observed that the light absorption wavelength was red shifted when a strong donor was introduced to the core of the molecule, making them potential light harvesting acceptors. However, there is still room to improve utilization of the full solar energy spectrum, which could be achieved by photoactive materials that absorbs in the NIR region.

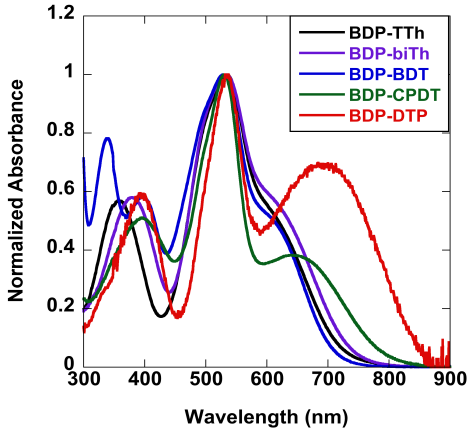

Figure 4.2 UV/vis spectra of previously reported BODIPY-based n-type small molecules without conjugation extension.

4.2. Molecular Design

Although extensive research on low band gap conjugated polymers for light harvesting p-type materials has been reported with favorable film forming properties for photovoltaic applications, there are several advantages of small molecules over polymeric molecules. They can be defined and characterized without batch to batch variations: their molecular structure is well-defined and their molecular weight is accurate with high purity, which would provide consistent device performance with good reproducibility.

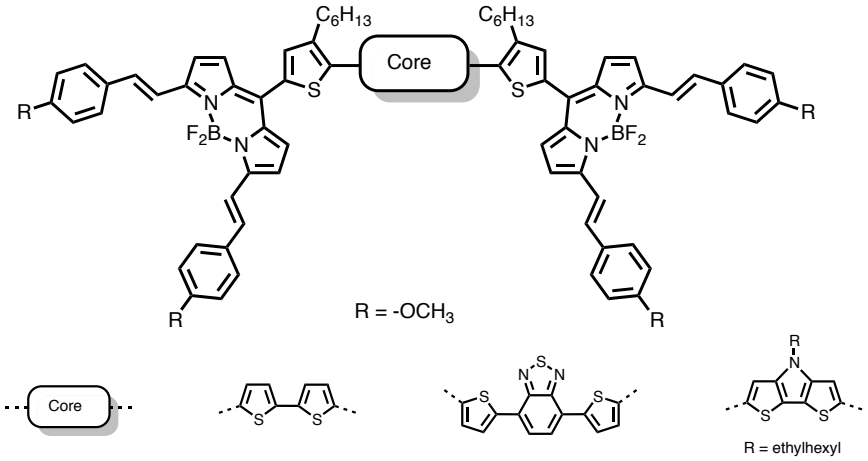

Figure 4.3 Molecular design of *alpha*-conjugation extended BODIPY with various cores.

Here in this chapter, a series of BODIPY molecules with extended conjugation through their *alpha*-position and bearing various electron rich moieties at their center were prepared, providing a symmetrical conjugated structure through their backbone (Figure 4.3). It is expected that the series of BODIPY derivatives could have expanded absorption into the NIR region, where a significant portion of solar energy is not utilized.

As electron rich core moieties, 2,2'-bithiophene (biTh), 2,1,3-benzothiadiazole (BTD) and *N*-(2-ehtylhexyl)-dithieno[3,2-*b*:2',3'-*d*]pyrrole (DTP) were chosen to be conjugated with two BODIPY molecules that possess further extended conjugation

through their *alpha* position, which are expected to possess a low band gap. Furthermore, 3-hexylthiophene was conjugated between the BODIPY moieties and the donor core through BODIPYs *meso* position. This was expected to reduce steric hindrance between the donor core and BODIPY structures, which could alter planarity of the entire molecule and impact the free flow of π-electrons through its conjugation backbone. In addition, as derived from P3HT, the aliphatic chain 2-ethylhexyl was incorporated to improve solvent solubility for processing and possibly provide beneficial morphology in the active layer for favorable charge transfer.

4.3. Experimental

4.3.1. Synthesis of *alpha*-conjugation extended BODIPYs

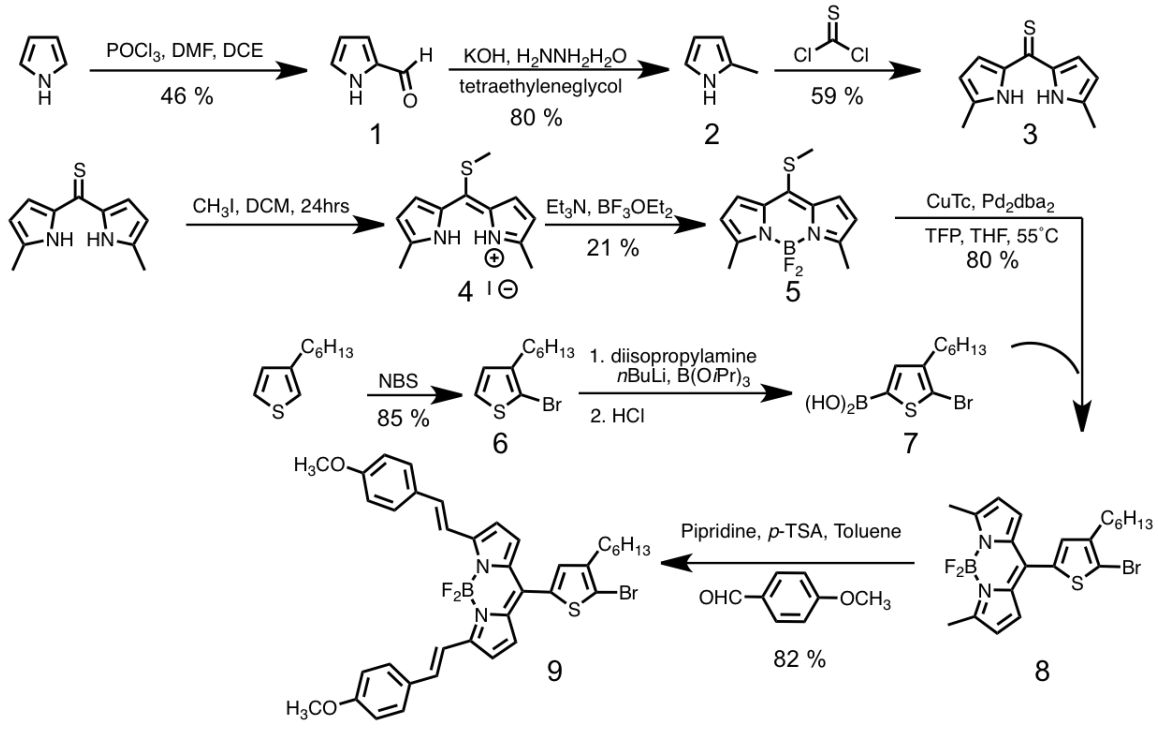

Scheme 4.1 Synthetic route of alpha-conjugation extended BODIPY cap, bearing 2-bromo-3-hexylthiophene functionality.

Synthesis of BODIPY with extended conjugation started with the reaction between pyrrole and dimethylformaldehyde (DMF) to form pyrrole-2-carbaldehyde, which was reduced in presence of hydrazine to produce 2-methylpyrrole. Reaction of two molecules of 2-methylpyrrole with thiophosgene yielded a thionyl derivative bearing two pyrrole rings, which was further reacted with methyliodide to convert the thionyl into a thiomethyl functionality. This was followed by the sequential reaction with triethylamine (TEA) and boron etherate to produce a BODIPY moiety with aromaticity on its entire cyclic structure. Separately, 3-hexylthiophene was mono-bromonated in the presence of *N*-bromosuccinimide (NBS) and glacial acetic acid, which was followed by functionalization of boronic acid on the 5 position of thiophene ring. The *alpha* proton of thiophene was deprotonated using lithium diisopropylamine (LDA), which allows the bromine on the 2-position to remain intact due to steric hindrance of LDA.[43,44] Then, the addition of triisopropylborate yielded 2-bromo-3-hexyl-5-diisopropylborothiophene, followed by acidification in the presence of hydrochloric acid. Separately, synthesized boronic acid-functionalized thiophene and thiomethyl BODIPY were conjugated in the presence of a palladium catalyst in mild basic condition through the Liebeskind-Srogl coupling reaction.[44,45] Then, a reduction reaction of methyl-BODIPY and *p*-methoxybenzaldehyde completed the synthesis of BODIPY cap with extended conjugation through its *alpha*-position, which is assigned as ExtBDP.

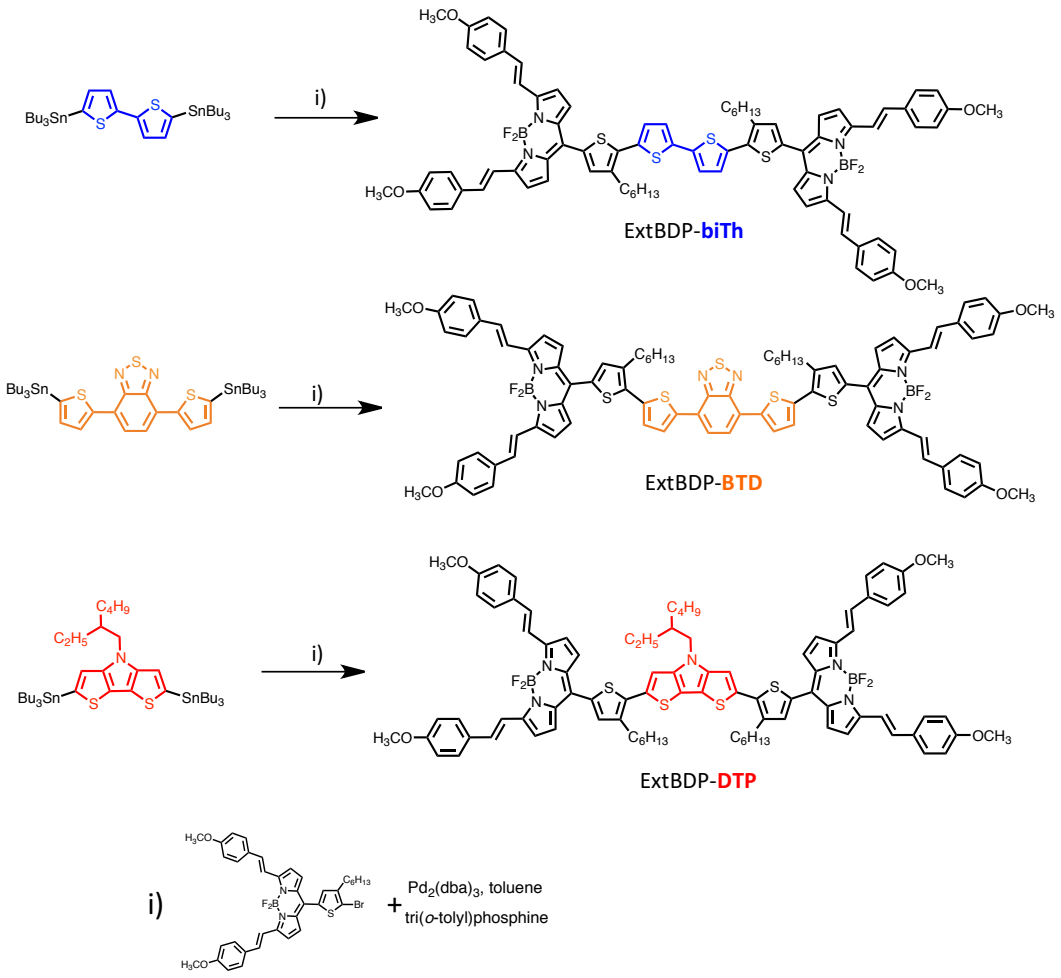

Scheme 4.2 Synthesis of *alpha*-conjugation extended BODIPY derivatives via Stille coupling reaction in the presence of palladium catalyst.

Synthesis of various core were achieved separately, then the *alpha*-conjugation extended BODIPY caps were installed at the final step, which provided a strategical approach to incorporate any compatible core. All cores were prepared with a bis(tributylstannyl)-functionality at both ends of the cores following a reported procedure.[71–77] The biTh core was lithiated using *n*-butyllithium, then reacted with tributyltin chloride to yield 5,5'-bis(tributylstannyl)-2,2'-bithiophene. The synthesis of BTD core starts from a Stille coupling reaction between 4,7-dibromobenzothiadiazole and 2-(tributyl)stannylthiphene in the presence of a palladium catalyst, followed by

lithiation using LDA to obtain 4,7-bis(5-(tributylstannyl)thiophene-2-yl)benzo[c][1,2,5]thiadiazole. The DTP core was synthesized from 2,2'-bithiophene reaction with bromine in the presence of acetic acid to give 3,3',5,5'-tetrabromo-2,2'-bithiophene, which was then reacted with zinc in acidic condition to generate 3,3'-dibromo-2,2'-bithiophene. Then, reaction between the bromo-functionalities on bithiophene and the primary amine of 2-ethyhexylamine providesd the DTP structure *via* ring closure, then finally, following stannylation, gave the final product, 4-(2-ethylhexyl)-2,6-bis(tributylstannyl)-4*H*-dithieno[3,2-*b*:2',3'-*d*]pyrrole.

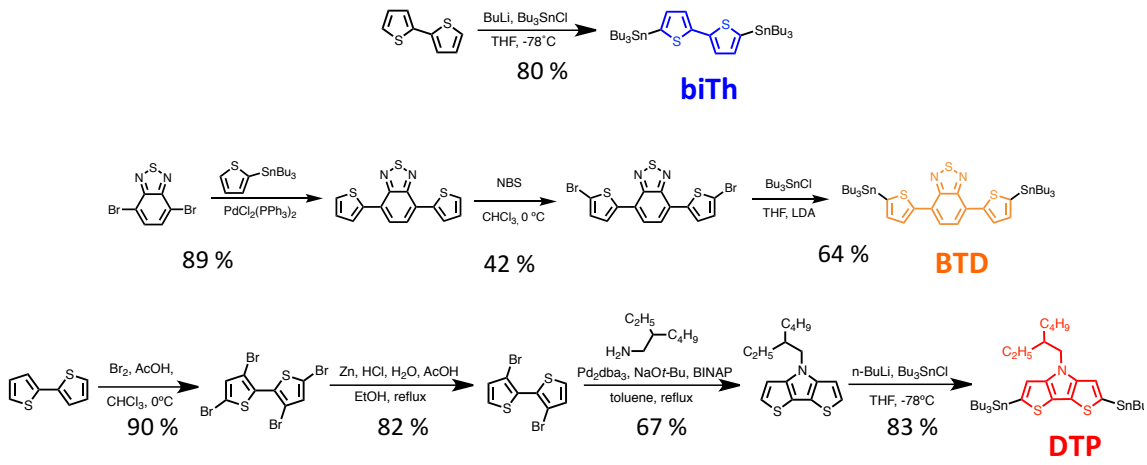

Scheme 4.3 Synthetic scheme of various cores: biTh[73], BTD[72,74,77] and DTP [71,75,76].

The synthesis of final targeted ExtBDP-core-ExtBDP compounds, bearing two symmetric ExtBDP on the varied middle core, was completed by Stille coupling between brominated ExtBDP and bis(tributylstannyl)-modified cores in the presence of a palladium catalyst and tri(*o*-tolyl)phosphine. All final compounds were achieved and identified by ^{1}H-NMR and mass spectrometry, however, high purity of the products could

not be achieved, which impacted our ability to perform purity-sensitive characterizations including cyclovoltammetry and device performances.

4.4. Optoelectronic Property

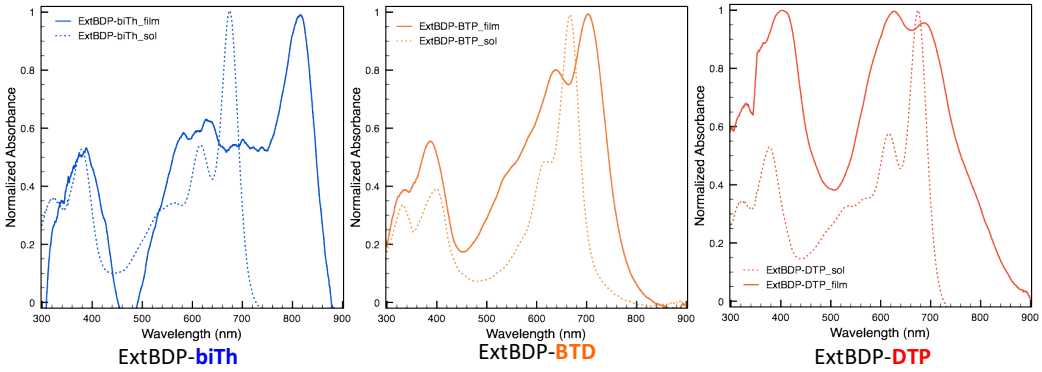

Figure 4.4 UV/vis spectra of *alpha*-conjugation extended BODIPYs, incorporated on various cores, in solution (solid line) and in film state (dotted line).

The absorption property of BODIPY derivatives with extended *alpha*-conjugation was compared to a BODIPY derivative without conjugation previously investigated in our group. The absorption spectra of synthesized ExtBDP-core-ExtBDP are shown in Figure 4.4 and their properties are summarized in Table 4.1. The dotted line and solid line in each plot indicate chloroform ($CHCl_3$) solution state and thin film state of the compounds, respectively. All the ExtBDP-core-ExtBDP molecules show a strong and sharp peak at around 670 nm, which is considerably red shifted compared to the BODIPY derivative that does not contain conjugation extension (Figure 4.6). In the film state, typical band broadening behaviors were observed in all the extended BODIPY-based compounds. Interestingly, ExtBDP-biTh showed a surprising feature of a λmax that was red shifted by 142 nm, providing λmax greater than 800 nm. Also, ExtBDP-DTP showed a great improvement in absorption intensity around 400 nm in the solid state compared to

the solution state. The optical band gap was calculated based on the onset wavelength in the film state. Interestingly, all ExtBDP-coreExtBDPs bandgaps were more and less same at 1.4 eV. The extinction coefficients of the species were obtained by the slope of absorbance vs. concentration based on Beer's law. All extended BODIPY compounds exhibited strong extinction coefficients with 10^5 magnitude. Specially, it was found that ExtBDP-biTh has a value of 3.3 x 10^5 M^{-1} cm^{-1}, about 3-fold the values compared to ExtBDP-BTD and ExtBDP-DTP. The combination of a strong extinction coefficient and a wide absorption profile of ExtBDP-biTh makes it a good candidate for light-harvesting for photovoltaics.

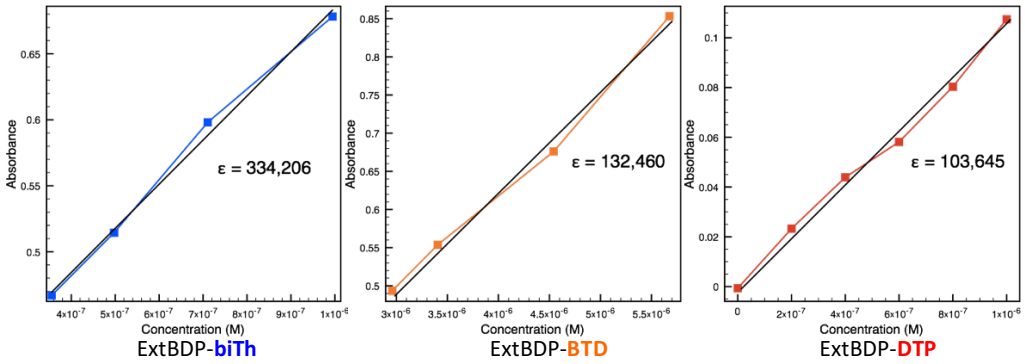

Figure 4.5 Absorption coefficients of BODIPY derivatives with *alpha*-conjugation extension.

The absorption properties of the solid state extended BODIPY derivatives were also compared to their corresponding BODIPYs that do not contain *alpha*-conjugation extension that have been previously reported in our group.

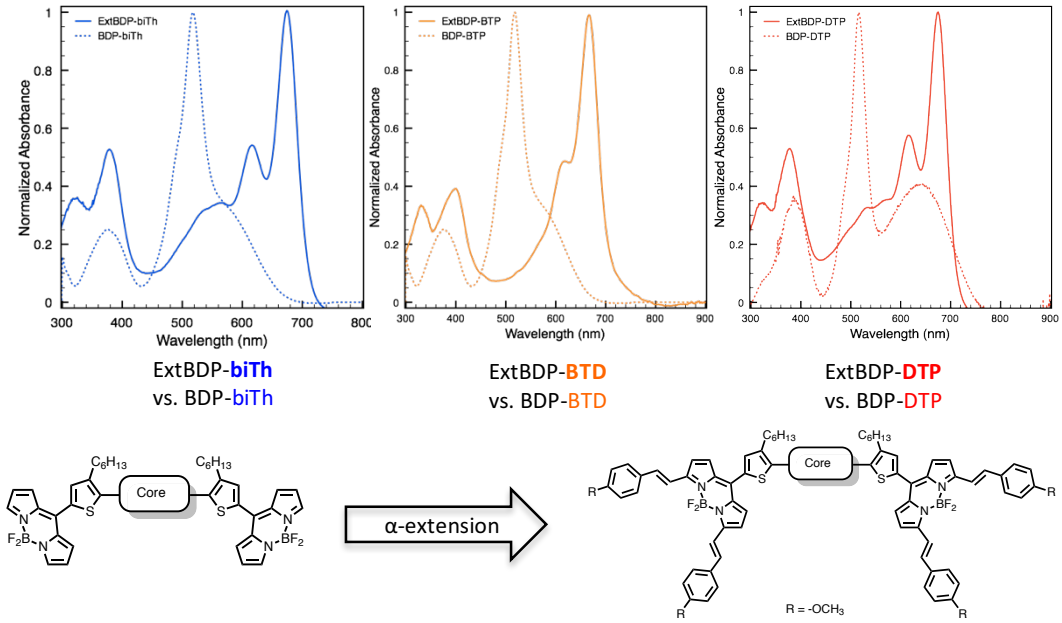

Figure 4.6 UV/vis spectra of *alpha*-conjugation extended BODIPY in solution, compared with those of BODIPYs without conjugation extension through *alpha* position.

The significant red shift of about 200 nm was observed for the alpha-conjugated BODIPYs compared to the non-extended BODIPY, which is characteristic of a π-π* transition in the BODIPY moiety. The shoulder peaks that are attributed to the core moiety remained almost the same in all cases, regardless conjugation extension.

Table 4.1 Summarized optical properties of alpha-conjugation extended BODIPY derivatives, obtained from UV/vis spectroscopy in solution and solid states.

	λ^{sol}_{max} (nm)	λ^{film}_{max} (nm)	ε (x 10^5 $M^{-1}cm^{-1}$)	λ^{film}_{onset} (nm)	ΔE_g^{opt} (eV)
ExtBDP-biTh	674	816	3.3	879	1.41
ExtBDP-BTD	667	704	1.3	858	1.45
ExtBDP-DTP	675	628	1.0	896	1.38

Figure 4.7 shows the fluorescence spectrum of ExtBDP-biTh. The excitation peaks are well matched with its absorption profile, and a typical bathochromic shift in fluorescence was observed. Due to the wavelength detection limit, the fluorescence of ExtBDP-BTD and ExtBDP-DTP were not clearly measured.

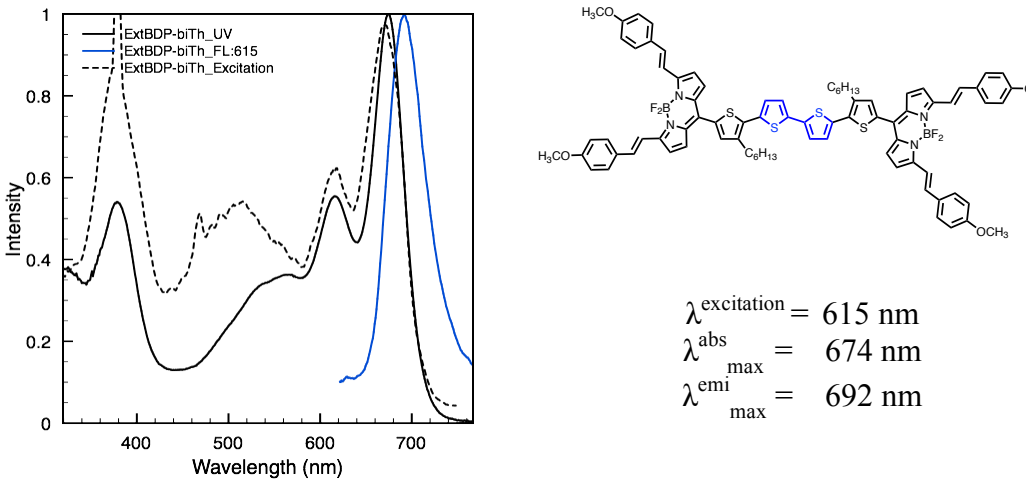

Figure 4.7 Fluorescence spectrum of ExtBDP-biTh, displayed with its UV/vis absorption profile as well as excitation spectrum. Fluorescence emission is measured upon excitation at 615 nm.

4.5. DFT Calculations

In order to investigate frontier orbital energy levels, density functional theory (DFT) calculations were used in the B3LYP/6-311G (d,p) level. The images of electron density in both the HOMO and LUMO levels for all BODIPY derivatives are shown in Figure 4.8.

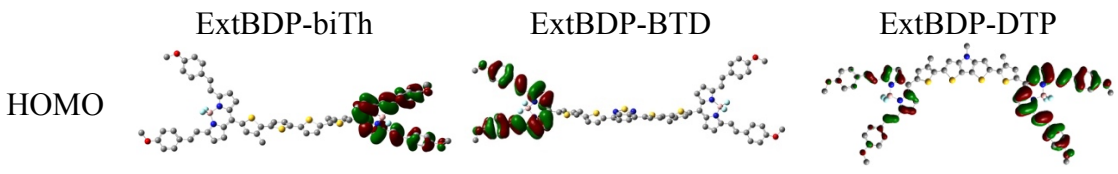

LUMO 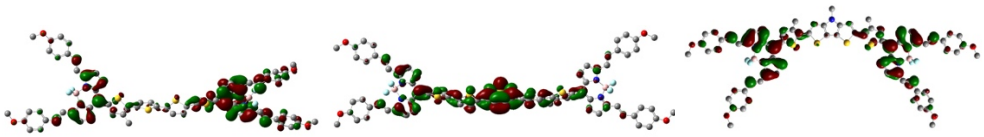

Figure 4.8 HOMO and LUMO electron density diagrams of alpha-conjugation extended BODIPY-based molecules, obtained by DFT calculations.

It was observed that the HOMO wave function was localized on the ExtBDP moiety of the ExtBDP-core-ExtBDP species regardless of core structure, limiting electronical communication through the core unit. Since the core moiety barely affects the electron density of the HOMO level, all three molecules show similar HOMO levels that are attributed from the same extended BODIPY structure at around -4.96 eV. This is very close to the HOMO of P3HT (-5.0 eV). The electron density of the LUMO levels, however, show more electronic communication through the core unit. Specifically, ExtBDP-BTD exhibits major contribution from the BTD core, while contribution from the extended BODIPY cap is limited. This explains the why the LUMO level of ExtBDP-BTD is lower than that of ExtBDP-DTP, which has more electron negativity but less contribution to LUMO electron density. In addition, ExtBDP-biTh displays a small contribution from the core unit in the electron density of the LUMO level, while the BODIPY cap moieties are still dominant.

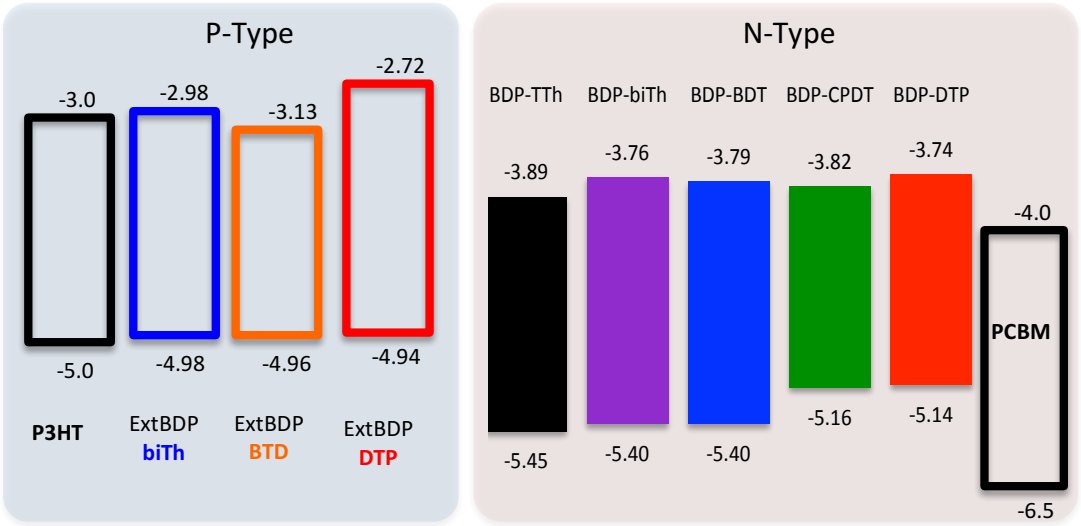

Figure 4.9 Illustration of frontier orbital energy alignment of ExtBDP-based p-type molecules compared with P3HT, and previously reported BDP-based n-type molecules compared with PCBM.

The HOMO levels of extended BODIPY derivatives are compatible with that of P3HT, and their LUMO levels are tunable based on electrochemical property of core. Furthermore, it was noticed that extended BODIPY derivatives exhibit p-type frontier energy levels, whereas previously investigated BODIPY derivatives without *alpha*-conjugation extension showed n-type properties. This is consistent with DFT results, for which the opposite trend was observed for previous BODIPYs: their HOMO levels were largely contributed from the core moieties, while LUMO electron density was more dominantly observed in non-extended BODIPY caps.

Table 4.2 Summarized frontier orbital energy levels and energy band gap, calculated based on DFT studies. The theoretical band gaps are compared with optical band gaps.

	ΔE_g^{opt} (eV)	ΔE_g^{Theo} (eV)	$HOMO^{Theo}$ (eV)	$LUMO^{Theo}$ (eV)
ExtBDP-biTh	1.41	2.00	-4.98	-2.98
ExtBDP-BTD	1.45	1.83	-4.96	-3.13
ExtBDP-DTP	1.38	2.22	-4.94	-2.72

4.6. Summary

In summary, a series of organic small molecules composed of various cores conjugated to two *alpha*-conjugation extended BODIPY caps through their *meso* position, containing a 3-hexylthiophene linker in between, were successfully synthesized. In the solution state, all these molecules showed a distinctive peak at around 670 nm, corresponding to the *alpha*-conjugation extended BODIPY moiety, while the various core molecules contributed to shoulder peaks between 450 ~ 650 nm. In the film state, a typical band broadening of conjugated molecules allowed significant coverage of a wide range of the UV/vis spectrum over 890 nm. Upon *alpha*-conjugation extension, the charge transfer band showed a significant red shift, resulting in a very low optical band gap of 1.41, 1.45, and 1.38 eV for ExtBDP-biTh, ExtBDP-BTD, and ExtBDP-DTP, respectively. Furthermore, it was confirmed that extension of BODIPY conjugation dramatically expand the absorption profile into the NIR region (~ 800 nm) with high extinction coefficients ($1 \sim 3 \times 10^5$ M^{-1} cm^{-1}), compared to their respective analogs that do not contain *alpha*-conjugation extension. Based on DFT studies, it was shown that the electron density of the HOMO mainly localized on ExtBDP moieties, whereas that of LUMO have slightly improved orbital overlap on the core units, which consistently supports their similar HOMO levels (-4.98, -4.96, and -4.94 eV) and core-dependent LUMO levels (-2.98, -3.13, and -2.72 eV) for ExtBDP-biTh, ExtBDP-BTD, and ExtBDP-DTP, respectively. Although further studies in device performance and well as charge transfer mobility should be pursued in the future with highly purified samples, we expect the optical properties of these BODIPYs to improve the light harvesting capability of solar cells. By creating a library of BODIPY-based p-type small molecules, we

expected to achieve a fine-tuning of molecular structure to develop active materials in photovoltaic application, especially when combined with BODIPY-based n-type molecules to improve J_{SC} due to its great light-harvesting property. For example, blending of BDP-biTh with ExtBDP-biTh shows a wide profile that covers absorption in the range of 300 ~ 900 nm (Figure 4.10). This is compatible with the P3HT:PCBM system, which has an absorption profile limited to 300 ~ 550 nm with a lower absorption coefficient. Based on these improved light-harvesting properties, we hope to observe enhanced J_{SC} and contribute to superior device performance.

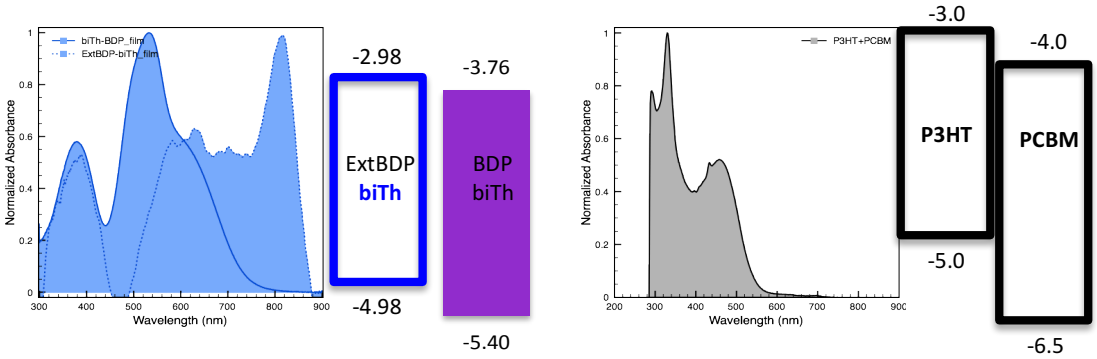

Figure 4.10 UV/vis absorption profiles of a ExtBDP-biTh and BDP-biTh (left) blend, compared with that of a P3HT:PCBM blend (right).

4.7. Experimental Section

4.7.1. Materials and Instrumentation

All chemicals and solvents were purchased from commercial sources and were used as received, unless otherwise described. Analytical techniques: ^{1}H NMR spectra were recorded on a 400 MHz Bruker NMR spectrometer using the residual proton resonance of the solvent as the internal standard. Chemical shifts are reported in parts per

million (ppm). When peak multiplicities are given, the following abbreviations are used: s, singlet; bs, broad singlet; d, doublet; t, triplet; m, multiplet. ^{13}C NMR spectra were proton decoupled and recorded on a 100 MHz Bruker spectrometer using carbon signal of the deuterated solvent as the internal standard. Fluorescence spectra were recorded using a JASCO FP-6500 spectrofluorimeter. FAB-MS spectra were measured on a JEOL JMS700. MALDI-TOF spectra were measured on a Bruker OmnifleX.

4.7.2. Synthesis

4.7.2.1. Synthesis of compound 1

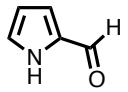

1

To 7 mL of DMF at 0ºC under argon, 7.5 mL of phosphorus oxychloride (12.57 g, 82.1 mmol) was added dropwise. The reaction was stirred for 15 min at room temperature. The solution was diluted with 1,2-dichloroethane (20 mL), cooled to 0 ºC, then a solution of pyrrole (5 g, 74.6 mmol) in 1,2-dichloroethane (20 mL) was added dropwise. The mixture was heated to reflux for 30 min, then cooled to 0 ºC. A solution of sodium acetate (30.59 g, 373.0 mmol) in water (80 mL) was added. The mixture was again heated at reflux for 30 min, then cooled to room temperature. The mixture was diluted with sat $NaHCO_3$ and extracted with methylene chloride. The solvents were removed under reduced pressure and the crude product was purified by column chromatography on silica gel (EA 20%) to give the product as orange crystals (3.26 g, 46%) ^1H NMR (400 MHz, DMSO-d_6): δ 12.14 ppm (bs, 1H), 9.51 (s, 1H), 7.25 (m, 1H),

7.03 (m, 1H), 6.31 (m, 1H). ^{13}C NMR (100 MHz, $CDCl_3$): δ 179.5, 132.8, 127.1, 121.9, 111.3.

4.7.2.2. Synthesis of compound 2

2

Compound 2 (2.4 g, 25 mmol) and KOH (4.3 g) were dissolved in tetraethylene glycol (30 mL), then hydrazine monohydrate (4.5 mL) was added. The reaction mixture was refluxed for 3 hours, during which time the yellow solid was dissolved. Distillation under reduced pressure produced water and 2-methyl pyrrole. The organic layer was extracted with ether and dried with Na_2SO_4. The solvent was evaporated to give 2-methylpyrrole (1.62 g, 80%): ^{1}H NMR (400 MHz, $CDCl_3$) δ 6.72 (s, 1H), 5.97 (s, 1H), 5.80 (s, 1H), 2.27 (s, 3H). ^{13}C NMR (100 MHz, $CDCl_3$) δ 181.0, 86.7, 84.5, 75.6, 65.0.

4.7.2.3. Synthesis of compound 3[78]

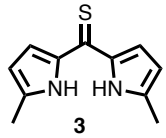

3

In a single neck 50mL flask, $CSCl_2$ (0.71g, 0.0062 mmol) was dissolved in toluene under Ar atmosphere, and the mixture was cooled to 0˚C. A solution of compound 3 (1g, 0.0123 mmol) in ethyl ether was added dropwise by syringe. The

mixture immediately darkened and was stirred at 0˚C for 10 min. An aq. 10mL of MeOH was added, and the mixture was raised to room temperature and stirred for 30 min. The solvents were evaporated and the residue was dissolved in methylene chloride and adsorbed on alumina. The column was run with ethylacetate:hexanes. ^{1}H NMR (400 MHz, $CDCl_3$): δ 9.58 (1H, br s), 6.90 (2H, d, J=6.0 Hz), 6.10 (2H, d, J=6.0 Hz), 2.78 (s, 6H). ^{13}C NMR (100 MHz, $CDCl_3$): δ 187.2, 139.5, 137.4, 115.8, 111.7, 14.0.

4.7.2.4. Synthesis of compound 4[78]

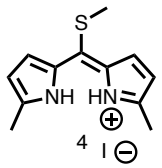

Compound 3 (0.64 g, 3.14 mmol) was dissolved in methylene chloride, then iodomethane (0.88 ml, 14.11 mmol) was added at room temperature. The mixture was stirred at room temperature for 24 hrs. The solvents were evaporated and the red gummy crude was used for the following step without further purification.

4.7.2.5. Synthesis of compound 5[78]

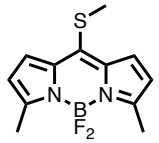

5

The crude of previous reaction mixture was dissolved in methylene chloride, then triethylamine (0.48 ml, 3.39 mmol) was added at room temperature. After stirring for 30 min, BF_3OEt_2 (0.39 ml) was added, then stirred for an additional 30 min at room temperature. After evaporation of solvents under vacuum, the crude product was

chromatographed on silica gel (using 15% EtOAc in hexanes) to yield the product as a dark red solid (0.28 g, 34 %). ^{1}H NMR (400 MHz, $CDCl_3$): δ 7.26 (d, J=5.2 Hz, 2H), 6.24 (d, J=5.2 Hz, 2H), 2.68 (s, 3H), 2.57 (s, 6H), ^{13}C NMR (100 MHz, $CDCl_3$): δ 156.8, 144.2, 135.3, 128.3, 119.1, 21.5, 14.8.

4.7.2.6. Synthesis of compound 6[79]

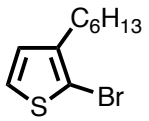

6

3-Hexyl thiophene (3.0 g, 18 mmol) was dissolved in acetic acid (50 mL) in an 50mL round bottom flask. *N*-Bromosuccinimide (3.2 g, 18 mmol,) was added and the solution was stirred for 30 min in the dark at room temperature. Water (50mL) was added and the organic layer was extracted with diethyl ether, washed with each $NaHCO_3$, water, and brine, then dried over Na_2SO_4. After filtration, the organic layer was concentrated under reduced pressure to yield a colorless oil (85%). The crude product was used in the next step without further purification. ^{1}H NMR (400Hz, $CDCl_3$) δ 7.19 (d, 1H), 6.81 (d, 1H), 2.57 (t, 2H), 1.62-1.56 (m, 2H), 1.35-1.30 (m, 6H), 0.92 (t, 3H). ^{13}C NMR (100Hz, $CDCl_3$) δ 142.1, 128.4, 125.3, 108.9, 77.4, 77.2, 76.9, 31.8, 29.9, 29.5, 29.0, 22.8, 14.2.

4.7.2.7. Synthesis of compound 7[75]

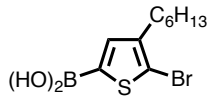

7

A cool solution of diisopropylamine (1.36 mL, 9.71 mmol) was added to *n*-BuLi (0.36 mL, 8.90 mmol) at -78˚C. The mixture was stirred for 30 min, then compound 6 (2 g, 8.09 mmol) was added dropwise in THF and the mixture was stirred for an additional 1hour. B(O*i*Pr)$_3$ (4.67 mL, 20.23 mmol) was then added in one portion. The reaction was raised to room temperature and stirred overnight. Finally, 10% aq. HCl was added and the mixture was stirred for a further 30 min. The mixture was extracted with EtOAc and dried over Na_2SO_4. The ratio of the product to unreacted starting material was calculated based on ^{1}H NMR spectroscopy. The reaction mixture was used without further purification

4.7.2.8. Synthesis of compound 8[75]

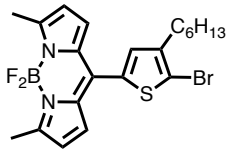

8

Compound 5 (0.399 g, 1.50 mmol) and compound 7 (1.31 g, 4.50 mmol) were dissolved in dry THF. A solid mixture of CuTC (0.858 g, 4.50 mmol), $Pd_2(dba)_3$ (34.3 mg, 0.037 mmol), and TFP (36.3 mg, 0.112 mmol) were added to the reaction flask in one portion. The reaction mixture was refluxed at 55 ˚C for 3 hours. The mixture was evaporated and purified by column chromatography to give compound 8 (80 %). ^{1}H-

NMR (400MHz, $CDCl_3$): δ 7.11 (s, 1H), 7.05-7.04 (d, *J* = 7.0 Hz, 2H), 6.30-6.29 (d, *J* = 6.2 Hz, 2H), 2.64 (m, 8H), 1.66-1.59 (m, 2H), 1.39-1.29 (m, 6H), 0.90 (t, J = 6.5 Hz, 3H). ^{13}C-NMR (100MHz, $CDCl_3$): δ 137.4, 136.1, 136.0 129.2, 125.0, 122.6, 119.1, 111.8, 108.4, 32.4, 30.0, 28.9, 28.6, 22.6, 15.5, 14.0, 9.3.

4.7.2.9. Synthesis of compound 9

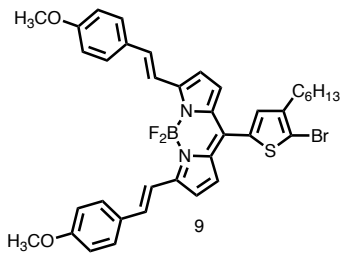

9

Compound 8 (216 mg, 0.464 mmol) and 4-methoxybenzaldehyde were dissolved in benzene, then piperidine and glacial acetic acid were added. The solution was refluxed using a Dean-Stark apparatus. Once the solution was concentrated, the reaction was monitored by TLC (20% ethyl acetate in hexanes) until the green-colored compound became the major product. Benzene was evaporated by a flow of air, then the reaction was extracted with $CHCl_3$ and water. The organic layer was dried with sodium sulfate and evaporated under reduced pressure. The product was purified by silica gel column chromatography using ethyl acetate:hexane as mobile phase. The fraction containing the product was collected then the solvent was removed under reduced pressure. 82%). ^{1}H-NMR (400MHz, $CDCl_3$): δ 7.66-7.59 (m, 6H), 7.32-7.28 (d, *J* = 16 Hz, 2H), 7.11-7.10 (m, 3H), 6.95-6.92 (m, 6H), 3.86 (s, 6H), 2.65 (t, J = 7.7 Hz, 2H), 1.65 (m, 2H), 1.41-1.33 (m, 6H), 0.91 (t, J = 6.9 Hz, 3H). ^{13}C NMR (100Hz, $CDCl_3$) δ 160.4, 137.4, 136.1, 136.0, 133.4, 129.2, 128.9, 126.3, 125.0, 122.6, 119.1, 114.7, 114.3, 111.8, 108.4, 55.4, 32.4,

30.0, 28.9, 28.6, 22.6, 14.0. MS (MALDI-MS): calc. for $C_{37}H_{36}BBrF_2N_2O_2S$: 701.5; found: 702.2

4.7.2.10. General synthetic procedure for ExtBDP-Core-ExtBDPs

Compound 9 (0.214 mmol) and a desired core molecule (0.097 mmol) were dissolved in degassed toluene, then $Pd_2(dba)_3$ (2.5 mol%) and tri(*o*-tolyl)phosphine (7.5 mol%) were added. The reaction was heated to reflux and stirred for 24 hr. The solvents were removed *in vacuo* and the crude was attempted to purify by silica gel column chromatography and dialysis against chloroform. However, successful purification with high purity was failed.

4.8. Reference

(1) Gorman, A.; Killoran, J.; O'Shea, C.; Kenna, T.; Gallagher, W. M.; O'Shea, D. F. In Vitro Demonstration of the Heavy-Atom Effect for Photodynamic Therapy. *J. Am. Chem. Soc.* **2004**, *126* (34), 10619–10631.

(2) Kochevar, I. E.; Redmond, R. W. Photosensitized Production of Single Oxygen. *Methods Enzymol.* **2000**, *319*, 20–28.

(3) Chen, X.; Li, Y.; Wang, A.; Zhou, L.; Lu, S.; Zhou, J.; Lin, Y.; Wei, S. Protonation Salt Derivative with Heavy-Atom Effect on Phthalocyanine for Enhanced in Vitro Photodynamic Therapy. *Dye. Pigment.* **2015**, *114* (C), 93–104.

(4) Yogo, T.; Urano, Y.; Ishitsuka, Y.; Maniwa, F.; Nagano, T. Highly Efficient and Photostable Photosensitizer Based on BODIPY Chromophore. *J. Am. Chem. Soc.* **2005**, *127* (35), 12162–12163.

(5) Rodriguez-Serrano, A.; Rai-Constapel, V.; Daza, M. C.; Doerr, M.; Marian, C. M. Internal Heavy Atom Effects in Phenothiazinium Dyes: Enhancement of Intersystem Crossing via Vibronic Spin-Orbit Coupling. *Phys. Chem. Chem. Phys.* **2015**, *17* (17), 11350–11358.

(6) Cui, G.; Fang, W. H. State-Specific Heavy-Atom Effect on Intersystem Crossing Processes in 2-Thiothymine: A Potential Photodynamic Therapy Photosensitizer. *J. Chem. Phys.* **2013**, *138* (4).

(7) Turro, N. J. The Triplet State. *J. Chem. Educ.* **1966**, *46* (1), 2–6.

(8) McClure, D. S. Spin-Orbit Interaction in Aromatic Molecules. *J. Chem. Phys.* **1952**, *20* (4), 682.

(9) Lower, S.; El-Sayed, M. The Triplet State and Molecular Electronic Processes in

Organic Molecules. *Chem. Rev.* **1966**, *66* (2), 199–241.

(10) Levine, I. N. Quantum Chemistry; Allyn and Bacon: Boston, 1970; pp 306–310.

(11) McClure, D. S. Triplet-Singlet Transitions in Organic Molecules. Lifetime Measurements of the Triplet State. *J. Chem. Phys.* **1949**, *17* (10), 905.

(12) Ermolaev, V. L.; Svitasbev, K. K. Quantum Yields of Phosphorescence and Fluorescence of Some 1-Derivatives of Naphthalene in Solutions at -196˚C.pdf. *Opt. Spectrosc.* **1959**, *1*, 399.

(13) Cowan, D. O. Elements of Organic Photochemistry. In *Elements of Organic Photochemistry*; Plenum Press: New York, N.Y., 1976; pp 250–262.

(14) Chock, P. B.; Stadtman, E. R. Superiority of Interconvertible Enzyme Cascades in Metabolite Regulation: Analysis of Multicyclic Systems. *Proc Natl Acad Sci U S A* **1977**, *74* (7), 2766–2770.

(15) Koshland, D. E.; Goldbeter, A.; Stock, J. B. Amplification and Adaptation in Regulatory and Sensory Systems Author (S): Daniel E . Koshland , Albert Goldbeter and Jeffry B . Stock Published by : American Association for the Advancement of Science Stable URL : http://www.jstor.org/stable/1689499 JS. **2017**, *217* (4556), 220–225.

(16) Chock, P. B.; Rhee, S. G.; Stadtman, E. R. Interconvertible Enzyme Cascades in Cellular-Regulation. *Annu. Rev. Biochem.* **1980**, *49*, 813–843.

(17) Bhalla and Ravi Iyengar, U. S. Emergent Properties of Networks of Biological Signaling Pathways. *Science (80-.).* **1999**, *283* (5400), 381–387.

(18) Weng, G. Complexity in Biological Signaling Systems. *Science (80-.).* **1999**, *284* (5411), 92–96.

(19) Jordan, J. D.; Landau, E. M.; Iyengar, R. Signaling Networks: The Origins of Cellular Multitasking. *Cell* **2000**, *103* (2), 193–200.

(20) Levine, S. N. Enzyme Amplifier Kinetics. *Science (80-.).* **1966**, *152* (3722), 651–653.

(21) Wald, G. Visual Excitation and Blood Clotting. *Science* **1965**, *150* (3699), 1028–1030.

(22) Brown, G. C.; Hoek, J. B.; Kholodenko, B. N. Why Do Protein Kinase Cascades Have More than One Level? *Trends Biochem. Sci.* **1997**, *22*, 288.

(23) Fozooni, T.; Ravan, H.; Sasan, H. Signal Amplification Technologies for the Detection of Nucleic Acids: From Cell-Free Analysis to Live-Cell Imaging. *Appl. Biochem. Biotechnol.* **2017**, 1–30.

(24) Wu, W.; Bazan, G. C.; Liu, B. Conjugated-Polymer-Amplified Sensing, Imaging, and Therapy. *Chem* **2017**, *2* (6), 760–790.

(25) Mittal, S.; Kaur, H.; Gautam, N.; Mantha, A. K. Biosensors for Breast Cancer Diagnosis: A Review of Bioreceptors, Biotransducers and Signal Amplification Strategies. *Biosens. Bioelectron.* **2017**, *88*, 217–231.

(26) Dewit, M. A.; Nazemi, A.; Karamdoust, S.; Beaton, A.; Gillies, E. R. Design, Synthesis and Assembly of Self-Immolative Linear Block Copolymers. *Non-Coventional Funct. Block Copolym.* **2011**, 9–21.

(27) Li, Y.; Liu, G.; Wang, X.; Hu, J.; Liu, S. Enzyme-Responsive Polymeric Vesicles for Bacterial-Strain-Selective Delivery of Antimicrobial Agents. *Angew. Chemie - Int. Ed.* **2016**, *55* (5), 1760–1764.

(28) Liu, G.; Wang, X.; Hu, J.; Zhang, G.; Liu, S. Self-Immolative Polymersomes for

High-Efficiency Triggered Release and Programmed Enzymatic Reactions. *J. Am. Chem. Soc.* **2014**, *136* (20), 7492–7497.

(29) Sauer, M.; Haefele, T.; Graff, a; Nardin, C.; Meier, W. Ion-Carrier Controlled Precipitation of Calcium Phosphate in Giant ABA Triblock Copolymer Vesicles. *Chem. Commun. (Camb).* **2001**, No. 23, 2452–2453.

(30) Sceince, P. Polymer Vesicles. *Science (80-.).* **2005**, *297* (17), 967–974.

(31) Wu, J.; Eisenberg, A. Proton Diffusion across Membranes of Vesicles of Poly(styrene-B-Acrylic Acid) Diblock Copolymers. *J. Am. Chem. Soc.* **2006**, *128* (9), 2880–2884.

(32) Gabrielli, L.; Mancin, F. Minimal Self-Immolative Probe for Multimodal Fluoride Detection. *J. Org. Chem.* **2016**, *81* (22), 10715–10720.

(33) Amir, R. J.; Pessah, N.; Shamis, M.; Shabat, D. Self-Immolative Dendrimers. *Angew. Chemie - Int. Ed.* **2003**, *42* (37), 4494–4499.

(34) Shamis, M.; Shabat, D. Single-Triggered AB6 Self-Immolative Dendritic Amplifiers. *Chemistry* **2007**, *13* (16), 4523–4528.

(35) Tan, X.; Li, B. B.; Lu, X.; Jia, F.; Santori, C.; Menon, P.; Li, H.; Zhang, B.; Zhao, J. J.; Zhang, K. Light-Triggered, Self-Immolative Nucleic Acid-Drug Nanostructures. *J. Am. Chem. Soc.* **2015**, *137* (19), 6112–6115.

(36) Niculescu-Duvaz, I.; Niculescu-Duvaz, D.; Friedlos, F.; Spooner, R.; Martin, J.; Marais, R.; Springer, C. J. Self-Immolative Nitrogen Mustard Prodrugs for Suicide Gene Therapy. *J. Med. Chem.* **1998**, *41* (13), 5297–5309.

(37) De Groot, F. M. H.; Albrecht, C.; Koekkoek, R.; Beusker, P. H.; Scheeren, H. W. "Cascade-Release Dendrimers" liberate All End Groups upon a Single Triggering

Event in the Dendritic Core. *Angew. Chemie - Int. Ed.* **2003**, *42* (37), 4490–4494.

(38) Shamis, M.; Lode, H. N.; Shabat, D. Bioactivation of Self-Immolative Dendritic Prodrugs by Catalytic Antibody 38C2. *J. Am. Chem. Soc.* **2004**, *126* (6), 1726–1731.

(39) Dresselhaus, M.S.; Thomas, I. . Alternative Energy Technologies. *Nature* **2001**, *414* (November), 332–337.

(40) Gregg, B. A.; Hanna, M. C. Comparing Organic to Inorganic Photovoltaic Cells: Theory, Experiment, and Simulation. *J. Appl. Phys.* **2003**, *93* (6), 3605–3614.

(41) https://energy.gov/eere/solar/downloads/research-cell-efficiency-records.

(42) Potscavage, W. J.; Sharma, a; Kippelen, B. Critical Interfaces in Organic Solar Cells and Their Influence on the Open-Circuit Voltage. *Acc. Chem. Res.* **2009**, *42* (11), 1758–1767.

(43) Carsten, B.; Szarko, J. M.; Son, H. J.; Wang, W.; Lu, L.; He, F.; Rolczynski, B. S.; Lou, S. J.; Chen, L. X.; Yu, L. Examining the Effect of the Dipole Moment on Charge Separation in Donor-Acceptor Polymers for Organic Photovoltaic Applications. *J. Am. Chem. Soc.* **2011**, *133* (50), 20468–20475.

(44) Yao, K.; Intemann, J. J.; Yip, H.-L.; Liang, P.-W.; Chang, C.-Y.; Zang, Y.; Li, Z.; Chen, Y.; Jen, A. K.-Y. Efficient All Polymer Solar Cells from Layer-Evolved Processing of a Bilayer Inverted Structure. *J. Mater. Chem. C* **2014**, *2* (3), 416.

(45) Takacs, C. J.; Sun, Y.; Welch, G. C.; Perez, L. A.; Liu, X.; Wen, W.; Bazan, G. C.; Heeger, A. J. Solar Cell Efficiency, Self-Assembly, and Dipole-Dipole Interactions of Isomorphic Narrow-Band-Gap Molecules. *J. Am. Chem. Soc.* **2012**, *134* (40), 16597–16606.

(46) Beaujuge, P. M.; Fréchet, J. M. J. Molecular Design and Ordering Effects in π-Functional Materials for Transistor and Solar Cell Applications. *J. Am. Chem. Soc.* **2011**, *133* (50), 20009–20029.

(47) Kallmann, H.; Pope, M. Photovoltaic Effect in Organic Crystals. *J. Chem. Phys.* **1959**, *30* (2), 585–586.

(48) Benanti, T. L.; Venkataraman, D. Organic Solar Cells: An Overview Focusing on Active Layer Morphology. *Photosynth. Res.* **2006**, *87* (1), 73–81.

(49) Yu, G.; Pakbaz, K.; Heeger, A. J. Semiconducting Polymer Diodes: Large Size, Low Cost Photodetectors with Excellent Visible-Ultraviolet Sensitivity. *Appl. Phys. Lett.* **1994**, *64* (25), 3422–3424.

(50) Dang, M. T.; Hirsch, L.; Wantz, G. P3HT:PCBM, Best Seller in Polymer Photovoltaic Research. *Adv. Mater.* **2011**, *23* (31), 3597–3602.

(51) Wu, P. T.; Xin, H.; Kim, F. S.; Ren, G.; Jenekhe, S. A. Regioregular poly(3-Pentylthiophene): Synthesis, Self-Assembly of Nanowires, High-Mobility Field-Effect Transistors, and Efficient Photovoltaic Cells. *Macromolecules* **2009**, *42* (22), 8817–8826.

(52) Gabe, Y.; Ueno, T.; Urano, Y.; Kojima, H.; Nagano, T. Tunable Design Strategy for Fluorescence Probes Based on 4-Substituted BODIPY Chromophore: Improvement of Highly Sensitive Fluorescence Probe for Nitric Oxide. *Anal. Bioanal. Chem.* **2006**, *386* (3), 621–626.

(53) Li, Y.; Wang, J.; Zhang, X.; Guo, W.; Li, F.; Yu, M.; Kong, X.; Wu, W.; Hong, Z. Highly Water-Soluble and Tumor-Targeted Photosensitizers for Photodynamic Therapy. *Org. Biomol. Chem.* **2015**, *13* (28), 7681–7694.

(54) Gee, K. R.; Archer, E. A.; Kang, H. C. 4-Sulfotetrafluorophenyl (STP) Esters: New Water-Soluble Amine-Reactive Reagents for Labeling Biomolecules. *Tetrahedron Lett.* **1999**, *40* (8), 1471–1474.

(55) Hendel, S. J.; Poe, A. M.; Khomein, P.; Bae, Y.; Thayumanavan, S.; Young, E. R. Photophysical and Electrochemical Characterization of BODIPY-Containing Dyads Comparing the Influence of an A–D–A versus D–A Motif on Excited-State Photophysics. *J. Phys. Chem. A* **2016**, *120*, 8794–8803.

(56) Gollnick, K.; Griesbeck, A. Singlet Oxygen Photooxygenation of Furans. *Tetrahedron* **1985**, *41* (11), 2057–2068.

(57) Morone, M.; Beverina, L.; Abbotto, A.; Silvestri, F.; Collini, E.; Ferrante, C.; Bozio, R.; Pagani, G. A. Enhancement of Two-Photon Absorption Cross-Section and Singlet-Oxygen Generation in Porphyrins upon ??-Functionalization with Donor-Acceptor Substituents. *Org. Lett.* **2006**, *8* (13), 2719–2722.

(58) Deng, P.; Zhang, Q. Recent Developments on Isoindigo-Based Conjugated Polymers. *Polym. Chem.* **2014**, *5* (10), 3298–3305.

(59) Lin, Y.; Li, Y.; Zhan, X. Small Molecule Semiconductors for High-Efficiency Organic Photovoltaics. *Chem. Soc. Rev.* **2012**, *41* (11), 4245.

(60) Zhang, Z.; Wang, J. Structures and Properties of Conjugated Donor–Acceptor Copolymers for Solar Cell Applications. *J. Mater. Chem.* **2012**, *22* (10), 4178.

(61) Zhou, H.; Yang, L.; You, W. Rational Design of High Performance Conjugated Polymers for Organic Solar Cells. *Macromolecules* **2012**, *45* (2), 607–632.

(62) Hou, J.; Huo, L.; He, C.; Yang, C.; Li, Y. Synthesis and Absorption Spectra of poly(3-(Phenylenevinyl)thiophene)s with Conjugated Side Chains.

Macromolecules **2006**, *39* (2), 594–603.

(63) Hou, J.; Tan, Z.; Yan, Y.; He, Y.; Yang, C.; Li, Y. Synthesis and Photovoltaic Properties of Two-Dimensional Conjugated Polythiophenes with Bi(thienylenevinylene) Side Chains. *J. Am. Chem. Soc.* **2006**, *128* (14), 4911–4916.

(64) He, G.; Li, Z.; Wan, X.; Liu, Y.; Zhou, J.; Long, G.; Zhang, M.; Chen, Y. Impact of Dye End Groups on Acceptor–donor–acceptor Type Molecules for Solution-Processed Photovoltaic Cells. *J. Mater. Chem.* **2012**, *22* (18), 9173.

(65) Liu, J.; Walker, B.; Tamayo, A.; Zhang, Y.; Nguyen, T. Q. Effects of Heteroatom Substitutions on the Crystal Structure, Film Formation, and Optoelectronic Properties of Diketopyrrolopyrrole-Based Materials. *Adv. Funct. Mater.* **2013**, *23* (1), 47–56.

(66) Yuan, J.; Huang, X.; Zhang, F.; Lu, J.; Zhai, Z.; Di, C.; Jiang, Z.; Ma, W. Design of Benzodithiophene-Diketopyrrolopyrrole Based Donor–acceptor Copolymers for Efficient Organic Field Effect Transistors and Polymer Solar Cells. *J. Mater. Chem.* **2012**, *22* (42), 22734.

(67) Sonar, P.; Ng, G.-M.; Lin, T. T.; Dodabalapur, A.; Chen, Z.-K. Solution Processable Low Bandgap Diketopyrrolopyrrole (DPP) Based Derivatives: Novel Acceptors for Organic Solar Cells. *J. Mater. Chem.* **2010**, *20* (18), 3626.

(68) Della Pelle, A. M.; Homnick, P. J.; Bae, Y.; Lahti, P. M.; Thayumanavan, S. Effect of Substituents on Optical Properties and Charge-Carrier Polarity of Squaraine Dyes. *J. Phys. Chem. C* **2014**, *118* (4), 1793–1799.

(69) Huang, X.; Zhu, C.; Zhang, S.; Li, W.; Guo, Y.; Zhan, X.; Liu, Y.; Bo, Z.

Porphyrin-Dithienothiophene π-Conjugated Copolymers: Synthesis and Their Applications in Field-Effect Transistors and Solar Cells. *Macromolecules* **2008**, *41* (19), 6895–6902.

(70) Benniston, A. C.; Copley, G. Lighting the Way Ahead with Boron Dipyrromethene (Bodipy) Dyes. *Phys. Chem. Chem. Phys.* **2009**, *11* (21), 4124.

(71) Oosterhout, S. D.; Savikhin, V.; Zhang, J.; Zhang, Y.; Burgers, M. A.; Marder, S. R.; Bazan, G. C.; Toney, M. F. Mixing Behavior in Small Molecule:Fullerene Organic Photovoltaics. *Chem. Mater.* **2017**, *29* (7), 3062–3069.

(72) Carlé, J. E. Polymers for Organic Photovoltaics Based on 1,5-bis(2-Hexyldecyloxy)-Naphthalene, Thiophene, and Benzothiadiazole. *J. Photonics Energy* **2011**, *1* (1), 11111.

(73) Guo, X.; Watson, M. D. Conjugated Polymers from Napthalene Bisimide. *Org. Lett.* **2008**, *10* (23), 5333–5336.

(74) Eggert Carlé, J.; Wenzel Andreasen, J.; Jørgensen, M.; Christian Krebs, F. Low Band Gap Polymers Based on 1,4-Dialkoxybenzene, Thiophene, Bithiophene Donors and the Benzothiadiazole Acceptor. *Sol. Energy Mater. Sol. Cells* **2010**, *94* (5), 774–780.

(75) Poe, A. M.; Della Pelle, A. M.; Subrahmanyam, A. V.; White, W.; Wantz, G.; Thayumanavan, S. Small Molecule BODIPY Dyes as Non-Fullerene Acceptors in Bulk Heterojunction Organic Photovoltaics. *Chem. Commun.* **2014**, *50* (22), 2913–2915.

(76) Matsumura, S.; Hlil, A. R.; Lepiller, C.; Gaudet, J.; Guay, D.; Shi, Z.; Holdcroft, S.; Hay, A. S. Ionomers for Proton Exchange Membrane Fuel Cells with Sulfonic

Acid Groups on the End-Groups: Novel Branched Poly(ether-Ketone)s. *Am. Chem. Soc. Polym. Prepr. Div. Polym. Chem.* **2008**, *49* (1), 511–512.

(77) Wakim, S.; Beaupré, S.; Blouin, N.; Aich, B.-R.; Rodman, S.; Gaudiana, R.; Tao, Y.; Leclerc, M. Highly Efficient Organic Solar Cells Based on a poly(2,7-Carbazole) Derivative. *J. Mater. Chem.* **2009**, *19* (30), 5351.

(78) Goud, T. V.; Tutar, A.; Biellmann, J. F. Synthesis of 8-Heteroatom-Substituted 4,4-Difluoro-4-Bora-3a,4a-Diaza-S-Indacene Dyes (BODIPY). *Tetrahedron* **2006**, *62* (21), 5084–5091.

(79) Rakstys, K.; Paek, S.; Gao, P.; Gratia, P.; Marszalek, T.; Grancini, G.; Cho, K. T.; Genevicius, K.; Jankauskas, V.; Pisula, W.; et al. Molecular Engineering of Face-on Oriented Dopant-Free Hole Transporting Material for Perovskite Solar Cells with 19% PCE. *J. Mater. Chem. A* **2017**, *5* (17), 7811–7815.

CHAPTER 5

SUMMARY AND FUTURE DIRECTIONS

5.1. Summary

In this thesis, organic small molecules and polymeric materials were designed, synthesized, and studied for their various applications, including photodynamic therapy, signal amplification, and organic photovoltaics. Although all different materials and aim of application, they have common feature of containing light responsive or light harvesting properties.

In chapter 2, BODIPY derivatives were discussed for use as photosensitizers, which is a light-harvesting that can become excited, undergo intersystem crossing, and induce chemical conversion of surrounding oxygen into reactive species that can damage cells in photodynamic therapy. Detailed characterization of electrochemical and photochemical properties of small molecule BODIPY derivatives were evaluated in organic solvents prior to *in vitro* PDT investigations. The structures of BODIPYs are varied in both conjugation extension length and bromination. Bromination of BODIPY molecules imparted a significant modification in their optoelectronic properties: 1) absorption coefficients dropped by about 10-fold, 2) their typical sharp charge transfer absorption band became broad and blue-shifted, absorbing a wider range of visible light, 3) the existence of triplet state was confirmed by transient absorption spectroscopy by observing triplet decay with a life time of 176 μs and 10 μs for BDP-Br and ExtBDP-Br, respectively, and 4) the capacity of singlet oxygen generation increased with a 7-fold

faster initial rate. Alternatively, extension of BODIPY conjugation through its *alpha* position caused different changes in their optoelectronic and physiochemical properties: 1) the absorption profile remained relatively intact but λmax red shifted by about 155 nm, with wide coverage over the NIR region contributed from a red shifted onset wavelength, whereas their extinction coefficient remained more or less the same, 2) for BDP-Br, a broad profile of the triplet state over 650 ~ 750 nm remained intact (700 ~ 800 nm) with a red shift of 50 nm, while its lifetime decreased significantly from 176 μs to 10 μs.

The photosensitizer cytotoxicity capability of BODIPY derivatives was then demonstrated by conjugation to naturally occurring polymer hyaluronic acid (HA). Since HA is well-known for binding with the CD44 receptor on tumor cells such as HeLa, BODIPY-modified HA was investigated for selectivity towards HeLa over CD44- normal cells, HepG2. Aside from target specificity, HA imparts biocompatibility and aqueous solubility to the BODIPY photosensitizers, which showed low toxicity in dark. Selective and controlled HeLa cell cytotoxicity was demonstrated with the HA-BODIPY photosensitizers with controlled LED NIR light treatment, supporting their candidacy for photodynamic therapy applications.

In chapter 3, a light-responsive self-immolative polymeric system was designed with properties such that light exposure caused structural degradation, with the aim of generating signal amplification behavior of a microscale input resulting in a macroscale detection. Here, we prepared a gel from a mixture of a polyanionic self-immolative polymer and a cationic polymer, such that irradiation of light would generate a macroscale morphological change to a solution state. The designed light-responsive material is based on carbamate polymer backbone with a light-sensitive cap at one end of

polymer backbone protecting its primary amine functionality, so that light cleavage generates self-immolation. Degradation of the synthesized polymer with carbamate backbone was characterized by ^{1}H NMR spectroscopy. Also, the cleavage of the end cap upon light exposure was confirmed by UV/vis spectroscopy. The degree of degradation reached 45% within the first 1 hour of light exposure and saturated over the course of light treatment for 7 hours. The homogeneous gel, consisting of negatively charged self-immolative oligomeric polymer and positively charged high Mw polymer, was optimized and used to further investigate rigidity changes as a function of light treatment. It was shown that on initiation of light exposure the rigidity of gel-like solution increased, followed by gradual rigidity decrease over the course of light treatment for 4 hours. Similar trends with different magnitudes of rigidity change was observed regardless of variation in concentration of P- and P+. The achieved demonstration of gel-to-sol transition upon light treatment implies successful manipulation of signal amplification. Readable morphological changes in the form of rigidity indicates a macroscopically amplified signal from microscopically triggered chemical signals in the polymeric mixture.

In chapter 3, BODIPY-based molecules were investigated for improved light-harvesting materials in photovoltaic applications. Novel BODIPY derivatives bearing various core units between two symmetrical BODIPY structures with conjugation extension through their *alpha* position were prepared, denoted ExtBDP-core-ExtBDP. These highly conjugated BODIPY structures exhibit high absorption coefficient up to 10^{5} $M^{-1}cm^{-1}$ in the solution state, as well as typical band broadening in the solid state UV/vis absorption compared to solution state. The derivatives were compared to an analog series

with non-conjugation extension in the structure previously reported in our group. The conjugation extension caused a red shift by 200 nm for these derivatives compared to the non-conjugation extension analogs, attributed to the π-π* charge transfer transition. Density functional theory (DFT) was used to study their frontier orbital energy levels, both the highest occupied molecular orbital (HOMO) and the lowest unoccupied molecular orbital (LUMO). The HOMO levels of ExtBDP-core-ExtBDP compounds showed very similar values of -4.94 ~ -4.98 eV, regardless or core unit, which was attributed to the BODIPY moieties in the compounds. In LUMO levels however involved increased contribution from the core structure, providing a fine tuning of LUMO levels from - 2.72 ~ -3.13 eV. Considering the compatible energy alignment, but wider range of light spectrum absorption with higher ε of ExtBDP-core-ExtBDP compared to P3HT, these derivatives could be a good candidate for p-type active layer materials for improved device efficiency in photovoltaic applications.

5.2. Future Directions

5.2.1. BODIPY-functionalized Hyaluronic Acids for Photodynamic Therapy

Although it was possible to estimate the approximate degree of BODIPY-substitution using UV/vis absorption spectroscopy, the low degree of substitution may cause error in quantification reliability. Because HeLa cells were shown to be very responsive to very low levels of photosensitizers upon LED irradiation, small changes in the degree of substitution can create a big difference in photodynamic effect. Accurate control and conjugation and evaluation of degree of BODIPY substitution on HA would be necessary to further optimize the system for clinical applications. In addition, although

HA-ExtBDP showed high viability in dark and successful cytotoxicity with light *in vitro* as a function of controlling factors such as incubation time, dosage of PS, and time of light exposure, HA-ExtBDP would need to be systemically evaluated *in vivo* for biocompatibility (safety), biodistribution, CD44+ targeting, and long term toxicity for clinical translation.

5.2.2. Light-sensitive Self-immolative Carbamate-based Polymer for Signal Amplification

In chapter 3, we observed the unexpected result that initiation of UV treatment to the gel P-/P+ mixture increased rigidity at the beginning of the degradation process. It is possible that released P- monomeric charged small molecules could further entangle the P+ and non-immolated P+ gel until it reaches a homogeneous equilibrium in solution. Comprehensive mechanistic investigation of the early stage will allow further understanding and optimization of this signal amplification process. In addition, successful optimization and demonstration of gel-to-sol transition based on P- and P+ would allow further designs of morphological transition using other stimuli-sensitive units. Development of a diversity of triggers would translate these gel-sol transitions to a variety of applications.

As discussed in chapter 3, the rigidity change of P-/P+ gel with light exposure treatment occurred over a slow period (4 hours). Considering that shorter P- chain could provide faster depolymerization, a faster and more dramatic signal amplification could be achieved by chain length optimization of P-. Too short a chain length may impact gel formation, and impart no significant morphological change before and after degradation, sacrificing amplification read out. Therefore, finding optimal P- length for rapid and

reliable signal amplification would be the key to highly tailor this system, which would require controlled modification of the P- degree of polymerization and chain length-based study of their degradation kinetics.

5.2.3. Alpha-extended BODIPY Derivatives for Photovoltaic Application

In chapter 4, we synthesized a series of *alpha*-conjugation extended BODIPY compounds. However, successful purification of these BODIPY-based materials in a high level of purity through recrystallization cycles would allow for cyclic voltammetry studies and evaluation of device performance. Chapter 4 showed improved light-harvesting properties of synthesized BODIPY-based small molecules. In order to evaluate these materials as active layer materials in organic photovoltaics, further studies, including charge mobility and morphology, would need to be considered to determine device efficiencies for photovoltaic applications.

BIBLIOGRAPHY

Gorman, A.; Killoran, J.; O'Shea, C.; Kenna, T.; Gallagher, W. M.; O'Shea, D. F. In Vitro Demonstration of the Heavy-Atom Effect for Photodynamic Therapy. *J. Am. Chem. Soc.* **2004**, *126* (34), 10619–10631.

Kochevar, I. E.; Redmond, R. W. Photosensitized Production of Single Oxygen. *Methods Enzymol.* **2000**, *319*, 20–28.

Chen, X.; Li, Y.; Wang, A.; Zhou, L.; Lu, S.; Zhou, J.; Lin, Y.; Wei, S. Protonation Salt Derivative with Heavy-Atom Effect on Phthalocyanine for Enhanced in Vitro Photodynamic Therapy. *Dye. Pigment.* **2015**, *114* (C), 93–104.

Yogo, T.; Urano, Y.; Ishitsuka, Y.; Maniwa, F.; Nagano, T. Highly Efficient and Photostable Photosensitizer Based on BODIPY Chromophore. *J. Am. Chem. Soc.* **2005**, *127* (35), 12162–12163.

Rodriguez-Serrano, A.; Rai-Constapel, V.; Daza, M. C.; Doerr, M.; Marian, C. M. Internal Heavy Atom Effects in Phenothiazinium Dyes: Enhancement of Intersystem Crossing via Vibronic Spin-Orbit Coupling. *Phys. Chem. Chem. Phys.* **2015**, *17* (17), 11350–11358.

Cui, G.; Fang, W. H. State-Specific Heavy-Atom Effect on Intersystem Crossing Processes in 2-Thiothymine: A Potential Photodynamic Therapy Photosensitizer. *J. Chem. Phys.* **2013**, *138* (4).

Turro, N. J. The Triplet State. *J. Chem. Educ.* **1966**, *46* (1), 2–6.

McClure, D. S. Spin-Orbit Interaction in Aromatic Molecules. *J. Chem. Phys.* **1952**, *20* (4), 682.

Lower, S.; El-Sayed, M. The Triplet State and Molecular Electronic Processes in Organic Molecules. *Chem. Rev.* **1966**, *66* (2), 199–241.

Levine, I. N. Quantum Chemistry; Allyn and Bacon: Boston, 1970; pp 306–310.

McClure, D. S. Triplet-Singlet Transitions in Organic Molecules. Lifetime Measurements of the Triplet State. *J. Chem. Phys.* **1949**, *17* (10), 905.

Ermolaev, V. L.; Svitasbev, K. K. Quantum Yields of Phosphorescence and Fluorescence of Some 1-Derivatives of Naphthalene in Solutions at -196˚C. *Opt. Spectrosc.* **1959**, *1*, 399.

Cowan, D. O. Elements of Organic Photochemistry. In *Elements of Organic Photochemistry*; Plenum Press: New York, N.Y., 1976; pp 250–262.

Chock, P. B.; Stadtman, E. R. Superiority of Interconvertible Enzyme Cascades in Metabolite Regulation: Analysis of Multicyclic Systems. *Proc Natl Acad Sci U S A* **1977**, *74* (7), 2766–2770.

Koshland, D. E.; Goldbeter, A.; Stock, J. B. Amplification and Adaptation in Regulatory and Sensory Systems Author (S): Daniel E . Koshland , Albert Goldbeter and Jeffry B . Stock Published by : American Association for the Advancement of Science Stable URL : http://www.jstor.org/stable/1689499 JS. **2017**, *217* (4556), 220–225.

Chock, P. B.; Rhee, S. G.; Stadtman, E. R. Interconvertible Enzyme Cascades in Cellular-Regulation. *Annu. Rev. Biochem.* **1980**, *49*, 813–843.

Bhalla and Ravi Iyengar, U. S. Emergent Properties of Networks of Biological Signaling Pathways. *Science.* **1999**, *283* (5400), 381–387.

Weng, G. Complexity in Biological Signaling Systems. *Science.* **1999**, *284* (5411), 92–96.

Jordan, J. D.; Landau, E. M.; Iyengar, R. Signaling Networks: The Origins of Cellular Multitasking. *Cell* **2000**, *103* (2), 193–200.

Levine, S. N. Enzyme Amplifier Kinetics. *Science.* **1966**, *152* (3722), 651–653.

Wald, G. Visual Excitation and Blood Clotting. *Science* **1965**, *150* (3699), 1028–1030.

Brown, G. C.; Hoek, J. B.; Kholodenko, B. N. Why Do Protein Kinase Cascades Have More than One Level? *Trends Biochem. Sci.* **1997**, *22*, 288.

Fozooni, T.; Ravan, H.; Sasan, H. Signal Amplification Technologies for the Detection of Nucleic Acids: From Cell-Free Analysis to Live-Cell Imaging. *Appl. Biochem. Biotechnol.* **2017**, 1–30.

Wu, W.; Bazan, G. C.; Liu, B. Conjugated-Polymer-Amplified Sensing, Imaging, and Therapy. *Chem* **2017**, *2* (6), 760–790.

Mittal, S.; Kaur, H.; Gautam, N.; Mantha, A. K. Biosensors for Breast Cancer Diagnosis: A Review of Bioreceptors, Biotransducers and Signal Amplification Strategies. *Biosens. Bioelectron.* **2017**, *88*, 217–231.

Dewit, M. A.; Nazemi, A.; Karamdoust, S.; Beaton, A.; Gillies, E. R. Design, Synthesis and Assembly of Self-Immolative Linear Block Copolymers. *Non-Coventional Funct. Block Copolym.* **2011**, 9–21.

Li, Y.; Liu, G.; Wang, X.; Hu, J.; Liu, S. Enzyme-Responsive Polymeric Vesicles for Bacterial-Strain-Selective Delivery of Antimicrobial Agents. *Angew. Chemie - Int. Ed.* **2016**, *55* (5), 1760–1764.

Liu, G.; Wang, X.; Hu, J.; Zhang, G.; Liu, S. Self-Immolative Polymersomes for High-Efficiency Triggered Release and Programmed Enzymatic Reactions. *J. Am. Chem. Soc.* **2014**, *136* (20), 7492–7497.

Sauer, M.; Haefele, T.; Graff, a; Nardin, C.; Meier, W. Ion-Carrier Controlled Precipitation of Calcium Phosphate in Giant ABA Triblock Copolymer Vesicles. *Chem. Commun. (Camb).* **2001**, No. 23, 2452–2453.

Sceince, P. Polymer Vesicles. *Science (80-.).* **2005**, *297* (17), 967–974.

Wu, J.; Eisenberg, A. Proton Diffusion across Membranes of Vesicles of Poly(styrene-B-Acrylic Acid) Diblock Copolymers. *J. Am. Chem. Soc.* **2006**, *128* (9), 2880–2884.

Gabrielli, L.; Mancin, F. Minimal Self-Immolative Probe for Multimodal Fluoride Detection. *J. Org. Chem.* **2016**, *81* (22), 10715–10720.

Amir, R. J.; Pessah, N.; Shamis, M.; Shabat, D. Self-Immolative Dendrimers. *Angew. Chemie - Int. Ed.* **2003**, *42* (37), 4494–4499.

Shamis, M.; Shabat, D. Single-Triggered AB6 Self-Immolative Dendritic Amplifiers. *Chemistry* **2007**, *13* (16), 4523–4528.

Tan, X.; Li, B. B.; Lu, X.; Jia, F.; Santori, C.; Menon, P.; Li, H.; Zhang, B.; Zhao, J. J.; Zhang, K. Light-Triggered, Self-Immolative Nucleic Acid-Drug Nanostructures. *J. Am. Chem. Soc.* **2015**, *137* (19), 6112–6115.

Niculescu-Duvaz, I.; Niculescu-Duvaz, D.; Friedlos, F.; Spooner, R.; Martin, J.; Marais, R.; Springer, C. J. Self-Immolative Nitrogen Mustard Prodrugs for Suicide Gene Therapy. *J. Med. Chem.* **1998**, *41* (13), 5297–5309.

De Groot, F. M. H.; Albrecht, C.; Koekkoek, R.; Beusker, P. H.; Scheeren, H. W. "Cascade-Release Dendrimers" liberate All End Groups upon a Single Triggering Event in the Dendritic Core. *Angew. Chemie - Int. Ed.* **2003**, *42* (37), 4490–4494.

Shamis, M.; Lode, H. N.; Shabat, D. Bioactivation of Self-Immolative Dendritic Prodrugs by Catalytic Antibody 38C2. *J. Am. Chem. Soc.* **2004**, *126* (6), 1726–1731.

Dresselhaus, M.S.; Thomas, I. . Alternative Energy Technologies. *Nature* **2001**, *414* (November), 332–337.

Gregg, B. A.; Hanna, M. C. Comparing Organic to Inorganic Photovoltaic Cells: Theory, Experiment, and Simulation. *J. Appl. Phys.* **2003**, *93* (6), 3605–3614.

https://energy.gov/eere/solar/downloads/research-cell-efficiency-records.

Potscavage, W. J.; Sharma, a; Kippelen, B. Critical Interfaces in Organic Solar Cells and Their Influence on the Open-Circuit Voltage. *Acc. Chem. Res.* **2009**, *42* (11), 1758–1767.

Carsten, B.; Szarko, J. M.; Son, H. J.; Wang, W.; Lu, L.; He, F.; Rolczynski, B. S.; Lou, S. J.; Chen, L. X.; Yu, L. Examining the Effect of the Dipole Moment on Charge Separation in Donor-Acceptor Polymers for Organic Photovoltaic Applications. *J. Am. Chem. Soc.* **2011**, *133* (50), 20468–20475.

Yao, K.; Intemann, J. J.; Yip, H.-L.; Liang, P.-W.; Chang, C.-Y.; Zang, Y.; Li, Z.; Chen, Y.; Jen, A. K.-Y. Efficient All Polymer Solar Cells from Layer-Evolved Processing of a Bilayer Inverted Structure. *J. Mater. Chem. C* **2014**, *2* (3), 416.

Takacs, C. J.; Sun, Y.; Welch, G. C.; Perez, L. A.; Liu, X.; Wen, W.; Bazan, G. C.; Heeger, A. J. Solar Cell Efficiency, Self-Assembly, and Dipole-Dipole Interactions of Isomorphic Narrow-Band-Gap Molecules. *J. Am. Chem. Soc.* **2012**, *134* (40), 16597–16606.

Beaujuge, P. M.; Fréchet, J. M. J. Molecular Design and Ordering Effects in π-Functional Materials for Transistor and Solar Cell Applications. *J. Am. Chem. Soc.* **2011**, *133* (50), 20009–20029.

Kallmann, H.; Pope, M. Photovoltaic Effect in Organic Crystals. *J. Chem. Phys.* **1959**, *30* (2), 585–586.

Benanti, T. L.; Venkataraman, D. Organic Solar Cells: An Overview Focusing on Active Layer Morphology. *Photosynth. Res.* **2006**, *87* (1), 73–81.

Yu, G.; Pakbaz, K.; Heeger, A. J. Semiconducting Polymer Diodes: Large Size, Low Cost Photodetectors with Excellent Visible-Ultraviolet Sensitivity. *Appl. Phys. Lett.* **1994**, *64* (25), 3422–3424.

Dang, M. T.; Hirsch, L.; Wantz, G. P3HT:PCBM, Best Seller in Polymer Photovoltaic Research. *Adv. Mater.* **2011**, *23* (31), 3597–3602.

Wu, P. T.; Xin, H.; Kim, F. S.; Ren, G.; Jenekhe, S. A. Regioregular poly(3-Pentylthiophene): Synthesis, Self-Assembly of Nanowires, High-Mobility Field-Effect Transistors, and Efficient Photovoltaic Cells. *Macromolecules* **2009**, *42* (22), 8817–8826.

Gabe, Y.; Ueno, T.; Urano, Y.; Kojima, H.; Nagano, T. Tunable Design Strategy for Fluorescence Probes Based on 4-Substituted BODIPY Chromophore: Improvement of Highly Sensitive Fluorescence Probe for Nitric Oxide. *Anal. Bioanal. Chem.* **2006**, *386* (3), 621–626.

Li, Y.; Wang, J.; Zhang, X.; Guo, W.; Li, F.; Yu, M.; Kong, X.; Wu, W.; Hong, Z. Highly Water-Soluble and Tumor-Targeted Photosensitizers for Photodynamic Therapy. *Org. Biomol. Chem.* **2015**, *13* (28), 7681–7694.

Gee, K. R.; Archer, E. A.; Kang, H. C. 4-Sulfotetrafluorophenyl (STP) Esters: New Water-Soluble Amine-Reactive Reagents for Labeling Biomolecules. *Tetrahedron Lett.* **1999**, *40* (8), 1471–1474.

Hendel, S. J.; Poe, A. M.; Khomein, P.; Bae, Y.; Thayumanavan, S.; Young, E. R. Photophysical and Electrochemical Characterization of BODIPY-Containing Dyads Comparing the Influence of an A–D–A versus D–A Motif on Excited-State Photophysics. *J. Phys. Chem. A* **2016**, *120*, 8794–8803.

Gollnick, K.; Griesbeck, A. Singlet Oxygen Photooxygenation of Furans. *Tetrahedron* **1985**, *41* (11), 2057–2068.

Morone, M.; Beverina, L.; Abbotto, A.; Silvestri, F.; Collini, E.; Ferrante, C.; Bozio, R.; Pagani, G. A. Enhancement of Two-Photon Absorption Cross-Section and Singlet-Oxygen Generation in Porphyrins upon ??-Functionalization with Donor-Acceptor Substituents. *Org. Lett.* **2006**, *8* (13), 2719–2722.

Deng, P.; Zhang, Q. Recent Developments on Isoindigo-Based Conjugated Polymers. *Polym. Chem.* **2014**, *5* (10), 3298–3305.

Lin, Y.; Li, Y.; Zhan, X. Small Molecule Semiconductors for High-Efficiency Organic Photovoltaics. *Chem. Soc. Rev.* **2012**, *41* (11), 4245.

Zhang, Z.; Wang, J. Structures and Properties of Conjugated Donor–Acceptor Copolymers for Solar Cell Applications. *J. Mater. Chem.* **2012**, *22* (10), 4178.

Zhou, H.; Yang, L.; You, W. Rational Design of High Performance Conjugated Polymers for Organic Solar Cells. *Macromolecules* **2012**, *45* (2), 607–632.

Hou, J.; Huo, L.; He, C.; Yang, C.; Li, Y. Synthesis and Absorption Spectra of poly(3-(Phenylenevinyl)thiophene)s with Conjugated Side Chains. *Macromolecules* **2006**, *39* (2), 594–603.

Hou, J.; Tan, Z.; Yan, Y.; He, Y.; Yang, C.; Li, Y. Synthesis and Photovoltaic Properties of Two-Dimensional Conjugated Polythiophenes with Bi(thienylenevinylene) Side Chains. *J. Am. Chem. Soc.* **2006**, *128* (14), 4911–4916.

He, G.; Li, Z.; Wan, X.; Liu, Y.; Zhou, J.; Long, G.; Zhang, M.; Chen, Y. Impact of Dye End Groups on Acceptor–donor–acceptor Type Molecules for Solution-Processed Photovoltaic Cells. *J. Mater. Chem.* **2012**, *22* (18), 9173.

Liu, J.; Walker, B.; Tamayo, A.; Zhang, Y.; Nguyen, T. Q. Effects of Heteroatom Substitutions on the Crystal Structure, Film Formation, and Optoelectronic Properties of Diketopyrrolopyrrole-Based Materials. *Adv. Funct. Mater.* **2013**, *23* (1), 47–56.

Yuan, J.; Huang, X.; Zhang, F.; Lu, J.; Zhai, Z.; Di, C.; Jiang, Z.; Ma, W. Design of Benzodithiophene-Diketopyrrolopyrrole Based Donor–acceptor Copolymers for Efficient Organic Field Effect Transistors and Polymer Solar Cells. *J. Mater. Chem.* **2012**, *22* (42), 22734.

Sonar, P.; Ng, G.-M.; Lin, T. T.; Dodabalapur, A.; Chen, Z.-K. Solution Processable Low Bandgap Diketopyrrolopyrrole (DPP) Based Derivatives: Novel Acceptors for Organic Solar Cells. *J. Mater. Chem.* **2010**, *20* (18), 3626.

Della Pelle, A. M.; Homnick, P. J.; Bae, Y.; Lahti, P. M.; Thayumanavan, S. Effect of Substituents on Optical Properties and Charge-Carrier Polarity of Squaraine Dyes. *J. Phys. Chem. C* **2014**, *118* (4), 1793–1799.

Huang, X.; Zhu, C.; Zhang, S.; Li, W.; Guo, Y.; Zhan, X.; Liu, Y.; Bo, Z. Porphyrin-Dithienothiophene π-Conjugated Copolymers: Synthesis and Their Applications in Field-Effect Transistors and Solar Cells. *Macromolecules* **2008**, *41* (19), 6895–6902.

Benniston, A. C.; Copley, G. Lighting the Way Ahead with Boron Dipyrromethene (Bodipy) Dyes. *Phys. Chem. Chem. Phys.* **2009**, *11* (21), 4124.

Oosterhout, S. D.; Savikhin, V.; Zhang, J.; Zhang, Y.; Burgers, M. A.; Marder, S. R.; Bazan, G. C.; Toney, M. F. Mixing Behavior in Small Molecule:Fullerene Organic Photovoltaics. *Chem. Mater.* **2017**, *29* (7), 3062–3069.

Carlé, J. E. Polymers for Organic Photovoltaics Based on 1,5-bis(2-Hexyldecyloxy)-Naphthalene, Thiophene, and Benzothiadiazole. *J. Photonics Energy* **2011**, *1* (1), 11111.

Guo, X.; Watson, M. D. Conjugated Polymers from Napthalene Bisimide. *Org. Lett.* **2008**, *10* (23), 5333–5336.

Eggert Carlé, J.; Wenzel Andreasen, J.; Jørgensen, M.; Christian Krebs, F. Low Band Gap Polymers Based on 1,4-Dialkoxybenzene, Thiophene, Bithiophene Donors and the Benzothiadiazole Acceptor. *Sol. Energy Mater. Sol. Cells* **2010**, *94* (5), 774–780.

Poe, A. M.; Della Pelle, A. M.; Subrahmanyam, A. V.; White, W.; Wantz, G.; Thayumanavan, S. Small Molecule BODIPY Dyes as Non-Fullerene Acceptors in Bulk Heterojunction Organic Photovoltaics. *Chem. Commun.* **2014**, *50* (22), 2913–2915.

Matsumura, S.; Hlil, A. R.; Lepiller, C.; Gaudet, J.; Guay, D.; Shi, Z.; Holdcroft, S.; Hay, A. S. Ionomers for Proton Exchange Membrane Fuel Cells with Sulfonic Acid Groups on the End-Groups: Novel Branched Poly(ether-Ketone)s. *Am. Chem. Soc. Polym. Prepr. Div. Polym. Chem.* **2008**, *49* (1), 511–512.

Wakim, S.; Beaupré, S.; Blouin, N.; Aich, B.-R.; Rodman, S.; Gaudiana, R.; Tao, Y.; Leclerc, M. Highly Efficient Organic Solar Cells Based on a poly(2,7-Carbazole) Derivative. *J. Mater. Chem.* **2009**, *19* (30), 5351.

Goud, T. V.; Tutar, A.; Biellmann, J. F. Synthesis of 8-Heteroatom-Substituted 4,4-Difluoro-4-Bora-3a,4a-Diaza-S-Indacene Dyes (BODIPY). *Tetrahedron* **2006**, *62* (21), 5084–5091.

Rakstys, K.; Paek, S.; Gao, P.; Gratia, P.; Marszalek, T.; Grancini, G.; Cho, K. T.; Genevicius, K.; Jankauskas, V.; Pisula, W.; et al. Molecular Engineering of Face-on Oriented Dopant-Free Hole Transporting Material for Perovskite Solar Cells with 19% PCE. *J. Mater. Chem. A* **2017**, *5* (17), 7811–7815.